TEMPLATE-ASSISTED ELECTROHYDRODYNAMIC ATOMISATION OF BIOACTIVE DEPOSITS ON ADVANCED BIOMATERIALS FOR ORTHOPAEDIC APPLICATIONS

Anouska Nithyanandan

Thesis submitted for the degree of

Doctor of Philosophy

December 2015

Department of Mechanical Engineering

University College London

Declaration

I, Anouska Nithyanandan, confirm that the work presented in this thesis is my own. Where information has been derived from other sources, I confirm that this has been indicated in the thesis.

Anouska Nithyanandan

Abstract

There is potential for template assisted electrohydrodynamic atomisation (TAEA) spraying, a novel ambient temperature patterning technique, to be an improved coating method compared to the current industry standard of vacuum plasma spraying metallic implants for orthopaedic applications. The reduction in temperature results in an increase in the range of coating materials and the ability to incorporate biological agents during manufacturing. This highly controllable process has been utilised to produce coatings with an ideal thickness, improves uniformity and homogeneity, and improved bond strength. The TAEA spraying of bioceramic suspension and polymer solutions in the stable cone jet mode was studied. It was found that the media concentration, the flow rate, the applied voltage and the spraying time had a significant influence on the morphology of the resultant coatings. A wide variety of predetermined topographical geometries have been achieved with a high degree of control. For the first time, TAEA has been used to pattern curved metallic surfaces with ceramics, and flat metallic substrates with polymer materials. A high degree of control over pattern line width, interline spacing and thickness were achieved. TiO_2 patterns with parallel lines have been successfully produced on both convex and concave Ti substrate diameters of ~25mm. Optimal results were obtained with 4 wt.% TiO_2 in ethanol suspension sprayed within the stable cone jet mode window at a flow rate of 20 $\mu l.min^{-1}$ for 300 s at 10 kV with a collection distance of 80 mm. Nanoindentation indicates good adhesion between pattern and substrate. The effect of heat treatment to further consolidate the patterned deposits was also investigated. Hardness of the patterns was not markedly affected by heating. For TiO_2 patterns at a loading rate of 1 $\mu N.s^{-1}$ and a hold time of 1 s, hardness decreases as load increases up to 7 μN and remains at 0·1 GPa up to higher loads. Elastic modulus behaves in a similar way. This decrease can be attributed to the microporosity observed in the TiO_2 deposits as higher loads are able to penetrate more easily into microporous structures. This work shows that TAEA is highly controllable and compatible on a range of substrate geometries. A clear correlation between the template shape and size and the achieved pattern was established, therefore the template can be chosen to reflect the specific clinical needs of the coating. Extending TAEA capabilities from flat to curved surfaces, enabling the bioactive patterning of different surface geometries, takes this technology closer to orthopaedic engineering applications.

Acknowledgements

Firstly I would like to thank Prof. Mohan Edirisinghe of University College London (UCL) for his primary academic supervision. His dedication and time throughout this doctorate are greatly appreciated. I would also like to thank Dr. Jie Huang (UCL) for her secondary academic supervision, and Prof. Edward Draper and Dr. Sarrawat Rehman (JRI Orthopaedics Ltd) for their industrial supervision. Thanks also to Dr. Sunthar Mahalingam and Dr. Muhammad Rafique Nangrejo for their academic and experimental guidance, and the Bio- and Functional Materials Processing and Forming Laboratory at UCL for their camaraderie and assistance. Thanks also to UCL and JRI Orthopaedics Ltd for financially supporting this work.

I am very grateful to the friends and family who have consistently encouraged and supported me as I completed this doctorate. In particular, I would like to thank my Grandpa, Vettivelu Veerasuntharam, for always being proud of me and continuing to be my greatest advocate. Thanks also to Dr. Matthew Grant and the Grant family for offering me much love and encouragement over the years.

Finally, there are three important people who celebrated with me when I began this doctorate, but are sadly no longer here as I complete it. Firstly my brave, resilient and loving Grandma, Mary-Josephine Veerasuntharam. Secondly my dear friend and respected mentor and teacher, Dr. Kajal K. Mallick. Thirdly my kind, talented and inspiring friend, Elisa Ly. This achievement is dedicated to them.

Table of Contents

Publications, Conferences and Awards

Journal publications

1. **Nithyanandan, A.**, Mahalingam, S., Huang, J., Rehman, S., Draper, E. and Edirisinghe, M. Bioinspired electrohydrodynamic ceramic patterning of curved metallic substrates. *Bioinspired, Biomimetic and Nanobiomaterials*, vol. 4, pp. 59-67, July 2014.

2. **Nithyanandan, A.**, Mahalingam, S., Huang, J., Rehman, S., Draper, E. and Edirisinghe, M. Template-assisted electrohydrodynamic atomization of polycaprolactone for orthopedic patterning applications. *Materials Science and Engineering C*, vol. 33, pp. 4608-4615, July 2013.

3. **Nithyanandan, A.**, Mahalingam, S., Huang, J., Rehman, S., Draper, E. and Edirisinghe, M. Template-assisted electrohydrodynamic atomisation on metallic substrates for orthopaedic implant applications. *(In preparation)*

4. **Nithyanandan, A.**, Mahalingam, S., Huang, J., Rehman, S., Draper, E. and Edirisinghe, M. Template-assisted electrohydrodynamic atomisation of biopolymers for hard and soft tissue implant applications. *(In preparation)*

5. **Nithyanandan, A.** Bio-engineering hips for the future: Smart patterning by template-assisted electrohydrodynamic atomisation (TAEA). Orthopaedic Research UK (ORUK) Impact Report 2015, September 2015.

Conference participation

1. **Nithyanandan, A.** Bio-engineering hips for the future: Smart patterning by template-assisted electrohydrodynamic atomisation (TAEA). JRI and ORUK exhibition stand. ***British Orthopaedic Association Annual Scientific Congress 2015,*** Liverpool, UK, September 2015.

2. **Nithyanandan, A.**, Mahalingam, S., Huang, J., Rehman, S., Draper, E. and Edirisinghe, M. Ambient temperature patterning of bioactive deposits on curved metallic substrates for orthopaedic implants. Poster presentation accepted by the ***26th European Society for Biomaterials Conference,*** Liverpool, UK, August 2014.

3. **Nithyanandan, A.** TAEA of bioactive deposits on curved substrates for orthopaedic applications. Oral presentation accepted by the ***International Conference in Progress in Additive Manufacturing 2014 (ICPro-AM'14)***, Nanyang Executive Centre, Nanyang Technological University, Singapore, May 2014.

4. **Nithyanandan, A.** TAEA of biopolymer and bioceramic surface patterns onto metallic substrates for orthopaedic implant applications. Oral presentation accepted by the ***International Symposium on Coatings Technology, International Materials Technology Conference and Exhibition 2014 (IMTCE'14)***, Putra World Trade Centre, Kuala Lumpur, Malaysia, May 2014.

5. **Nithyanandan, A.**, Mahalingam, S., Huang, J., Rehman, S., Draper, E. and Edirisinghe, M. TAEA Patterning of Bioactive Deposits on Advanced Biomaterials for Orthopaedic Applications. Oral and poster presentation accepted by the ***UCL Mechanical Engineering PhD Conference 2013****,* University College London, UK, June 2013.

6. **Nithyanandan, A.**, Draper, E., Huang, J. and Edirisinghe, M. TAEA patterning of bioactive deposits on advanced biomaterials for orthopaedic applications. Invited oral presentation at the ***1st JRI Technology Innovation Day****,* JRI Orthopaedics Ltd., Sheffield, UK, October 2012.

7. **Nithyanandan, A.**, Nangrejo, M., Huang, J., Draper, E. and Edirisinghe, M. TAEA Patterning of Bioactive Deposits on Advanced Biomaterials for Orthopaedic Applications. Oral and poster presentation accepted by the ***UCL Mechanical Engineering PhD Conference 2012****,* University College London, UK, June 2012.

8. **Nithyanandan, A**. Participated and co-organised the ***4th Biomaterials, Particles, Bubbles, Capsules & Fibres for Healthcare Research Symposium****,* University College London, UK, April 2012.

Awards

1. ***Young Person's Lecture Competition Winner London 2014.*** **Nithyanandan, A**. Bio-engineering hips for the future: An introduction to TAEA. The Institute of Materials, Minerals and Mining, London, UK, February 2014.

2. ***Royal Society Brian Mercer Feasibility Award (£30,000), 2013-2014*****.** Edirisinghe, M. with co-applicants Huang, J., Mahalingam, S. and **Nithyanandan, A.** Template-assisted Electrohydrodynamic Atomisation (TAEA) Patterning of Bioactive Materials on Curved Metallic Substrates. Royal Society, London, November 2013.

List of Figures

List of Tables

1. Introduction

1.1 Background

At least 50,000 hip replacement operations are carried out each year in the UK, with 85% lasting for 20 years before needing revision surgery (National Joint Registry 2012). This percentage needs to increase in order to accommodate for an increasing aging population. Total hip replacements (THRs) simulate the anatomy of a healthy hip joint, and are implanted to replace one that is failing. An acetabular cup implanted into socket part of the hip joint in the pelvis, and a femoral stem is inserted into the femur for fixation. These implants, particularly the femoral stem, are made up from metallic biomaterials such as medical grade stainless steels, and titanium and its alloys. Studies show that whilst their mechanical properties are sufficient for load-bearing applications, their chemical bioactivity and high stiffness can lead to bone loosening in the long term as well as high stress concentrations *in vivo*. This contributes to the relatively limited functional lifetime of THRs. Therefore this lifetime needs to increase in order to minimise the number of revision surgeries that patients need to endure.

The application of bioactive coatings such as hydroxyapatite has been found to improve bone ingrowth of implants as it has a similar mineral composition to bone mineral (Hench, 1998, Coathup et al., 2000, Capello et al., 1997). This material has insufficient mechanical properties if used alone, but it can be applied as a coating onto metallic implants such as the femoral stems of THRs to improve the direct biological fixation of the tissue to the implant surface. Optimising the surface topography of this coating can also up-regulate cellular activity and increase the biological response (Curtis and Wilkinson, 1997).

The bioengineering task of effectively and efficiently coating the surface of metallic load bearing joint prostheses with bioactive materials can enhance direct biological fixation, resulting in shorter recovery times and fewer revision surgeries for patients. The current industrial method for manufacturing coatings is vacuum plasma spraying (Sun et al., 2001). This expensive high-temperature method is capable of producing adequate (uniform and continuous) coatings commercially. However, there are several inherent limitations including their tendency to detach and or resorb over time (Radin and Ducheyne, 1992), reducing their long term stability and thus functional lifetime. This process is also incapable of optimising surface topography using patterned deposition.

Template-assisted electrohydrodynamic atomisation (TAEA) is an electrohydrodynamic process where a high voltage is applied to a liquid flow ejected out of a needle, which then splits into small droplets that are attracted to a grounded substrate. This occurs due to the electric stress of the liquid from the large potential difference between the needle and substrate. The process is mainly affected by liquid flow rate, the voltage applied to the liquid and needle, the properties of the liquid such as electrical conductivity and density, and process parameters such as collection distance between the needle and substrate. These collective parameters affect the nature of the liquid jet as it emerges from the needle. There are several distinctive modes of jetting, but the mode best suited to creating homogenous coatings required by orthopaedic implants is the cone jet mode. This mode is the most stable and produces droplets that are small (micro- and nano-metre range) and with a low size distribution. Here, the liquid emerges from the needles in a conical shape, and extends to a fine liquid jet made up of liquid particles.

TAEA spraying has the potential to provide an improved regular and uniform coating method. Reasons for this include reduced processing temperatures, increased coating

material range, greater controllability, greater variety of predetermined topographical geometries and simple set up with lower energy requirements.

Further developing the TAEA process for use with a wider range of coating materials and substrate geometries will improve the functionality and commercial viability of this process, whist improving the quality, longevity and applicability of coated orthopaedic implants.

1.2 Aims and objectives of the research

The aim of this doctorate is to develop template-assisted electrohydrodynamic atomisation (TAEA) spraying into a generic patterning process for bioactive materials and substrates for clinical use in orthopaedic implant technology. This approach should take advantage of the ambient temperature processing conditions (≈20°C) and the potential to use traditional ceramic and novel polymer coating materials on flat and curved substrates, whilst optimising the geometry of the interlocked coating microstructure.

Key objectives of project include:

1. To manufacture and characterise TAEA coatings using a range of coating materials and substrate geometries.
2. To utilise ambient temperature conditions (≈20°C).
3. To optimise key process parameters (e.g. voltage, flow rate, collection distance) to produce repeatable ideal coatings suitable for clinical use.

1.3 Structure of the thesis

Chapter 1 introduces the background of the project and the motivation for improving the quality and longevity of orthopaedic implants via bioceramic materials and surface modification. The limitations of current coating techniques are given, and the novel template-assisted electrohydrodynamic atomisation (TAEA) process is briefly introduced. The aim and objectives of this research are stated, the structure of the thesis explained, and the benefits of this research elucidated.

Chapter 2 is dedicated to reviewing the literature relevant and associated with this research. The structure and nature of bone tissue are explained, as well as the function of bones the skeletal system. This leads the reader to the mechanical properties and requirements of bone tissue, and why joints may need replacing with artificial implants such as total joint replacements. The role of orthopaedic implants in the body, specifically total hip replacements (THRs), is discussed. Their structure is also described. The different types of THRs and their failure mechanisms are explained to justify the focus on improving the quality of fixation and thus bioactive coatings for patients. The concept of biomaterials is introduced, including their fundamental requirements and the rationale for choosing the ceramic, metallic and polymeric materials used in this study. Current coating techniques are discussed, thus their inherent limitations and the potential for TAEA to be an improved method. The process and mechanisms involved in TAEA are explained, including the functional modes of spraying and the Taylor cone. Key processing parameters and their effect on the resultant jet are discussed.

Chapter 3 gives a detailed description of the experimental procedures employed in this study. The coating and substrate materials that are used are stated, as well as how they are sourced and prepared. The preparation of coating suspensions, solutions and sols are

described here, as well as the methods used to characterise them. The experimental set up is shown and explained, and the techniques used to characterise the resultant patterns and coatings are explained and justified.

Chapter 4 presents the development of TAEA onto curved metallic substrates. This area is introduced, and the challenges involved with spraying curved substrates are explained. The strategy for assessing coating homogeneity is explained as well. The chapter goes on to elucidate the physical properties of the suspensions and sols, and the voltage-flow maps for these. Resultant patterns are included in this chapter, as well as an analysis of their geometry. A systematic investigation into the effect of substrate curvature is contained here, as well as the mechanical properties of the patterns derived via nanoindentation techniques.

Chapter 5 presents the development of TAEA using biopolymers as the coating material. This chapter reveals that TAEA is compatible with a range of polymers, and that macroporosity can also be introduced and controlled into deposits. The solutions were characterised and the results given and explained. The jetting modes of these solutions were also described. The geometry of the resultant patterns were analysed, and systematic investigations into the effect of flow rate and solution concentration were carried out. The mechanical properties of PCL patterns were also examined.

Chapter 6 presents the development of TAEA spraying interlocked TiO_2 and HA coatings on a range of metallic substrates, and the mechanical effects of heat-treating titanium dioxide buffer layers on titanium substrates. Suspension properties were stated and explained, and this chapter includes images of the resultant patterns.

Chapter 7 states the conclusions derived from this study, based on the results and discussion from Chapters 4, 5 and 6. Chapter 7 offers several future areas of research based on these findings.

1.4 Benefits of the research

This research will increase our understanding of the TAEA process and its applicability and versatility in biomaterials processing and orthopaedic implant applications. This will further interest in this process within industry and academia, as it elucidates the potential for this process in real-world applications. This research shows that TAEA is a relatively simple and cheap process that is capable of producing highly controllable patterned biocompatible coatings for clinical use.

The controllability of droplet size and homogeneity in spray processes such as TAEA is hugely relevant to many industries, not just medical implants. These include aircraft, aerospace and automotive coatings, high performance coating for the protection of structural steelwork (e.g. bridges, oil and gas rigs), and marine coatings. This novel technique can improve the surface properties of materials with ideal bulk properties.

2. Literature Review

Bone is a living tissue that can remodel itself in response to stress and load requirements. Biomaterials are materials that interact with biological systems to repair and reconstruct of the body. In this chapter, the author will present the background to bone implant technology and the current work. This will give the reader sufficient knowledge to understand the relevance and motivation of the author's work on developing an improved method for coating orthopaedic implants.

An understanding of the microstructure and properties of natural bone will aid the design of materials and processes specific to orthopaedic applications. Many techniques to coat metallic surfaces have been developed with bioceramics, particularly since the development of hydroxyapatite-coated hip replacements. TAEA offers a range of advantages, including low costs, simple set-up and ambient temperature processing, therefore this chapter will introduce its physical mechanisms, as well as classifying its processing parameters. This will offer the reader a comprehensive understanding of TAEA in order to understand the relevance and mechanisms further developed in this study.

2.1 Bone and orthopaedic engineering

Effective orthopaedic engineering works aims to utilise the natural properties of bone tissue to successfully integrate biomaterials in order to support muscular-skeletal function (Place et al., 2009). The clinical requirements of bone tissue are therefore defined by it macro and microstructure, composition and mechanical properties, which in turn determine the properties of bioactive coatings for orthopaedic implants.

2.1.1 The composition of bone

Bone structure has a number of hierarchical levels, which are depicted in **Figure 2.1**.

Figure 2.1: Macro-, micro- and ultra-structure of mature bone (Park, 1987)

At the microscopic scale collagen fibres make up lamellar sheets that have a thickness of around 1-7 µm. Each osteon is made up of concentric rings of 4-20 lamellae, which go around the Haversian canal (Park, 1987). Each of these lamellae has the collagen orientated individually. The ultrastructure of bone is made up of the mineral component (apatite mineral crystals such as calcium phosphate crystals that increase bone stiffness) and the organic component (collagen fibres). These apatite crystals can be in the form of needles or plates, ranging in length from 40-60 nm long, width around 20 nm and thickness between 1.5-5 nm. Apatite crystals in the ultrastructure lay parallel to collagen fibres (Currey, 1983). Collagen microfibres make up a matrix, and collagen fibres themselves have a diameter between 100-2000 nm. Collagen increases the toughness and elasticity of bone tissue.

At the macroscopic scale, bone is made up of two types of tissue, dense cortical/compact bone and less dense trabecular/cancellous bone. This is shown in **Figure 2.2**.

Figure 2.2: Transverse cross-sectional view through a human long bone (Kumar, 2005)

The outer layer of bone is made up of cortical bone, whilst the centre is made up of spongy trabecular bone. Trabecular bone is made up of interconnected rods that orientate themselves in response to the loads placed upon them externally, and is approximately 50% dense with an apparent density typically 0.3 $g.cm^{-3}$. Thus bone is described as being 'dynamically modelled'. Bone can change its shape and structure to accommodate for varying metabolic and mechanical demand (Katz, 2000).

Cortical bone is hard and stiff due to the increased proportion of needle-like apatite crystals, yet strong (i.e. less likely to fracture or be brittle) due to the effect of collagen fibres. The apparent density of cortical bone is 1.85 $g.cm^{-3}$.

Bone is highly vascularised, with blood vessels and nerves running vertically through the central core of trabecular bone. This supplies the bone tissue with essential nutrients and metabolites. Both red and white blood cells are produced in the bone marrow within trabecular bone. Essential minerals for the body are also stored here, including phosphorus and calcium. The ability for tissues to grow or regenerate on a scaffold or an implant is one

way in which cells and their associated extra-cellular matrix can be characterised (Kawanishi et al., 2004). Another is the range of mechanical properties of the tissue. On average, 65% of bone tissue is a mineral inorganic phase like calcium phosphate or hydroxyapatite. Around 10% is water, with the rest, 25%, being organic bone matrix. Of this, 90% is collagen and the remaining 10% is non-collagenous protein. This emphasises the crucial role of the mineral inorganic phase in bone as a biocomposite. This is displayed schematically in **Figure 2.3**. The specific proportions vary with respect to the location of the bone in the body, water content of the tissue, and the age and health of the individual.

Figure 2.3: The composition of human bone

2.1.2 The function of bone and the human skeletal system

The human skeletal system facilitates movement by providing a lightweight framework onto which muscles can attach and operate, whilst also being strong enough to support and protect internal organs. Bones also provide shock absorption when the body is in motion and encounters impact (Haywood, 2008).

Functions of the skeletal system also include the production of elements of the blood in the red marrow of the bones (haematopoiesis), the storage of energy reserves (lipids) and minerals (calcium and phosphates) in the yellow marrow of the bones.

2.1.3 The mechanical properties of bone

As discussed, the combination of constituents renders bone a biocomposite material that is comprises of a flexible organic phase of collagen with a rigid inorganic phase of mineral apatites. However, the direction in which the load is applied also affects mechanical properties including Young's modulus, compressive strength and tensile strength. These have been found to be higher when the load is applied parallel to the longitudinal direction down into the end of the femur for example ($1.79x10^8$ Nm^{-2}, $1.33x10^8$ Nm^{-2}, and $2.03x10^8$ Nm^{-2} respectively), rather than in a perpendicular direction ($1.01x10^8$ Nm^{-2}, $0.41x10^8$ Nm^{-2}, and $1.51x10^8$ Nm^{-2} respectively) (Reilly and Burstein, 1975, Reilly et al., 1974).

2.1.4 Regeneration of bone tissue

The body has the capacity to signal the proliferation of bone cells and the regeneration of bone tissue upon tissue damage. Three types of bone cells facilitate this regeneration. Firstly, growth factors and hormones activate the production of bone matrix as osteoprogenitor cells differentiate into osteoblasts. Osteoblasts develop into osteocytes as they mature, and are located in microscopic channels that follow through the osteons of cortical bone called canaliculi. Mineral apatites like calcium phosphates and hydroxyapatite attach onto the bone matrix and forms bone tissue. Osteoclasts break down bone tissue during repair and maintenance (Lieberman and Friedlaender, 2005).

In summary, osteoblast aid tissue production, osteocytes aid maintenance of tissue, and osteoclasts are responsible for cell absorption (through the release of proteolytic enzymes). Osteoblasts are usually in a rounded plump form, but when in close contact with the surface of bone (and not participating in bone formation) they have a more flattened shape that lies parallel to the surface. Cells can also adjust their shape in response to other surface morphologies such as the implant interface. For example, osteoblast can elongate along a

surface with grooves with a diameter similar to its own. When bone is remodelling, osteoblasts can mineralise and differentiate into osteocytes. Osteocytes have a less rounded shape and supply bone tissue with nutrients, metabolites and oxygen, as well as minerals.

Biological and pathological factors can affect bone's capacity to heal. Age increases the incidence of certain bone diseases such as osteoporosis, which reduces bone's capacity to regenerate. Age also positively correlates with declining populations of osteoprogenitor cells, thus is another limiting factor. Anti-inflammatory medicines, nicotine and other drugs can reduce blood supply to a defect site and inhibit healing and regeneration. Vitamin D and calcium deficiencies caused by poor diet can also lower cell proliferation (Narayan, 2009).

2.1.4 The role of orthopaedic implants in the body

Human joints are susceptible to trauma and degenerative and inflammatory diseases, all of which can cause pain, reduced mobility and diminished quality of life. The most common degenerative diseases are osteoarthritis and rheumatoid arthritis (Woolf and Pfleger, 2003), and have been found to affect 90% people over the age of 40 (Lowman, 1955).

Surgery is usually required to remove damaged articulating tissue and replace it with artificial materials when weight-bearing joints deteriorate (Lee and Goodman, 2008). Total hip replacements (THR) are well-established orthopaedic techniques. At least 50,000 hip replacement operations are carried out each year in the UK, with 85% lasting for 20 years before needing revision surgery (National Joint Registry 2012). This percentage needs to increase in order to accommodate for an increasing aging population. The global population of those aged 65 and over is projected to increase year on year as life expectancy and quality increase, improved (less invasive) surgeries and techniques are developed, and

orthopaedic technology innovates new solutions and thus creates a greater and wider demand for orthopaedic implants (Hing, 2004).

2.2 Total hip replacements

Total hip replacement (THR) is a surgical procedure where the whole hip joint (including the acetabulum, femoral head and femoral stem) is replaced by a prosthetic implant. Prostheses generally consist of three elements, which are shown in **Figure 2.4**.

1. A metallic ball to replace the original femoral head.
2. A metallic femoral stem that is surgically inserted into the femur.
3. A plastic acetabular component that is inserted in the hip socket of the pelvis.

Figure 2.4: Typical hip replacements *in vivo* (a) schematic diagram (b) X-ray radiograph (Bradbury, 2013)

2.2.1 Types of total hip replacement

There are approximately 60 different types of hip prostheses used in the UK today. The most common way to classify them is the method by which they are fixed into the body. THRs can be cemented into the femur using bone cement, cementless (where the femoral stem is shaped or surface treated for fixation) or hybrid (where a cemented stem is implanted with a cementless cup).

Historically, cemented stems caused frequent early failure, post-implantation (Learmonth et al., 2007). This was caused by osteolysis (bone cell damage and resorption) from local inflammatory response to cement particles (Harris et al., 1976). This encouraged the development of un-cemented prostheses.

Without bone cement, THRs had to provide enough initial mechanical stability to encourage bone osteointegration (bone growth) onto the implant. This had the greatest design implication on the metallic femoral stem. Whilst the surface could be made porous to encourage bone cells to attach, and tapered to allow the implant to 'hold' in the femur, the chemical and biological properties of metals are not favourable to cell growth. In addition, some patients complained of thigh pain caused by the discrepancy between the elastic behaviour of the rigid metallic femoral stem adjacent to the dynamically modelled femur *in vivo* (Lavernia et al., 2004).

Therefore, the next major development of uncemented THRs was the application of bioactive bioceramic coatings onto the surface of the femoral stem, to enhance bone in-growth and enhance long-term biological fixation (D'Antonio et al., 2001). Currently, the choice between cemented and uncemented fixation is based on the quality of the patient's bone tissue. If the patient is young and otherwise healthy, the uncemented approach is preferable due to its improved initial adhesion and healing. However, in the case of older

patients with underlying bone health issues, surgeons are more likely to choose the cemented approach, as the long-term effects are historically favourable. As the quality of uncemented, coated THRs improve, there is a shift in preference from cemented to cementless THRs (Yamada et al., 2009).

2.2.2 Total hip replacement failure mechanisms and revision

Although THRs are relatively successful and common orthopaedic procedures, there are several inherent issues that limit long-term effectiveness. This can be measured by implant service life (how long they last before needing to be revised), as well as the improvement in joint function and quality of life for the patient. The patients themselves are changing demographics, to younger and more active individuals that need their joint replacements to both minimise pain and increase mobility for longer (Lee and Goodman, 2008, Drake et al., 2002). Complications may therefore arise that mean the original surgery requires revision years later. Also, despite the current popularity of THRs, artificial joints ultimately have a shorter lifetime when compared to the human body's natural joints.

When THRs need to be revised, the success rate of surgery is lower than the initial implantation. The process is more difficult as more tissue needs to be removed and replaced. Therefore, the average hospital stay is increased, as well as the risk of complications and additional damage to the joint. This results in an average 33% increase to healthcare costs (Nag and Banerjee, 2012). The annual global cost of revision surgery exceeds $3billion (Bourne et al., 2004). There are several reasons why primary THRs fail or need revision. The main reasons and their relative frequency are presented in **Table 2.1**.

Table 2.1: Indications for revision THR in Swedish Hip Register (Malchau et al., 2002)

Reason	Number	Percentage (%)
Aseptic loosening	10,610	75
Deep joint infection	948	7
Dislocation	810	6
Fracture	716	5
Technical error	425	3
Implant fracture	215	1
Other	357	3

Total hip replacements can fail due to a range of reasons. **Table 2.1** shows the relative frequency of a variety of failure mechanisms for patients in the Swedish Hip Registry who had primary THRs.

These failure modes occur due to several problems. The prostheses can become infected during the operation or follow-up or the hip can fracture (though this is rare following primary THR). Dislocations can occur if the THR is improperly aligned *in vivo* or improperly managed during follow-up, and poor design or size choice can cause mechanical loosening to occur. However, the most common form of failure, and hence revision surgery, is aseptic loosening.

2.2.3 Aseptic loosening

Aseptic loosening can be caused by inadequate initial fixation, poor mechanical bonding, or inadequate biologic fixation due to osteolysis from wear particles. It generally affects patients between 10 and 20 years after their initial joint replacement procedure. Repeated

wear of THR materials can generate wear debris that causes osteolysis and the resorption of bone (Abu-Amer et al., 2007). Although wear debris is created primarily from the articular surface (at the moving surface around the ball of the joint), the quality of initial implant fixation is also critical in enabling aseptic loosening.

Implant fixation is dependent on the interface between the implant and the living tissue. The method of fixation (cement or coatings), and the texture and shape of the implant all affect how quickly and strongly the implant is fixed in the body. This means the choice and quality of implant fixation is a key to the long-term effectiveness of the implant. Modifying the tissue-implant interface to enable improved initial and long-term fixation will further results in the success of THR in orthopaedic medicine.

2.2.4 Surface modification at the implant-tissue interface

The interaction at the tissue-implant interface is critical in influencing biological response and long-term success of medical implants in the body. Load bearing joint prostheses require the bulk mechanical properties of titanium alloys (high yield strength, high tensile strength, resistance to creep deformation and cyclic loading) (Wang, 2009, Paital and Dahotre, 2009). Modifying the surface composition can increase osteoconductivity, enabling direct biological fixation, enhanced cell adhesion, accelerated cell attatchment, extended functional service life, minimised fixation times and reduced aseptic loosening (Wang et al., 2011).

The ability to pattern of bioactive materials onto the surface of metallic orthopaedic implants is a crucial feature in influencing cell response, orientation and growth (Wang, 2009, Munir et al., 2011). Initial cellular response has been shown to have considerable influence on tissue regeneration, and the orientation of the cells attaching onto the implant

significantly affect the structure of resultant tissue. For instance, increased scar tissue formation was observed when the cells attached onto an implant in a random manner during wound healing (Monsees et al., 2005).

2.3 Biomaterials

Any material that, when implanted into a human body, will elicit a biological response over time (Hench, 1991). Biomaterials are materials specifically designed to do so in a way that aids the regeneration and repair of living tissue without adverse effect. There are four types of biological responses to implants in contact with living tissue in the body (Hench, 1998):

1. If the material is toxic, the surrounding tissue will die.
2. If the material is nontoxic and biologically inactive (almost inert), a fibrous tissue of variable thickness will form around it.
3. If the material is nontoxic and biologically active (bioactive), an interfacial bond will form.
4. If the material is nontoxic and degrades, the surrounding tissues grow to replace it.

As such, biomaterials are classified into bioinert (where there is no direct chemical interaction between the material and the tissue), bioactive (where there is a direct chemical bond) and biodegradable (where the material degrades into the body over time and the host tissue ideally regenerates at a similar rate).

2.3.1 Biomaterial requirements of orthopaedic coatings

When manufacturing novel techniques for the coating metallic implants for orthopaedic applications, the following properties are required (Dearnley, 1999).

i.) Biocompatibility

Coatings must be non-toxic and integrate into the biological environment without rejection or adverse effect.

ii.) Architecture

Coating microstructure must facilitate the attachment, orientation and proliferation of cells. The tissues must be vascularised in such a way that nutrients and waste can be transported to and from cells.

iii.) Mechanical and chemical properties

The mechanical (such as attachment and load bearing properties) and chemical properties (specifically pertaining to cell proliferation and metabolism) of the coatings must be able to support bone for full lifetime of the implant or until its need is fulfilled.

iv.) Resorption

The coating must resorb into the body at a controlled rate that is close to the rate at which cells are proliferating. Any dissolution products should be safely metabolised by the body.

v.) Secondary requirements

The coating process needs be economically viable, and able to meet clinical standards. The manufacturing process should be cost-effective, simple, repeatable and scale-able. Coatings should encourage a strong interface with the host tissue.

2.3.2 Ideal coatings for orthopaedic implants

Ideal coatings on metallic implants should have strong cohesive strength and substrate adhesion, a high degree of material purity and phase stability (Tsui et al., 1998). Coating thickness also affects strength. It has been found that coatings >100µm may be susceptible to fatigue fractures, and coatings <30µm may resorb too quickly and produce a weak bond. An ideal thickness 50-75µm would avoid fatigue failure but have consistent apposition (Jaffe and Scott, 1996).

Coatings also need to be optimised in terms of adhesion strength, phase stability, surface roughness and thickness amongst others measures. If there is insufficient tensile strength for example, cracking can occur, compromising the attachment of the implant and causing failure. Roughness and porosity should be optimised to encourage cell bioactivity and attachment, but not reduce the adhesion of the coating.

The bioengineering task is to effectively and efficiently coat the surface of metallic load bearing joint prostheses with bioactive materials to enhance direct biological fixation and extend functional service life. This means shorter recovery times and fewer revision surgeries for patients.

2.4 Metallic implant materials

Metallic implant materials such as titanium, titanium alloys and 316L stainless steel have been widely used in load bearing orthopaedic and dental implants for many decades. This is primarily due to their mechanical properties and corrosion resistance *in vivo*. Titanium metals have relatively low elastic moduli, which minimises areas of high stress concentration between the implant and the living tissue (Kutz, 2003). They are also more machinable and formable when compared to stainless steels and cobalt-based alloys. However, they do have a high coefficient of friction when in contact with bone tissue, and are also relatively bioinert due to the oxide layer that forms at their surface *in vivo*. This means that they cannot form a direct bond with living tissue. This is necessary for long-term stability. Therefore, surface modifications such as coatings have been applied to metal implants to improve tissue interactions and circumvent this issue.

2.4.1 Titanium and titanium alloys

Commercially pure titanium and titanium alloy Ti_6Al_4V are currently the most widely used metallic implant material. This is primarily due to their biocompatibility (they form a bioinert oxide layer on their surface in the biological environment) and relatively low elastic moduli, which minimises stress concentrations between the implant and the tissue. This is especially in important load-bearing implant applications (Kutz, 2003). These metals are also highly machinable and formable, which is important in manufacturing, and have good fatigue strength and corrosion resistance *in vivo* (generally relative to stainless steels and cobalt-based metallic alloys).

There are some drawbacks however. Both titanium and its alloys have a high coefficient of friction in tribological applications, which can cause wear particles to form. The fine oxide

layer that improves their compatibility also inhibits their ability to bond directly to organic bone tissue. Together this compromises the long-term stability of the orthopaedic implants in which they feature. A current aim of orthopaedic implant technology is the make implants that have greater long-term stability, to reduce the frequency of revision surgeries. Improving the osteointegration on the surface of such implants would improve direct biological fixation, and the functional service life of the implant (Sebbowa et al., 2011).

The titanium alloy Ti_6Al_7Nb has improved corrosion resistance due to the presence of niobium (Nb). Nb increases how thermodynamically and kinetically stable titanium is within the alloy. It is sometimes used in preference to Ti_6Al_4V dues to the absence of vanadium (V), which has been found to be cytotoxic when tested in isolation (Krzakala et al., 2013).

The titanium alloy $Ti_{78.8}Mo_{16}Nb_3Al_3SiO_{0.2}$ also exhibits high corrosion resistance and is relatively light compared to its strength. It also lacks vanadium. The presence of silicon dioxide is beneficial in orthopaedic applications, as some studies have found silicon to support bioactivity and the formation and growth of bone tissue (Xiao et al., 2009). When incorporated into hydroxyapatite, silicon has also been found to act as a calcifying agent, increasing the proliferation rate of bone cells and improving cell attachment to implants both *in vitro* and *in vivo*.

Ti_6Al_4V is the most commonly used titanium alloy. This alloy has higher ultimate tensile strength, fatigue limit and corrosion resistance. It is biocompatible and supports osteointegration (Mansur et al., 2013). Despite the presence of vanadium (V), it has been found to be safe when used in this context due to nitric passivation pre-processing. The procedure involves etching with nitric acid to increase in the surface area of the implant, then sand-blasting to remove any particle remnants (Velasco-Ortega et al., 2010).

2.4.2 316L stainless steel

Steels that contain >12% of the element chromium are referred to as stainless steels. Chromium increases corrosion resistance in many steel types, as it encourages the formation of an oxide layer that is more chemically stable. 316L stainless steel is the most commonly used stainless steel in medical implant applications. This is mainly due to high corrosion resistance (which is due to the oxide layer that forms on its surface and the addition of molybdenum to the alloy), high ultimate tensile strength (465-950MPa) and Young's modulus (200GPa) (Long and Rack, 1998). Economically, this 316L is also much cheaper (up to a fifth of the price) than other typical metallic biomaterials, and it is also easier to process. Conversely, the elastic modulus of this metal is much higher than that of cortical bone, which can result in stress shielding and the loosening of the implant over time. Also, in areas of the body where there is insufficient oxygen to maintain the oxide layer on the metal's surface, corrosion and some nickel toxicity is also possible. Wear resistance can also be improved by laser surface treatments (Popa et al., 2011). The application of bioactive coatings encourages osteointegration, improves corrosion resistance and minimises wear (Xiao et al., 2009).

2.4.3 Cobalt-chromium alloys

The benefits of using cobalt-based alloys over stainless steels lie in its improved corrosion resistance, wear properties, tensile strength and compressive strength. Common alloys include Co-Cr-Mo alloy and Co-Ni-Nr-Mo alloys. These are modifications of the alloy vitallium, which was the first cobalt-based alloy used in orthopaedics. The main drawback from the use of these alloys is the potential for the release of chromium, a possible carcinogen (Black and Hastings, 1998). This drawback is being overcome via improved processing of this alloy and the development of replacement alloys.

2.5 Ceramics

Ceramics are polycrystalline, refractory materials that are generally brittle and hard with have good compressive strength. Bioceramics are ceramics that are designed to support the repair and regeneration of biological tissues and/or organs. Ceramics that are biodegradable are called apatites, and are usually calcium phosphates. Bioceramics can vary a great deal. They can be amorphous or crystalline, dense or porous, and synthetic or natural.
Ceramic coatings can be successfully applied via vacuum plasma spraying due to their high melting points. However, if the coating process temperature could be reduced to ambient temperature conditions, a greater range of materials could be used including biodegradable polymers and ceramic-polymer composites.

2.5.1 Bioceramics

Typical coatings for metallic orthopaedic implants are HA bioceramic coatings. These have been used successfully in orthopaedic applications for several decades (De Groot et al., 1998). HA forms the inorganic constituent of human bone, therefore applying it to the implant surface improves biological response *in vivo* (Thian et al., 2010). Its chemical formula is $Ca_{10}[PO_4]_6[OH]_2$, and it has a calcium-to-phosphate ratio of 1.67, a ratio closest to the natural calcium apatites found in bone. The mechanical behaviour of HA is acceptable when under low-load conditions and it exhibits excellent biocompatibility, although it degrades slowly *in vivo* (Paital and Dahotre, 2009).

The literature shows that applying a patterned layer of TiO_2 (titania) before applying HA significantly improves interfacial adhesion, therefore the TAEA application of both TiO_2 and HA on curved titanium substrate should be investigated (Kim et al., 2004, Lin and Yen, 2005). In order to create titanium dioxide coatings, titanium isopropoxide needs to be

hydrolysed. This can be carried out using distilled water or ethanol, but ethanol was chosen due to its electrical and spray properties (Li et al., 2008).

TiO_2 (titania) coatings have found to improve the corrosion resistance of titanium substrates (the thicker the coating the greater the resistance (Cabrini et al., 1997)) and thus their functionality in load-bearing orthopaedic applications (Kurzweg et al., 1998). The outer HA layer enhances the bioactivity and osteoconductivity initially, and the inner TiO_2 layer prevents the titanium substrate from corroding, even after the HA layer has completely resorbed into the body. The titania pattern interlocks with the HA coating on the titanium (Ti) substrate, and improves mechanical strength and chemical bonding, thus clinical functionality.

2.5.2 Calcium phosphates

Calcium phosphates are a family of mineral bioceramics that primarily contain calcium ions, and various phosphates. These materials make up the majority of the inorganic material of bone and are able to bond directly with this tissue. Thus, they are used widely in orthopaedic engineering. Notable calcium phosphates include hydroxyapatite (HA), which is widely used. Tricalcium phosphate (TCP) $Ca_3(PO_4)_2$ has a Ca:P ratio of 1.5, and is used due to its high biocompatibility, osteoconductivity and versatility. Studies have shown that the addition of manganese ions can improve surface bonding of implants with tissues. Due to the brittle nature of ceramics, only tin films are applied onto metallic surfaces, so as to utilise the bulk properties of the metallic substrates. It should also be noted that when the calcium-to-phosphorus ratio is lower, increase acidity and water-solubility is observed (Legeros, 1993). There are only two forms of calcium phosphate that are stable *in vivo* (i.e. at body temperature 37°C): below pH 4.2 that phase is dicalcium phosphate ($CaHPO_42H_2O$), and above pH4.3, the phase is HA.

2.5.3 Hydroxyapatite

Hydroxyapatite ($Ca_{10}(PO_4)_6(OH)_2$) (HA) is highly biocompatible and osteoconductive ceramic. It has a hexagonal crystalline lattice structure. Its network of phosphate groups give HA its stability (Elliott and Young, 1967). It has an elastic modulus of around 20GPa.

At high temperatures, HA decomposes to phases of other calcium phosphates. At around 1000-1360°C, OH^- ions are lost in a process called dehydroxylation, and the HA converts into oxyhydroxyapatite (OHA) then oxyapatite (OAP). When the temperature reaches above 1360°C, OAP then converts into TCP (Posner et al., 1958). HA is therefore stable up to 1000°C, so processing should be kept below this temperature to avoid the presence of other calcium phosphates which are not as stable in the biological environment. HA has a lower dissolution rate that other calcium phosphates such as TCP and OHA.

HA is used primarily for non-load bearing applications due to its low fracture toughness of 0.9 - 1.3 $MPa.m^{0.5}$. By comparison, compact bone has a fracture toughness around 2 – 12 $MPa.m^{0.5}$ (Behiri and Bonfield, 1984). Additionally, the Weibull modulus (*n*), which measures the variability in material strength of brittle materials such as ceramics, is low (*n* = 5-12) in wet environments such as *in vivo* (Suchanek and Yoshimura, 1998). This means it can be unreliable for use in load bearing implants. For THRs, the combination of HA's biological properties suits the mechanical and load bearing properties of bulk materials such as metals.

HA is usually produced in two ways: wet methods such as precipitation, hydrothermal techniques and hydrolysis of calcium phosphates, and solid state reactions (Okayama et al., 1991). Each technique yields HA with different morphologies, stoichiometries and levels of crystallinity. For example, the precipitation wet technique can occur below 100°C and produce nano-sized HA crystals in various shapes (needles, rods, particles), whilst solid state

reactions usually produce well-crystallised stoichiometric HA with low sinterability, but require long heat treatment times and high temperatures.

HA provides the bonding interface between a coated metallic implant and the tissues in the biological environment. This is because the HA phase is structurally and chemically similar to the mineral phase in bone, resulting in interfacial bonding (Hench, 1991). This is believed to occur through two processes that occur simultaneously. Firstly, bone cells, and thus bone tissue, grows into the HA layer and mechanically locks into the implant onto which it is laid. Secondly, a dissolution/precipitation reaction occurs reciprocally at the tissue-implant interface by calcium, hydroxide and phosphate ions. Ions from body fluid get deposited on both the coating and the bone, resulting in biological fixation (Sergo et al., 1997).

2.6 Polymers

Polymers are a versatile type of biomaterials due to the range of physical and mechanical properties that they can exhibit to match those required for different biological environments. Polymers are widely used biomaterials, thus a natural progression of work on TAEA (Balasundaram and Webster, 2006). Polymer TAEA has potential applications in joint prosthesis coatings, scaffolds for hard and soft tissue engineering, low wear interfaces, orthopaedic fixation tools (Ciccone et al., 2001). Bioactive polymer coatings have exhibited bone-bonding properties and cell-mediated osteogenesis comparable with that of hydroxyapatite and other calcium-phosphate coatings (Heimke and Griss, 1980). Results from stress-analysis studies also suggest that a polymer coating and its associated flexibility, may have mechanical advantages compared with traditional ceramic coatings which are more brittle (De Groot et al., 1993).

Polyurethane (PU) is widely used in bioengineering due to its excellent mechanical properties (Chen et al., 2008). Polymethylsilsesquioxane (PMSQ) is used in this work as it can be converted directly to silicon oxycarbide (a ceramic) via a pyrolysis reaction (Ma et al., 2002). PMSQ is a biocompatible polymer with good slip properties (Luo et al., 2010). Most recently, biopolymers have been developed to demonstrate the bioactivity, biocompatibility and mechanical strength required in over a specific time frame.

2.6.1 Biodegradable polymers

Biodegradable polymers degrade into metabolites normally found *in vivo* and can be completely eliminated by the body safely. The degradation products of biodegradable polymers should be non-toxic, the mechanical properties suitable, and the rate of degradation should match the required application (Velema and Kaplan, 2006). The main benefit of using biodegradable polymers (rather than biostable polymers that do no degrade *in vivo*) is that a second surgery is not required to remove the implant once its mechanical and chemical use has been fulfilled. Also, the long-term biocompatibility concerns are alleviated as they can be completely degraded and metabolised at a controllable time. Stress-shielding associated with metallic implant materials can be circumvented by using biodegradable polymers that slowly transfer the load as it degrades.

In addition to their mechanical properties, polymers have the scope to provide drug-delivery capabilities, where medications can be delivered intact to the implant-tissue interface via a polymer that can control its administration (Panyam and Labhasetwar, 2003). Biodegradable polymers are an ideal material for drug-delivery carriers. They have been observed to enhance drug-targeting specificity, lower systemic drug toxicity, improve treatment absorption rates and protect pharmaceuticals from biochemically degrading (Reed and Gilding, 1981). Polyesters like poly(lactic acid) (PLA), poly (lactic-co-glycolic acid) (PLGA) and

poly(ε-caprolactone) (PCL) are generally considered the most suitable biodegradable polymers as they have low toxicity and immunogenicity. Mechanical properties can also be controlled by varying molecular weight and functionalisation (Anderson and Shive, 1997).

Biodegradable polymers can be derived naturally or synthetically. Natural polymers can exhibit good biocompatibility, unique mechanical properties due to their structures, and can degrade via enzymes or hydrolysis. However, they can be difficult to source reliably, may pose risks associated with viral infection, natural variations in material properties and antigenicity (Barbucci, 2002). However, synthetic polymers are highly reproducible, eliminating supply issues with natural polymers, and their structures are highly controllable.

PCL is a preferred choice as a drug delivery carrier as small drug molecules easily diffuse into the polymer, it does not create an acidic environment when degrading *in vivo*, and it blends well with other polymers. It also has a slower degradation rate than PLGA which makes it a more appropriate choice for long-term drug delivery systems (>1year) (Aberturas et al., 2002).

2.7 Ceramic-polymer composites

Ceramic-polymer bioactive composites can be developed to combine the ideal properties of each component and to optimise the biological and mechanical properties required for orthopaedic applications (Bonfield, 1988). The application of ceramics to reinforce biodegradable polymers is carried out to improve the mechanical and biological properties of both compared to pure polymers and pure ceramics (Ignatius et al., 2001, Kim et al., 2005, Qiu et al., 2007, Ural et al., 2000). Ceramic-polymer composite coatings may improve the mechanical properties of pure bioceramic, such as HA, by releasing the residual stresses

present within them (Garcia-Alonso et al., 2012), and bioresorbable polymers such as PCL may also enhance the coatings' biological behaviour. However, due to differing thermal properties, there is a major challenge associated with spraying ceramic and polymeric materials together (Ural et al., 2000). TAEA spraying is an ambient temperature process, so has potential to overcome this challenge.

'Sandwich' coatings may also improve performance of orthopaedic implant coatings. A deeper layer of HA can be applied to the implant with surface layer of a more rapidly dissolving bioactive polymer coating on top. This has resulted in improved initial osteointegration and long-term stability (Jaffe and Scott, 1996).

2.8 Current coating techniques

There are several technologies that have been developed to apply bioactive coatings on metallic implant materials. This is due to the marked improvement of coated implants in terms of biocompatibility, bioactivity, cell attachment, service life, corrosion resistance and many other parameters when compare to un-coated metallic implants used for load-bearing orthopaedic applications. Overall, the surface modification of traditional orthopaedic implants improves the biological interactions of the implant *in vivo*, reducing recovery times for patients and increasing overall service life. These coating techniques can be broadly split into three different types: wet techniques, physical vapour techniques and spray techniques. Each produces coatings specific to their manufacturing method. **Table 2.2** presents a summary of some of the main techniques, and the advantages and disadvantages of each. They are discussed in more detail later in the chapter.

Table 2.2: Coating techniques employed to coat metallic implants with bioceramics

Coating technique	Method	Advantages	Disadvantages
Sol-gel deposition (Gross et al., 1998)	A homogeneous precursor metallic solution (sol) is deposited onto the substrate and undergoes hydrolysis (breaks down molecule due to reaction with water). This produces a hydrated metal oxide gel that is dried and sintered.	Good for glass and ceramic thin films (coatings very thin at <1µm). Can coat complex substrate geometries. Dense coatings	High degree of process control required. Precursor solutions are expensive. Limited thicknesses can be achieved. Wet technique.
Biomimetic deposition (Tanahashi et al., 1994)	Metallic substrates are immersed in a simulated body fluid (SBF) to promote the development of calcium apatites (much like bone).	Low cost and simple technique. Not limited by complex geometry. High temperatures not required. Coating thickness <35µm.	Very low deposition rate. Difficult to regulate SBF composition and pH. Limits on substrate materials. Wet technique.
Electrophoretic deposition (EPD) (Wei et al., 1999)	The substrate is a charged electrode and is immersed in coating particles/ions that are oppositely charged in suspension, therefore get deposited on the substrate surface.	Simple, low cost process, suitable for complex geometries. Coating thickness 25-35µm.	Require fine coating powder particles (nano-sized). Coating prone to cracking. Low deposition rate. Low bond strength. Wet technique.

Vacuum plasma spraying (VPS)(Gledhill et al., 1999)	In a vacuum, a direct current electric arc is created between two electrodes. This turns a stream of gas into plasma across it (~15000°C) at a speed of <400 $m.s^{-1}$. The coating powder (metal or ceramic) is fed into the plasma, which softens and is directed to the substrates. On contact, it cools and solidifies to create a coating.	High deposition rate, good adhesion, dense coatings, can spray ceramics of metals. Current industry standard method of coating metallic THRs with ceramic coatings.	Expensive technique due to vacuum environment and high temperatures. Thick coatings of 50-200µm. Cumbersome equipment. Limited batch size. Requires grit-blasting pre-treatment. Cannot pattern coatings.

2.9 Wet deposition techniques

Wet techniques involve immersing the substrate in an aqueous medium over time, and therefore require relatively low temperatures and compared to thermal methods. This also has the added benefit of reducing manufacturing costs. The three main types of wet coating techniques are sol-gel deposition, biomimetic deposition and electrophoretic deposition.

2.9.1 Sol-gel deposition

Sol-gel deposition is a versatile, low temperature process. A sol-gel is a material where solid colloidal particles are distributed within a gel. This deposition process was first developed when a silicon alkoxide solution converted into a transparent solid in a humid environment,

and when heat was then applied, formed silicon dioxide (Reuter, 1991). Now it is commonly used to manufacture ceramic thin films and glasses.

The three main processing steps are:

1. Preparation of a homogenous precursor metal solution.
2. Deposition and hydrolysis of sol onto the substrate forming a gel of hydrated metal oxide.
3. Drying, compacting and sintering the resultant gel to produce a ceramic/glass at lower temperatures.

For bioceramic coatings, the original solution must contain the ceramic elements required, and post drying and compacting, the material must be sintered to remove any organic materials. Resultant coatings are dense, stable, and have good adhesive properties. Their purity is limited by the purity and homogeneity of the materials making up the precursor solution (which can drive up cost), and the whole process relies on the strict control of all processing parameters. Complex three-dimensional geometries can be coated via this method.

Dipping deposition is a process that developed out of sol-gel deposition, and is particularly suited to coating orthopaedic implants. It has a higher deposition rate and can cope with more complex geometries. However, thicker coatings are susceptible to cracking and delamination.

2.9.2 Biomimetic deposition (BMD)

Biomimetic deposition (BMD) is where the substrate is submerged into simulated body fluid (SBF) supersaturated in coating apatite. The temperature is kept at 37°C for several days. Apatite crystals then nucleate on the surface of the substrate, creating the coating. The process is called biomimetic deposition because the apatite crystals of the coating have been observed to be similar to natural bone apatites in terms of composition and crystallinity. This simple process is possible at ambient temperatures and can be used to coat complex geometries (Liu et al., 2006). Drawbacks include the constant monitoring of pH and replenishing of SBF over the several days that the coating is being carried out.

2.9.3 Electrophoretic deposition (EPD)

This process involves applying a low voltage electric field on the solution with the substrate acting as the electrode (see **Figure 2.5**). Ions in solution migrate to the electrode and create the coating. This means thick and thin coatings can be manufactured, but the substrate must be electrically conductive. The powder particles in suspension must be nanoparticles in order to be fine enough for this process to work. After coating, a densification process is also required via sintering. This comes with inherent risks of cracking and shrinkage. EPD is simple with low apparatus costs, and is capable of coating substrates with complex geometries as it is not a line-of-sight process.

2.10 Physical vapour deposition techniques

This type of process usually involve the following steps:

1. Boil or sublime a source material (for the coating) and create a vapour.
2. Transport the vapour towards the substrate.
3. Allow the vapour to condense onto the substrate surface creating a film/coating.

The three main physical vapour deposition techniques are magnetron sputtering, pulsed laser deposition (PLD) and ion beam sputtering (IBS), which are discussed in detail here.

2.10.1 Magnetron sputtering

Magnetron sputtering involves collecting atoms of a coating material onto a substrate that have been removed via ion bombardment. It can effectively produce coatings reproducibly, with a uniform thickness, constant apposition, good adhesion and with a high density (Kukla, 1997). **Figure 2.6** shows the system schematically.

Figure 2.6: Schematic diagram of a magnetron sputtering system

A substrate is placed into the sputtering chamber in which a working gas forms plasma. Atoms are deposited onto the substrate surface by the sputtering target. The greater the power input and lower the pressure, the greater the deposition rate. Limitations include non-uniformity of the coating surface and heat transfer to the substrate. The heat also limits the range of materials that can be used for coatings. Overall, the process has high operation and equipment costs.

2.10.2 Pulsed laser deposition (PLD)

In PLD, atoms of the coating material are ejected from its surface onto the substrate by pulses of a laser, and directed at the substrate surface (Jayadevan and Tseng, 2002). Generally, this process produces dense coatings with uniform morphology, at a stable deposition rate. Coatings have good adhesion but an overall low deposition rate.

2.10.3 Ion bean sputtering (IBS)

Ion beam sputtering (IBS) is another physical vapour technique. Here, an ion beam cleans the substrate whilst it is mounted on a rotating stage in a chamber of inert gas. It is then moved to the coating position where another ion bean knock atoms of the coating material and directs them onto the substrate. Again, coatings are dense but uniform and with good adhesion. The operation costs are high and the deposition rate is relative low, though stable (Ong et al., 2002).

2.11 Spraying techniques

Plasma spraying and vacuum plasma spraying are types of spraying techniques for coating orthopaedic implants. A novel technique, template-assisted electrohydrodynamic atomisation spraying will also be introduced here.

2.11.1 Plasma spraying

This coating technique is one of the most common methods used to make ceramic coating on metallic orthopaedic implants (Deram et al., 2003). A direct electric arc is created between two electrodes. When gas is passed through this arc it turns into a stream of plasma at speeds of 400m.s^{-1} and a temperatures around 20,000°C. The coating material is fed into this plasma stream in the form of a powder, and each particle softens due to the heat, so that when it collides with the substrate surface is cools and solidifies and hardens onto it, creating a coating.

Coatings produced by this method are usually dense and adhere well to the substrate, and are also uniform in their morphology. With this process, both the coating material and the substrate must be able to withstand the high temperatures involved.

2.11.2 Vacuum plasma spraying

Similar to plasma spraying, vacuum plasma spraying (VPS) involves injecting a coating powder (metal or ceramic between 10 and 50 microns in particle diameter) into a hot gaseous plasma at around 15,000°C. This melts the powder particles and directs these now molten droplets onto the desired substrate at a high velocity, which builds to a coating. VPS is conducted in a vacuum environment. This is shown in **Figure 2.7**. The spray environment is evacuated of air and filled with an inert gas, which is kept at a low pressure of around

100MBar. The vacuum environment minimises the risk of oxidation or the uptake of nitrogen, especially at high temperatures, which could affect the phase stability of the coatings. The coating particles also collide with the substrate with greater energy, as they are not hindered by friction and energy losses when travelling towards the target, so coatings are more dense. This enables VPS coatings to be almost 100% dense and with improved adhesion to ordinary plasma spraying (Davis, 2004).

Figure 2.7: Schematic diagram of vacuum plasma spraying (Gledhill et al., 1999)

It is common for a grit-blasting pre-treatment to be carried out on metallic substrates for orthopaedic implants before ceramic coating in order to roughen the surface and improve adhesion between the coating and the metal substrate.

Thick (40µm) and dense HA coatings have previously been produced on titanium via VPS by (Gledhill et al., 1999). These coatings exhibited good adhesion with the substrate, no visible cracks through its thickness, but there was evidence of surface microcracks. The resultant coating also had lower levels of crystallinity compared to the original coating powder, reducing its stability *in vivo*. When applying much thicker calcium phosphate coatings of

500µm on titanium, Tsui et al. found that more HA decomposed into different phases as crystallinity increased, and porosity decreased. Microcracking was observed to reduce, increasing the interfacial adhesion (Tsui et al., 1998).

2.12 Template-assisted electrohydrodynamic atomisation (TAEA) spraying

Template-assisted electrohydrodynamic atomisation (TAEA) spraying is an adapted form of electrohydrodynamic deposition (EHD). Here, a liquid is subjected to an electric field as it passes through a needle, and under this electric field the droplets break up into smaller particles that settle onto the grounded substrate surface creating a coating. When the electric field is sufficiently high, and the meniscus of the liquid elongates and forms a cone shaped jet, the droplets have a relatively uniform size distribution in the micro- and nanometre scale. This creates homogenous and even coatings with very good adhesion to the substrate at ambient temperature. When combined with templating, EHD becomes even more powerful. Highly specific, repeatable topographies can be produced with geometric features just a few micrometres in size.

Zeleny first developed the electrohydrodynamic process, from which TAEA was adapted, over one hundred years ago. A high voltage was applied to a needle with a liquid passing through it onto a ground electrode (Zeleny, 1914). Fifty years later, though the work of Taylor, the mechanisms by which particles formed from the jet was better understood (Taylor, 1964). This work showed that the conical formation of the liquid meniscus as it exits the needles, was obtained when the applied electric field and the surface tension of the conducting liquid were in equilibrium. The geometry of the conical shape was also analysed and it was found to have a sharp apex at a semi-vertical angle at 49.3° so that this equilibrium can be achieved. This formation is now referred to as the Taylor cone, and is

formed during stable cone jetting during electrohydrodynamic (EHD) spraying. Once this was established, EHD was further investigated as a processing technique, thus the parameters that affect jetting were also established. Jones and Thong found that the size of the spray droplets was mainly attributed to liquid flow rate (Jones and Thong, 1971). Another study found that the liquid required electrical conductivity between specific limits to achieve stable cone jetting (Mutoh et al., 1979), and droplet diameter can be reduced by increasing applied voltage and varying the physical properties of the liquid such as surface tension, electrical conductivity, density and viscosity (Smith, 1986).

The functional modes of electrohydrodynamic spraying were classified by Cloupeau and Prunetfoch, and are discussed in detail later in the chapter (Cloupeau and Prunetfoch, 1990). It was found that when the physical properties of the liquid and its flow rate are kept constant, variations in applied voltage can be detected visually through the shape of the liquid meniscus as it exits the needle, and the size and distribution of the resultant droplets. Jaworek and Krupa further characterised these modes and suggested EHD as a deposition technique for biomedical implant applications (Jaworek and Krupa, 1999).

Template-assisted electrohydrodynamic atomisation (TAEA) spraying uses ground electrode configurations and templates with electrohydrodynamic atomisation (Leeuwenburgh et al., 2006) to deposit well-defined patterns on a substrate surface. The process consists of a nozzle (needle) that is connected to a high voltage supply and a ground electrode. A suspension or solution containing the desired coating material fed through the nozzle at a controlled flow rate through a syringe pump. This simple set-up is shown schematically in **Figure 2.8**.

Figure 2.8: TAEA equipment set-up

A copper template with the desired pattern is placed over the ground substrate. The electric field created between the nozzle (electrode) and the substrate, forms a liquid jet from the needle. This breaks up into smaller droplets as the applied voltage increases, and it eventually breaks up into fine and uniform droplets in the nano- or micro-metre scale (Jaworek and Krupa, 1999). The spray collects on the grounded substrate and template to produce a fine coating that can be easily controlled by varying process parameters such as flow rate and applied voltage. After coating, the solvent evaporates away and the template can be removed, leaving the inverted template pattern on the substrate. The templating process is described in detail in Chapter 3. TAEA has the potential to circumvent the inherent limitations of the coating techniques discussed in this chapter. The later sections of this chapter discuss this process in more detail.

2.12.1 TAEA vs. vacuum plasma spraying

The current industry standard for manufacturing coatings on metallic implants is vacuum plasma spraying (VPS). VPS is capable of producing adequate coatings commercially, but there are several inherent limitations that prevent further optimisation such as improved

quality and biological fixation, and their associated increase in functional service life and faster healing (Cheang and Khor, 1996).

VPS requires high temperatures (~15,000°C), which means it cannot incorporate biological agents such as growth factors, antibiotics and proteins into the coating as it is being manufactured. These agents would deteriorate when subjected to the heat. VPS ceramic coatings are also not patterned, so cannot exploit the observed control and guidance of primary human osteoblast cells onto controlled HA topographies on titanium substrates (Munir et al., 2011). VPS coatings are relatively thick (50-200µm), thus have the associated problems of variations in bond strength, non-uniformity of coating density, and microcracks from a grit-blasting pre-treatment. These can introduce defects that serve as crack initiators *in vivo*, shortening function service life (Liu et al., 2004). The VPS process also requires very high temperatures and a vacuum environment, which is highly energy intensive with high equipment and operational costs. Circumventing these issues could greatly improve the functionality, cost and service life of orthopaedic implants.

There is potential for template assisted electrohydrodynamic atomisation (TAEA) spraying, a novel ambient temperature patterning technique invented at UCL (Li et al., 2008), to be an improved coating method compared to the current industry standard of VPS. The reduction in temperature results in an increase in the range of coating materials (such as polymers) and the ability to incorporate biological agents during manufacturing. This highly controllable process could produce coatings with an ideal thickness, improves uniformity and homogeneity, and improved bond strength.

A wide variety of predetermined topographies with a range of geometries can also be achieved with a high degree of control (Li et al., 2011). Printing patterns can result in much more favourable biological response than depositing a continuous coating (Huang et al.,

2004). The simple set up and lower energy requirements result in a larger commercially viable batch size and reduced lead time (Ahmad et al., 2006).

2.12.2 Modes of electrohydrodynamic atomisation

Electrohydrodynamic jetting modes are characterised in two ways (Jaworek and Krupa, 1999). Firstly the shape of the liquid as it exits the needle, and secondly how the liquid breaks up into droplets. **Figure 2.9** shows the various jetting modes schematically. **Figure 2.10** shows the forces acting on the liquid jet when the potential difference across the needle and liquid is applied. **Figure 2.11** shows these modes visually during jetting.

Figure 2.9: TAEA jetting modes (Jaworek and Krupa, 1999)

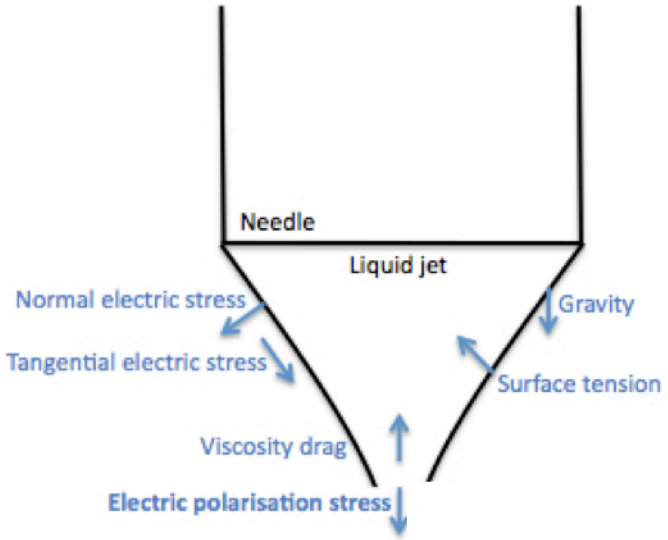

Figure 2.10: Forces acting on the liquid jet during TAEA

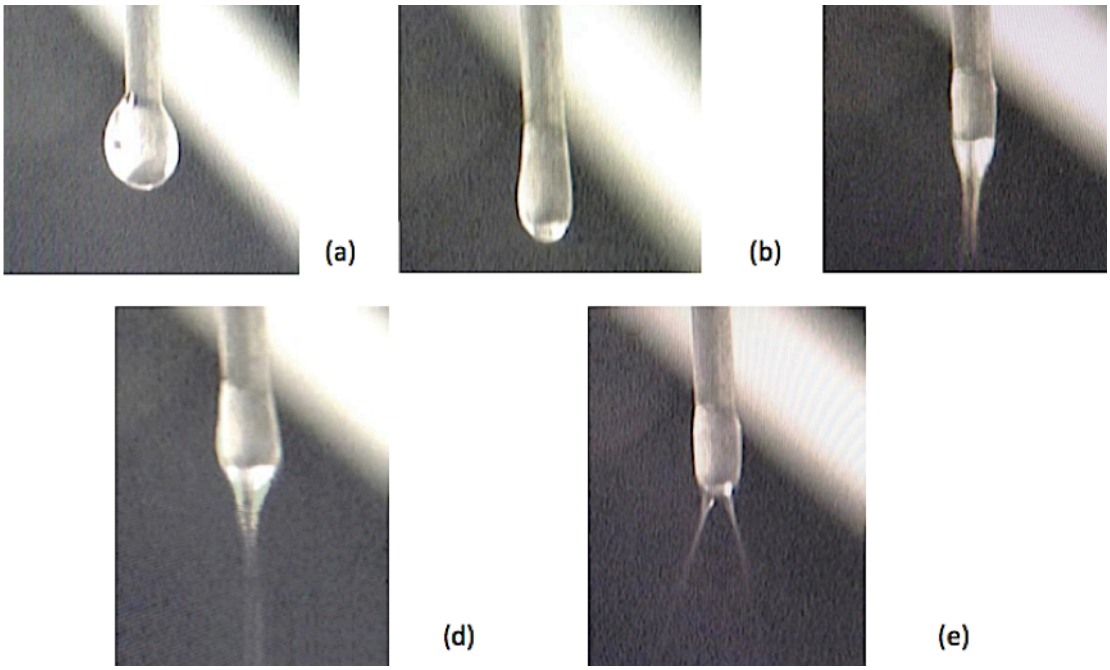

Figure 2.11: The geometry of the liquid (6wt.% TiO_2 in ethanol) at the exit of the needle during the functional modes of EHD spraying. (a) Dripping mode (b) Micro-dripping mode (c) Unstable cone jet mode (d) Stable cone jet mode (e) Multi-jet mode

The dripping mode is obtained at zero to low applied voltage. The drops are spherical in shape as they detach from the needle under gravity. The gravitational and electric force overcomes the surface tension of the liquid and the droplet forms (Cloupeau and Prunetfoch, 1990). Once the droplet detaches from the jet, the liquid meniscus contracts back towards the needle to a curved, hemispherical shape before increasing in size again to form the next droplet. The time taken to form a droplet is much longer than the time taken for the droplet to fall, therefore the charge of the former droplet itself does not affect the formation of the next droplet. When the processing parameters are constant, the rate of droplet emission and droplet size is also constant. No additional smaller droplets form when the main droplet breaks off and the meniscus retracts. These smaller secondary droplets are

known as satellite droplets, and can be minimised by spraying within the applied voltage range for stable cone-jetting, which is specific to the coating material and processing parameters.

As the applied voltage increases, the meniscus of the liquid as it exits the needles elongates and the droplets become smaller. They also form and detach at a higher frequency. This is because the surface tension of the liquid decreases as the electric field goes up. The electric stress on the surface causes the electrostatic pressure to act in the opposite direction to the capillary pressure, attracting the droplet towards the substrate, i.e. away from the needle. When the droplet does detach, the meniscus retracts back towards the needle exit. When the voltage and other parameters are kept constant, the size and regularity of the drops also remains constant (Cloupeau and Prunetfoch, 1990).

The mode is described as micro-dripping when the voltage is increased to the point where the liquid meniscus does not contract back towards the needle exit after the droplet detaches. This is compounded by the increasing charge of detaching droplets. The droplets are smaller in this mode as the electric field is greater, and droplet emission is no longer regular.

The unstable cone jet mode is obtained when the voltage increases more and the droplets become more frequent and irregular. The liquid meniscus and the droplets are elongated towards the grounded substrate, so the shape can be referred to as a jet. It is not continuous, however, and flickers between droplets of varying sizes (generally 300-1000µm) and a continuous jet (Jaworek and Krupa, 1999). This is why the mode is called the unstable cone jet mode.

A stable cone jet is achieved when the voltage is again increased, and a regular, constant jet is formed at the needle exit at the end of a spherical cone (Taylor cone). A thin (10-100μm) continuous jet extends from it for a few millimetres, before detaching into very fine particles. At this point of detachment, the jet is subject to two types of instability. Varicose instabilities cause waves on the surface of jet, whilst kink instabilities cause the jet to move away from the axis of the needle, thus droplets detach due to electrical and inertial forces. At the point of detachment, the electric stress and surface tension are equal. This mode is most stable as the droplets are smaller and more homogenous than for other modes. It is most suitable for deposition because the spray forms a cone shape of around 50-60° to deposit the coating onto the substrate, and the particles are attracted to the grounded substrate. This means that TAEA in the cone jet mode is not a line-of-sight process.

When the voltage is increased beyond the stable cone jet mode, the multi-jet mode is obtained. Here, the increased charge on the surface of the Taylor cone causes its depth and jet diameter to reduce skew, causing the jet to point away from the needle. Several jets with short cones will form due to the instability of the now flattened meniscus, and their direction can change. The particles produces have a much larger size distribution. Small droplets form due to kink instabilities in the surface of the jets, and a fine mist forms around them. The spray is not homogenously scattered in a cone as before, but is rather concentrated in the direction of the multiple jets. As the voltage keeps increasing, so does the number of jets. Each additional jet narrows as the shear stresses between the jets increase. The particles have a greater size distribution than those produced in the stable cone jet mode (Jaworek and Krupa, 1999).

2.13 Mechanism of the electrohydrodynamic stable cone jet mode

The geometry of the jet and the resultant droplets that are sprayed are dependant on the jetting mode that is achieved by the particular applied voltage (Jaworek and Krupa, 1999). The steadiest mode of spraying, and the mode that produces the finest and most uniform droplets, is called the cone jet mode. These droplets are just a few micrometres in diameter (Hartman et al., 2000).

The spray is created from the jet as the spray media is accelerated from the needle and a cone forms. Its velocity is dependant on the flow rate that the infusion pump delivers spray media to the needle. The geometry and stability of the cone is dependant on parameters such as the velocity and pressure of the media liquid, its surface tension and viscosity, as well as electrical properties. From this cone, the media travels towards the grounded substrate in the form of a jet. The high voltage applied across the needle and spray media result in a highly charged jet that moves towards the grounded substrate. This jet breaks up into droplets with a droplet size distribution that is ideally small to create an even coating. These droplets then land on the substrate, and the solvent evaporates away to leave a coating.

The distance between the needle and the substrate also affects droplet size, as solvent can evaporate away in transit. This means greater collections distances result in smaller droplets and thinner coatings. Needle size also influences the velocity at which the spray media exit the needle, therefore the stability of the jet. The liquids also need to be electrically conductive enough, as the process is drive by an electric field through the liquid (Cloupeau and Prunetfoch, 1990).

The jet breaks up from the Taylor cone during EHD due to two reasons (Hartman et al., 1999). Firstly, some ions, atoms and droplets do separate from the jet due to small instabilities caused by the high applied voltage (Rulison and Flagan, 1994). The second reason is more common. It is because charges are conducted via charge convection at the tip of the Taylor cone. When the flow rate is too low, instabilities in the direction of flow are sufficient enough to break up the jet non-uniformly, so a stable cone jet is not possible. However, at higher flow rates, there is more current passing through the cone and the surface charge increases. Now it is only lateral instabilities (perpendicular to the direction of flow) that can affect the jet. As they do so, the size distribution of the droplets reduces and uniform coating in the stable cone jet is possible. This is why there is a specific 'window' for achieving a stable cone jet. The flow rate needs to be above a minimum value, and the voltage must be high enough to get a Taylor cone but not so high to split into a multi-jet.

2.14 Droplet evaporation

Some solvent evaporates as the particles travel from the needle towards the substrate. This can be significantly affected by the properties of the solvent and the environment (Wilhelm et al., 2003). The droplets created via stable cone jetting are highly charged. When their size decreases, a measure of charge called the Rayleigh limit can be reached. At this point the Rayleigh limit charge is below that of the original droplet, which can then split into smaller droplets and further reduce the average size of the particles.

The Rayleigh limit (Q_R measured in coulombs, C) can be calculated using the following equation:

$$Q_R=8\pi(\gamma\varepsilon_0 r_d^{\,3})^{0.5} \qquad \text{(equation 1)}$$

Where γ is the surface tension measured in Nm^{-1}, r_d is the radius of the droplet measured in m, and ε_0 is the constant $8.85 \times 10^{-12} Fm^{-1}$ (Rayleigh, 1978).

2.15 The effect of physical properties of the liquid to electrohydrodynamic spraying

Flow rate, applied voltage and other processing parameters affect whether a stable cone jet can be achieved. This section will discuss these effects so that they can be optimised in experimentation.

2.15.1 Electrical conductivity

TAEA is an electric-field assisted process, therefore the electrical conductivity of the spraying media is very important. It facilitates the stability of the cone jet and the size of the resultant droplets. The electric field passes through the liquid and affects the shape of the meniscus and the jet. If it is too low, insufficient charge will build up in the liquid and a cone jet will not form. The tangential stress cause by the applied charges would not be great enough (Cloupeau and Prunetfoch, 1990). If the conductivity is too high, however, some charge would discharge through the ions in the air and again, the stable cone jet will not form (Hartman et al., 2000).

2.15.2 Surface tension

The surface tension of the coating media is important because the surface tension has to be overcome by the electric stresses applied during TAEA to achieve a stable cone jet. This affects the size and shape of the resultant droplets. When the surface tension is high, more voltage needs to be applied to achieve the Taylor cone, and the risk of charge discharging through the air increases. Up to that point though, the higher the surface tension, the higher the required applied voltage (Smith, 1986).

2.15.3 Viscosity

Viscosity also plays an important role in the formation and break-up of the EHD jet. It also affects the size of the droplets, as when the viscosity increases, droplet size also increases. There are also fewer droplets caused by jet instability when the viscosity is higher. There are two main reasons for these observations. Firstly, the increased viscosity reduces the oscillations caused when a droplet detaches from the meniscus. Secondly, the increased viscosity causes the resultant droplets to be more spherical in shape, and the size of relics produced via EHD increases (Jayasinghe and Edirisinghe, 2002).

2.16 Controlling parameters of TAEA spraying

This chapter has outlined why key process parameters like flow rate, applied voltage and solution properties affect TAEA processing. Flow rate affects the speed at which the coating media exits the needle and therefore the necessary applied voltage for a stable cone jet, as well as droplet size (Jayasinghe et al., 2004). Applied voltage affects the strength of the electric field that drives the process. In this study, the influences of several key process parameters on TAEA spraying of various bioactive coating materials on different substrate geometries will be investigated. This includes flow rate, applied voltage, collection distance and collection time. The physical properties of the coating media will also be investigated to better understand how these affect the process and the resultant coatings and patterns. These were systematically varied to observe their effect on resultant coating microstructure.

3. Experimental Details

3.1 Materials

The main materials involved in this project are titanium dioxide (TiO_2), hydroxyapatite (HA) and polycaprolactone (PCL), of which the sol, suspension and solutions were prepared specifically and the preparation is described in Section 3.2. The solvents used for these preparations, as well as substrate materials such as titanium and stainless steel are introduced in detail here.

3.1.1 Coating materials

Titanium (IV) isopropoxide ($Ti[OCH(CH_3)_2]_4$) and hydroxyapatite (nanopowder, <200nm) was purchased from Sigma-Aldrich (Poole, UK). Polycaprolactone (Mw=14000 kDa) was also purchased from Sigma-Aldrich (Poole, UK). All reagents were of analytical grade and were used as received.

3.1.2 Substrate materials

3.1.2.1 Titanium

The flat titanium (Ti) substrates used in Chapters 5 and 6 for TAEA deposition were Grade 1 (ASTM F67) commercially pure Ti of 0.5 mm thickness, and were purchased from Advent Research Materials (Oxford, UK). The Ti plate was cut into individual 10 mm x 10 mm

squares. The curved titanium substrate used for deposition was Grade 1 (ASTM F67) commercially pure titanium tubing (Advent Research Materials, Oxford, UK) of 0.5mm thickness, which was cut lengthways to produce small curved plates which could have both the inner and outer surface prepared for coating. Convex (outer) diameter was 25.4mm and concave (inner) diameter was 23.6mm. The Ti plates were then polished using silicon carbide grinding papers (No.800, No.1200, No.2400 and No.4000). Prior to TAEA deposition, each plate was degreased with acetone and rinsed with the solvent used for deposition, and then air-dried.

3.1.2.2 Titanium alloys

The titanium alloy substrates used in Chapter 6 for template-assisted electrohydrodynamic atomisation (TAEA) deposition was commercially pure Ti90-Al6-V4 and Ti 78.8-Mo15-Nb3-Al3-SiO0.2, of 0.5 mm thickness. These were obtained from Advent Research Materials (Oxford, UK). Plates were cut into individual 10 mm x 10 mm squares. These were then polished using silicon carbide grinding papers (No.800, No.1200, No.2400 and No.4000). Prior to TAEA deposition, each plate was degreased with acetone and rinsed with the solvent used for deposition, and then air-dried.

3.1.2.3 Stainless steel

Flat stainless steel (316L) of thickness 0.5mm (commercially pure) was obtained from Advent Research Materials (Oxford, UK). The titanium alloy substrates used in Chapter 6 for TAEA deposition was commercially pure Ti90-Al6-V4 and Ti 78.8-Mo15-Nb3-Al3-SiO0.2, of 0.5 mm thickness. These were obtained from Advent Research Materials (Oxford, UK).

Plates were cut into individual 10 mm x 10 mm squares. These were then polished using silicon carbide grinding papers (No.800, No.1200, No.2400 and No.4000). Prior to TAEA

deposition, each plate was degreased with acetone and rinsed with the solvent used for deposition, and then air-dried.

3.1.2.4 Cobalt chromium alloy

Cobalt chromium alloy was obtained from Advent Research Materials (Oxford, UK). The titanium alloy substrates used in Chapter 6 for TAEA deposition was commercially pure Ti90-Al6-V4 and Ti 78.8-Mo15-Nb3-Al3-SiO(0.2), of 0.5 mm thickness. These were obtained from Advent Research Materials (Oxford, UK). Plates were cut into individual 10 mm x 10 mm squares. These were then polished using silicon carbide grinding papers (No.800, No.1200, No.2400 and No.4000). Prior to TAEA deposition, each plate was degreased with acetone and rinsed with the solvent used for deposition, and then air-dried.

3.1.3 Solvents for coating materials

Pure ethanol (99.7 %wt) was obtained from BDH laboratory Supplies, Poole, UK, for all TiO_2 and HA sols and suspensions. Dimethylacetamide (DMAC, 99%) was used as the solvent for PCL solutions. Pure ethanol was taken as a standard material to calibrate devices used for characterisation of coating liquids.

At ambient temperature of 20°C, DMAC evaporates more slowly than the ethanol, is more dense (938 $kg.m^{-3}$ rather 790 $kg.m^{-3}$), has a higher surface tension (30 $mN.m^{-1}$ rather 23 $mN.m^{-1}$) and has higher electrical conductivity (6 $S.m^{-1}$ rather than 1 $S.m^{-1}$).

3.1.4 Templates for TAEA

Copper templates (100 mesh copper, 3.05mm) were purchased from Agar Scientific (Stansted, UK).

3.1.5 Grinding papers

Silicon carbide grinding papers No.800, No.1200, No.2400 and No.4000 were used to polish the substrate surface.

3.2 Preparation of coating suspensions, sol and solutions

3.2.1 Preparation of HA suspension

For TAEA processing, ethanol was added as a liquid carrier to the HA to create a suspension with 6wt.% concentration. The HA and ethanol mixtures were then stirred using a magnetic stirrer for 60 minutes. A concentration of 6wt.% was prepared, investigated and kept constant because it achieved electrohydrodynamic spray deposition in the stable cone jet mode with ease, as found in the literature (Ahmad et al., 2006). However, a range of concentrations (2wt.% to 15wt.%) were initially investigated to verify this hypothesis. Suspensions containing 6wt.% of HA was found to be most suitable. 2wt.% suspension did not dry sufficiently to enable homogenous coating, and 10wt.% and above suffered from sedimentation in the syringe during spraying.

3.2.2 Preparation of TiO_2 sol

Titanium (IV) isopropoxide ($Ti[OCH(CH_3)_2]_4$) was used as a precursor for titanium dioxide (TiO_2). Specific volumes of the precursor and ethanol were mixed together. These mixtures were subsequently magnetically stirred for 2 hours at ambient temperature to create homogenous sols. 2, 4 and 6wt.% TiO_2 sols were found to be stable with no sedimentation, and a stable cone jet was achieved during the TAEA process. For these reasons, these concentrations were used for this study.

3.2.3 Preparation of PCL solution

Specific amounts of polycaprolactone (PCL) were dissolved in the solvent dimethylacetamide (DMAC) to create suitable polymer solutions at a range of concentrations. The polymer to the solvent weight ratios were as follows: (PCL:DMAC) 1:99, 2:98, 5:95, 10:90, and 15:85, i.e. 1, 2, 5, 10 and 15 wt.% PCL in DMAC, respectively. The polymer solutions were mechanically stirred for 60 min at the ambient temperature (20 °C) to ensure that the polymer was completely dissolved and the solutions were homogenous. A range of solution concentrations was used to investigate the effect of this variable of TAEA processing.

3.3 Characterisation of coating suspensions, sol and solutions

The physical properties of the coating liquids are important for the TAEA process. Density, surface tension, viscosity and electrical conductivity of all suspensions, sols and solutions were measured. The equipment used for measuring these properties were calibrated beforehand using pure ethanol, and the reading validated by reference data. The equipment and characterisation method for each physical property are described and discussed in this section.

3.3.1 Density

Density was calculated using a standard 25ml density bottle (VWR International, UK) and a high precision scale (to six decimal places). The mass of density bottle was measured on the scale, and then the bottle filled with solution and measured again. This was repeated five times for each measurement and the mean values calculated and reported in this study. All the measurements were carried out at ambient temperature. The density bottle was calibrated with ethanol.

3.3.2 Electrical conductivity

The electrical conductivity of solutions was measured using a HI-8733 Hanna Instruments probe (Hanna Instruments Ltd., Bedfordshire, UK). The probe was cleaned with distilled water prior to each experiment. Around 25ml of solution was placed into a clean glass beaker, and the liquid gently rotated to remove any air bubbles. The electrode was then immersed into the liquid up to the specified mark, and held until a constant reading settled on the monitor. This was repeated five times for each measurement and the mean values calculated and reported in this study. All the measurements were carried out at ambient temperature. The electrical conductivity meter was calibrated with ethanol.

3.3.3 Surface tension

The surface tension was measured using a tensiometer (Kruss K100SF, Kruss GmbH, Hamburg, Germany) and the standard Wilhelmy's plate method. 50ml of solution was placed into a clean glass beaker so that the surface tensiometer plate could be completely submerged. The platform was then lowered slowly, lifting the plate out of the liquid. The surface tension measurement was displayed on the monitor, and was recorded at the point where the surface of the liquid was just about to detach from the plate, lifting it completely out of the liquid. This was repeated five times for each measurement and the mean values calculated and reported in this study. All the measurements were carried out at ambient temperature. The surface tensiometer was calibrated with ethanol. The plate was washed using deionised water, then the solvent used in the solution to be investigated, and then air dried prior to each measurement to minimise the risk of contamination and ensure an accurate reading.

3.3.4 Viscosity

When calculating the viscosity of the spray media, the time taken by samples to travel between the two marked regions in the U-tube viscometer (t) was measured in seconds using a stopwatch with accuracy to the millisecond. The kinematic viscosity (v) was calculated by multiplying the viscometer constant (C, 0.003 for Type A U-tube) with the time (t).

$$v = Ct \qquad \text{(equation 2)}$$

In order to find the dynamic viscosity (η), (v) was multiplied by the relative density (ρ) of the media, measured earlier and described in Section 3.3.1.

$$\eta = v\rho \qquad \text{(equation 3)}$$

The viscometer was calibrated using ethanol before the measurement. The mean value of five separate measurements was calculated for each solution in this study.

3.4 Experimental set-up and equipment

The TAEA process uses ground electrode configurations and templates with electrohydrodynamic atomisation spraying (Leeuwenburgh et al., 2006) to deposit well-defined patterns on a substrate surface. The experimental set-up of the template assisted electrohydrodynamic atomisation process is described here. The experimental design and the specification of each component used are also introduced.

3.4.1 Equipment configuration

The equipment configuration of template-assisted electrohydrodynamic atomisation spraying is illustrated in **Figure 3.1.** The equipment consists of a nozzle (needle) that is held in epoxy resin and is connected to a high voltage supply and a syringe held in a syringe pump and connected by silicone tubing. The syringe pump controls the flow rate of the spray media in the needle. The distance between the tip of the needle and the substrate a ground electrode is referred to as the collection distance. This was varied in order to investigate its effect on the resultant pattern morphology. The substrate and the platform on which it rests was grounded, and acted as a ground electrode.

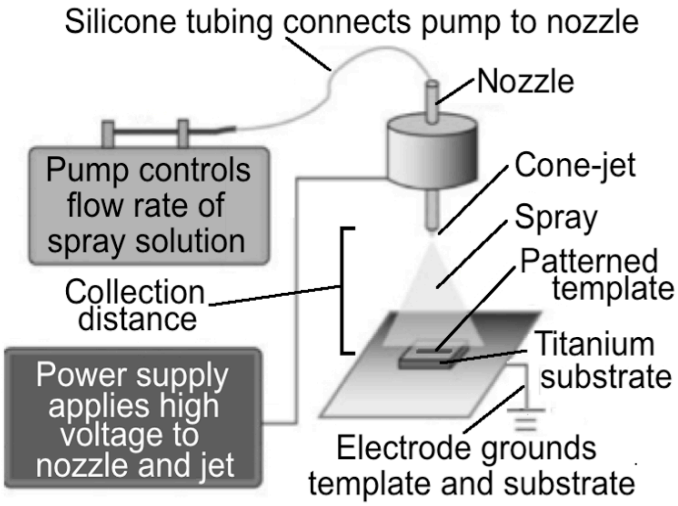

Figure 3.1: Schematic diagram equipment configuration for template-assisted electrohydrodynamic atomisation processing

A camera with illumination was also used to observe the tip of the needle and the shape of the liquid jet as it emerged from the needle at varying applied voltages. The image was displayed on a computer screen, and images could be recorded and saved from there. A stable cone jet was necessary homogenous spraying via TAEA, and this was achieved by adjusting the applied voltage and flow rate. For a specific flow rate, there was a specific range of applied voltages that would achieve a stable cone jet. This was investigated in order to optimise the conditions under which TAEA spraying was possible.

3.4.2 Ground electrode configurations

The electric stress required for electrohydrodynamic processing is determined by the electric field across the collection distance, i.e. between the needle with the applied voltage and the grounded substrate. Varying the collection distance and observing the effect on the process helped further optimise TAEA.

3.4.3 Electrohydrodynamic atomisation processing

In order to achieve homogenous deposition, the position, collection distance, shape (i.e. substrate geometry), and material of the substrate influence the generated electric field. A suspension or solution containing the desired coating material fed through the needle/nozzle at a controlled flow rate through a syringe pump. The electric field created between the needle (electrode) and the substrate, forms a liquid jet from the needle. This breaks up into smaller droplets as the applied voltage increases, and it eventually breaks up into fine and uniform droplets in the nano- or micro-metre scale (Jaworek and Krupa, 1999). The spray collects on the grounded substrate and template to produce a fine coating where its morphology can be easily controlled by varying process parameters such as flow rate and applied voltage.

3.4.4 Template-assisted electrohydrodynamic processing

The use of templates in the EHD process enables the user to further control the properties of the coating deposits by determining their architecture. The templates used in this study were made of copper. A copper template with the desired pattern is placed over the ground substrate. After coating via EHD, the solvent evaporates away and the template can be removed using tweezers, leaving the inverted template pattern on the substrate. This system is shown schematically in **Figure 3.2**.

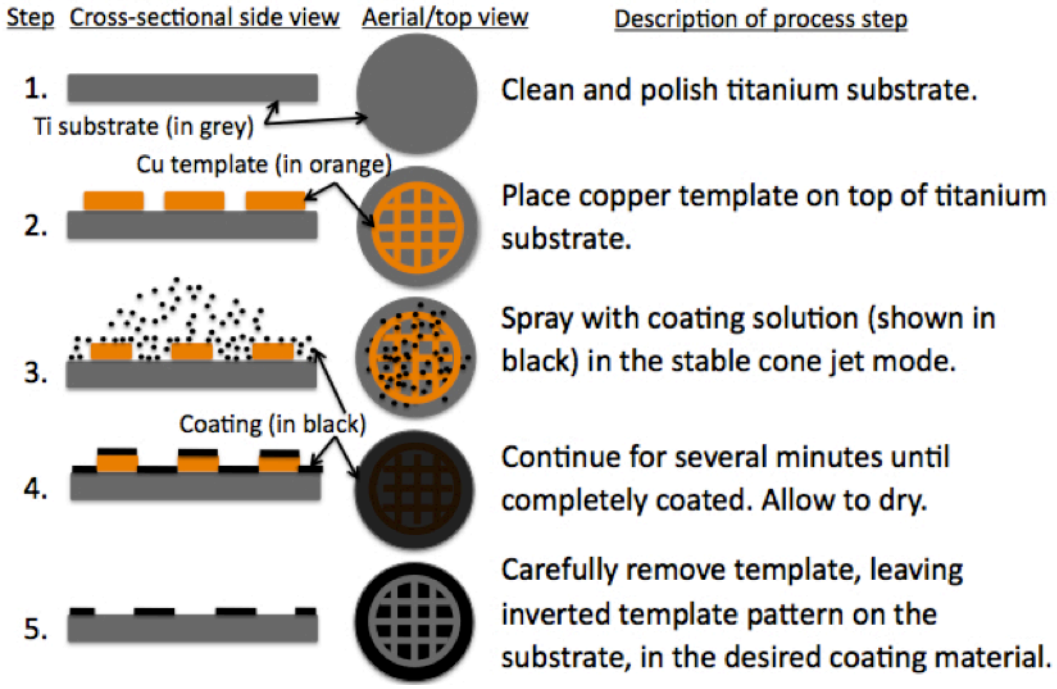

Figure 3.2: Schematic diagram of the templating process

3.4.5 TAEA needle

The needle used in this study was kept constant throughout all experiments. It is made from stainless steel with a 300µm inner diameter, and it is mounted in insulated epoxy resin as shown in **Figure 3.3**. The needle had a blunt tip, i.e. its end face is perpendicular to the needle length. The electrically conductive stainless steel capillary was connected with a wire, and mounted in epoxy resin for 24 hours to insulate and impart rigidity. This made the needle easier to handle and mount for experiments.

3.4.6 Syringe pump

A syringe pump is used to control the rate at which the coating media passes through the needle, and subsequently affects the TAEA deposition rate. The pump is an Infuse/Withdraw PHD 4400 Hpsi programmable syringe pump (Harvard Apparatus Ltd., UK), with a microcontroller that controls a small distance stepper motor. This stepper motor enables the pump to be accurate at low infuse rates, and the motor drives a lead screw and a pusher

blocker. The target volume, infuse rate, syringe type amongst other parameters can be selected via the operation keypad. In this study, 10 ml plastic syringes (BD Plastipaktm, VWR, Lutterworth, UK) were used throughout experimentation. The pump was calibrated using silicone oil 500 (VWR, Lutterworth, UK, density 971 kg.cm^{-3}) before use.

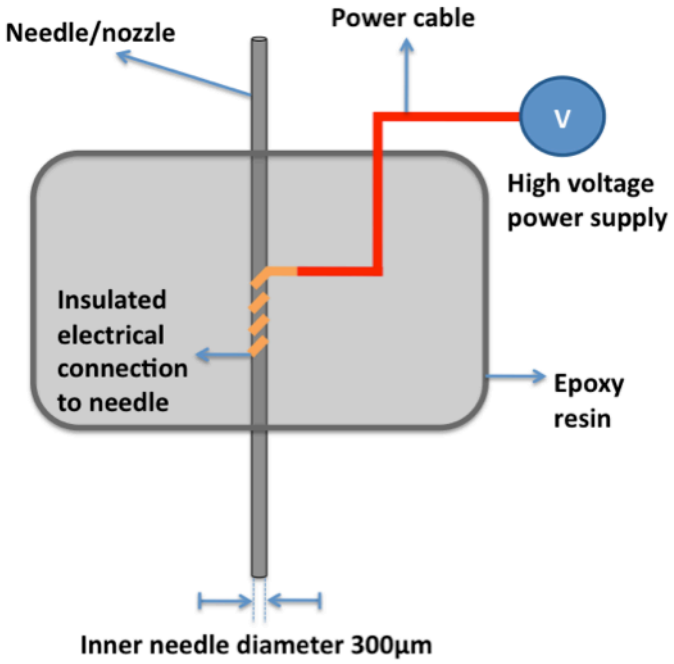

Figure 3.3: Schematic diagram illustrating the needle design used in this study for electrohydrodynamic processing

3.4.7 High voltage power supply

The high voltage supply used in this study is a FC30 P4 120 W regulated high voltage DC power supply (Glassman Europe Ltd., Hampshire, UK). The output voltage range is 0-30 kV and the output current range of this device is 0-4 mA. The operating temperature can vary between -20°C to 50°C, but in this study all experimentation was carried at ambient temperature of 20°C.

3.4.8 Data recording

A Leica S6D microscope (Leica Microsystems UK Ltd., Milton Keynes, UK) was used in conjunction with a JVC TK-C1481BEG digital camera (JVC Professional Europe Ltd., London, UK) to observe the jet during TAEA processing. A computer was connected to the camera to display and record the image on the screen. The applied voltage was set and read from the high voltage power supply unit monitor screen. The flow rate was set and read from the syringe pump monitor screen.

3.4.9 Furnace

A furnace was used in Chapter 6 to heat treat TiO_2 patterns on flat titanium plates. This was a Lenton Eurotherm 2216E laboratory chamber furnace (Lenton Thermal Design Ltd., UK) where heating was carried out in air. The temperature of this furnace could increase up to 1600°C, and output power to 5 kW. The target temperature, hold time and the ramp rate could be set on the controller.

3.5 Characterisation of bioactive TAEA deposits

For the studies that were carried out in Chapters 4, 5 and 6, the morphology and microstructure of the TAEA deposits were observed and characterised using optical microscopy (OM), field emission scanning electron microscopy (SEM), nanoindentation and profilometry. The experimental procedures and the equipment used for these techniques are introduced in detail here.

3.5.1 Optical microscopy

Optical microscopy was used to observe the morphology of the TAEA deposits so that the resultant coatings could be compared to the processing conditions. In this way, the relationship between the two could be better understood, and the process parameters adjusted to achieve the desired morphology.

Optical microscopy (OM) is a standard tool for examining the microstructural features of the surface of materials. The condenser lens, objective lens then projective lens focuses a beam of light onto a photographic plate for observation.

In the study, a Zeiss Axiotech fitted with a Nikon Eclipse Nikon ME600 camera (Nikon, Japan) was used to examine the resultant deposits. The microscope has illumination from either above (for opaque samples such as Ti), or below, for analysing particles on glass slides or the template on its own. There are five lenses on this microscope with magnifications x5, x10, x20, x50 and x100.

The dimensions of the deposits were measured using standard OM images coupled to an imaging tool program, which allowed the mean measurements of geometric features to be calculated via direct link-up analysis of imaging and magnification. The dimension (width and gap) of the patterns were measured using image analysis software where n = 50.

3.5.2 Scanning electron microscopy (SEM)

The morphology and structure of the coatings were also examined using scanning electron microscopy (JEOL JSM-6301F field emission, SEM). This SEM is high resolution, and is fitted with a field emission emitter that can achieve a resolution of ~1.5 nm. The accelerating

voltage can be set between 0.5 kV and 30 kV, and the working distance (the emitter-objective distance) varies between 15-35 mm.

Scanning electron microscopy achieves far greater magnifications than optical microscopy, up to 500,000 times magnification. Electrons are generated in a source and accelerated by a strong electrical voltage gradient down the microscope in a vacuum environment. They then collide with the sample surface, causing some surface electrons to be ejected. A detector then detects, amplifies and measured the strength of the backscattered secondary electrons as they move away from the surface. This signal is then relayed and synchronised with the beam of incident electrons, which creates an image of the detailed variations in the topography of the sample surface. The images obtained through SEM depict large three-dimensional areas as it is capable of including a greater depth of field (Shackelford, 2005).

Samples analysed using SEM were mounted onto an aluminium stub with carbon sticker and sputter-coated with gold for 120s prior to examination, which releases the electrons to minimise charging in the SEM chamber. An acceleration voltage range of 5–10 kV with a working distance of 15 mm was used for all analysis.

The dimensions of the generated deposits were measured using standard OM and SEM images coupled to an imaging tool program, which allowed the mean measurements of geometric features to be calculated via direct link-up analysis of imaging and magnification. The dimension (width and gap) of the patterns in was measured using image analysis software where n = 50.

3.5.3 Sputter coating

Sputter coating is the most common sample preparation method for SEM analysis (Kuo, 2007), and is shown schematically in **Figure 3.6**. A fine coating of gold is deposited onto the sample surface rapidly. For each round of coating, up to six samples were placed inside the chamber in which a vacuum environment was created (via a pump) to prevent contamination. Argon (an inert gas) was then pumped into the chamber ionised via an applied electric field. This created positively charged Ar^+ ions as electrons from their atomic outer shell were removed. These now positive ions are then attracted to the gold target above which is negatively charged, knocking gold atoms away from its surface and depositing them on the sample surface.

Figure 3.4: Schematic diagrams of sputter coating for SEM (Kuo, 2007)

3.5.4 Nanoindentation

Nanoindentation can be adopted to investigate the indentation load-displacement behaviour of materials. An indenter is the main component for indentation tests (see **Figure 3.5**). The load-displacement data can be used to determine the elasticity modulus, hardness, yield strength, wear properties, scratch hardness and fracture toughness of materials.

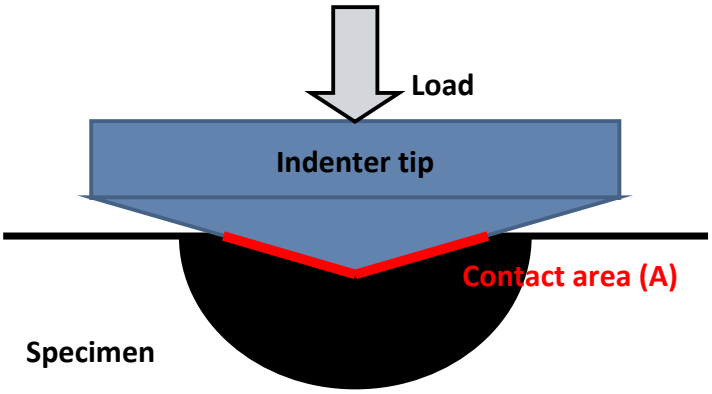

Figure 3.5: Indentation testing

A hard tip indenter whose mechanical properties are known (e.g. diamond) is pressed, at a prescribed load, into a specimen sample whose properties are unknown. As the tip penetrates further into the specimen, the applied load on the indenter tip is increased until it reaches a user-defined value (eg. 14µN in this study). Load and depth measurements are taken throughout testing. The load may be held constant for a defined amount of time, or removed as soon as the prescribed maximum load is reached. The area of the indentation left on the material by the indenter is measured (A). The hardness (H) is defined as the maximum load, P_{max}, divided by the area A.

$H=P_{max}/A$ (equation 4)

Different indenter tips can up used for nanoindentation (see **Figure 3.6** below). The shape used depends on the type of material and mechanical properties being investigated. For titanium dioxide testing, Berkovich is most appropriate due to its sharp and well-defined tip geometry and well-defined plastic deformation into the specimen surface, which make hardness and elastic modulus simpler to calculate. For a Berkovich indenter, A is equal to 24.5x(displacement at P_{max})^2.

Figure 3.6: Indentation tip shapes (b) Berkovich used in this study

During a typical nanoindentation test, an indenter tip is pressed into the test material's surface in a specified loading and unloading cycle, and force and displacement are recorded. A load-displacement curve is then plotted, as the shape of the curve reflects the mechanical properties of the specific material. The gradient of the slope is equal to the stiffness (S). Elastic modulus is a measurement of a material's tendency to be elastically deformed due to an applied force. It can be measured by the gradient of the stress–strain curve in the elastic deformation region. Materials with a high elastic modulus are described as being stiff. Elastic modulus (Pa) = stress/strain. Stress is the force caused by the deformation of a solid per unit area (measured in Pa); and strain is the deformation of a solid as a result of stress.

3.5.5 Profilometry

Profilometry was adopted to investigate the thickness of TAEA deposits, so that it could be compared to collection time and solution concentration. The surface profilometer used in this study was a Bruker DektakXT surface stylus profilometer (Bruker Corporation, Massachusetts, USA). A stylus needle was drawn along the surface of the pattern and it followed the topography of the pattern. This meant that the vertical distance between the substrate surface and the pattern surface could be measured. This optical profilometer has

a vertical resolution of 5 nm. The length of the test was 500µm, with duration of 5 s. The stylus force was 5 mg. Three separate readings were taken for each sample, and the mean values were calculated.

4. Electrohydrodynamic patterning of curved titanium substrates with bioactive ceramics

4.1 Introduction

The development of TAEA for application on curved substrates is a natural progression of research, which has been exclusively on flat surfaces to date since its invention (Li et al., 2007, Li et al., 2010) and is a key milestone towards commercial viability. This work aims to further develop TAEA for the application of bioceramic patterns onto curved titanium (Ti) substrates for the first time.

There are not only similarities but also characteristic differences between flat and curved surface TAEA. The substrate, whether curved or flat, remains grounded; however, the collection distance between the needle and the top surface of a curved substrate varies with the curvature (see **Figure 4.1**). This affects the electric polarisation stress parallel to the needle acting on the liquid meniscus on application of the electric potential. The relationship between collection distance and the dimensions of the liquid droplets is well documented in the literature (Jaworek and Krupa, 1999, Hartman et al., 2000, Enayati et al., 2010). As the collection distance increases, liquid droplet size decreases as the solvent carrier evaporates in transit, resulting in smoother coatings. As the collection distance decreases, liquid droplet size increases as less solvent carrier evaporates in transit, resulting in rougher coatings. This greatly affects the integrity and uniformity of resultant coatings.

Therefore, increased collection (working) distances are preferable so that the difference in height across the substrate is less significant compared to the average collection distance.

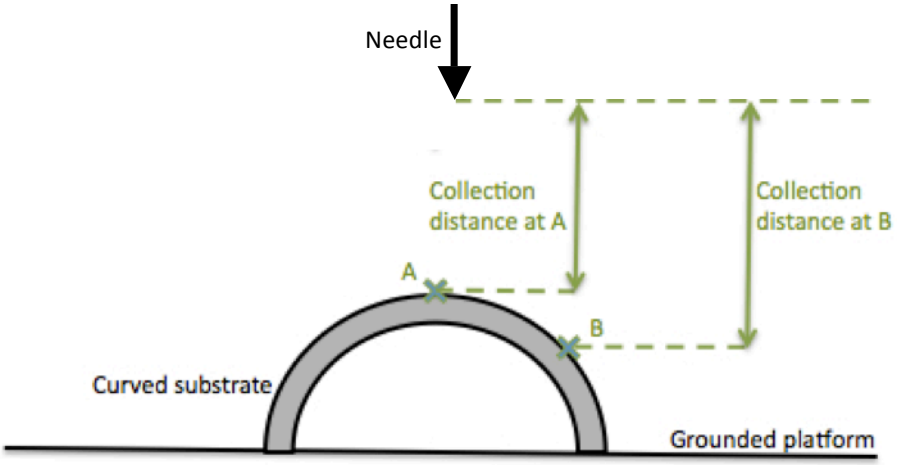

Figure 4.1: How collection distance varies with substrate curvature

The bioceramic hydroxyapatite (HA) is typically used when coating metal prostheses for controlled implant or tissue interfacial response. The mechanical behaviour of HA is acceptable when under low- load conditions and it exhibits excellent biocompatibility, although it degrades slowly *in vivo* (Paital and Dahotre, 2009). However, applying a patterned layer of titania (TiO_2) before applying HA significantly improves interfacial adhesion of the HA layer with the titanium. This is due to the ionic interactions between the buffer titania buffer layer with the titanium, and the HA coating on the titania. The stability of the oxide layer that forms on titanium and its alloys *in vivo* may be affected in the biological environment. This can result in increased metal ion release, in low enough amounts that it does not negatively impact cell viability (0.01 to 100 $ng.ml^{-1}$), but could inhibit phytohemagglutinin-induced T-cell or liposaccfaride-induced B-cell proliferation and reduce mineral

formation (Ku et al., 2002). Titanium also exhibits poor osteointegration properties, compromising biological fixation (Nie et al., 2000). A buffer layer of titania at the titanium substrate surface acts as a chemical barrier, preventing the release of these aforementioned metal ions, but also increases adhesion strength between the titanium substrate and the HA coating via chemical bonding.

In addition, TiO_2 coatings have been found to improve the corrosion resistance of titanium substrates (Cabrini et al., 1997) and thus their functionality in load-bearing orthopaedic applications (Kurzweg et al., 1998). The outer HA layer enhances the bioactivity and osteoconductivity initially, and the inner TiO_2 layer prevents the titanium substrate from corroding, even after the HA layer has completely resorbed into the body (Munir et al., 2012). The TiO_2 pattern interlocks with the HA coating on the Ti substrate, in an enhanced manner in TAEA, and improves mechanical strength and chemical bonding, thus clinical functionality (Li et al., 2007). Therefore the TAEA application of both TiO_2 and HA on curved Ti substrate warrants investigation (Kim et al., 2004, Lin and Yen, 2005).

In order to compare the uniformity of the TAEA spraying across the curved substrate, mean line widths were measured at different points across the curve. These positions are shown in **Figure 4.2**. The Ti substrate was in the same position for all three experimental set-ups; it was only the template position that was varied. Comparing the mean width for each position will give an indication on how uniform the coating is across the curve. A mean closest to 100 μm (template width) indicates the most accurate templating, as the pattern exactly resembles the negative of the template. A mean that varies more greatly from the original template width indicates less accurate templating and more particle spread. In this way, the effect of template

position on resultant microstructure can be assessed. This investigation is relevant because, for TAEA to be translated to curved surfaces, the resultant patterns need to be as homogenous as on flat surfaces.

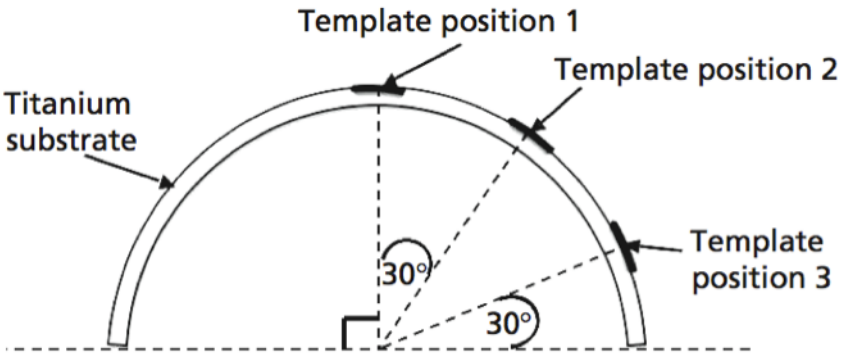

Figure 4.2: Schematic illustration of the three template positions for investigating curved surface TAEA

4.2 Characteristics of ceramics and their sol/suspensions

The TAEA process of producing the patterns is electric field assisted; therefore it is controlled by both the processing parameters of the technique (such as flow rate and applied voltage) as well as the physical properties of the suspensions (such as density, viscosity, surface tension and electrical conductivity). A combination of processing parameters and physical properties determines the different jetting modes of the various suspensions (Jaworek and Krupa, 1999, Sebbowa et al., 2011). **Table 4.1** shows how the measured physical properties of the suspension vary with respect to concentration, from 100 wt.% ethanol to 10 wt.% TiO_2 in ethanol. Results for ethanol were verified with the literature (Grace and Marijnissen, 1994). The electrical conductivities of the suspensions were in the range $0{\cdot}1\text{-}0{\cdot}8 \times 10^{-4}$ $S.m^{-1}$. TiO_2 addition caused the density to increase by 2%. However, viscosity and surface tension

increased by 62% and 52%, respectively, with the addition of 10 wt.% TiO_2. This affects the ability and readiness of the suspension material to achieve stable jetting under the influence of an electric field. Therefore, it was found that 2-4 wt.% TiO_2 was ideal for coating in the stable cone jet mode (not too viscous but electrically conductive enough), which is necessary to generate homogeneous droplets.

Table 4.1: Titania in ethanol sol properties

Suspension	**Density ($kg.m^{-3}$)**	**Viscosity (mPa.s)**	**Surface tension ($mN.m^{-1}$)**	**Electrical conductivity ($S.m^{-1}$)**
Ethanol	790	1.3	23	$0.1x10^{-4}$
1wt.% TiO_2 in ethanol	790	1.3	24	$0.5x10^{-4}$
2wt.% TiO_2 in ethanol	791	1.5	26	$0.6x10^{-4}$
4wt.% TiO_2 in ethanol	794	1.7	29	$0.6x10^{-4}$
6wt.% TiO_2 in ethanol	799	1.8	32	$0.7x10^{-4}$
8wt.% TiO_2 in ethanol	802	1.9	34	$0.7x10^{-4}$
10 wt.% TiO_2 in ethanol	808	2.1	35	$0.8x10^{-4}$

The voltage–flow rate map for 4 wt.% TiO_2 (**Figure 4.3**) was also plotted as a reference for obtaining a stable cone jet under different conditions. It was found that at a flow rate increased from 5 to 20 µl.min^{-1}, the applied voltage window for stable cone jetting increased from 0·75 to 1·5 kV, that is, it doubled in range. This made stable cone jetting easier to achieve at a 20 µl.min^{-1} flow rate.

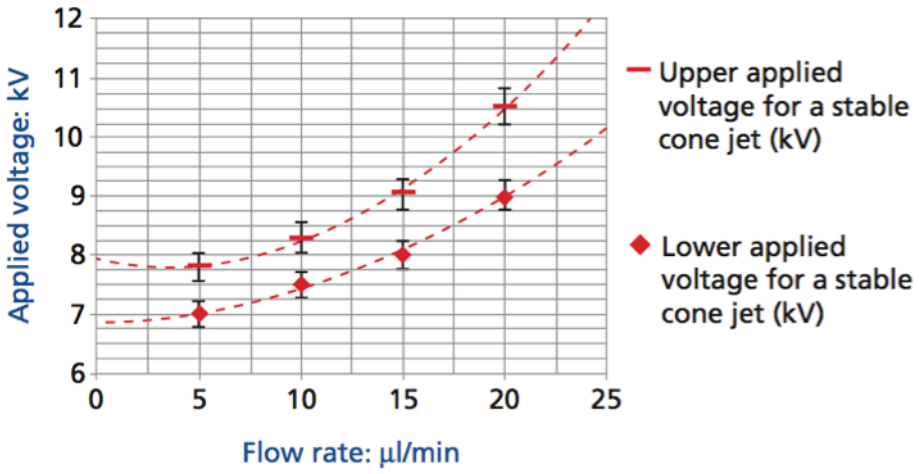

Figure 4.3: Applied voltage variation with flow rate for 4 wt.% TiO_2 for stable cone jet mode electrohydrodynamic atomisation jetting with collection distance of droplets maintained at 80 mm

4.3 TAEA spraying parameter investigation for ceramic patterns

In this study, TAEA is further developed for the application of predetermined TiO_2 patterns on curved Ti substrates for the first time. We show that this is indeed possible, with results comparable to that of existing research on exclusively flat substrates. However, further work is needed to scale-up the process to larger curved surfaces and substrates, and ongoing and future work will address this. The results obtained are verified by way of analysis of the pattern morphology, and mechanical testing by nanoindentation. A systematic study on the relationship between heating

the patterns and their resultant mechanical properties was also carried out (Nithyanandan et al., 2015).

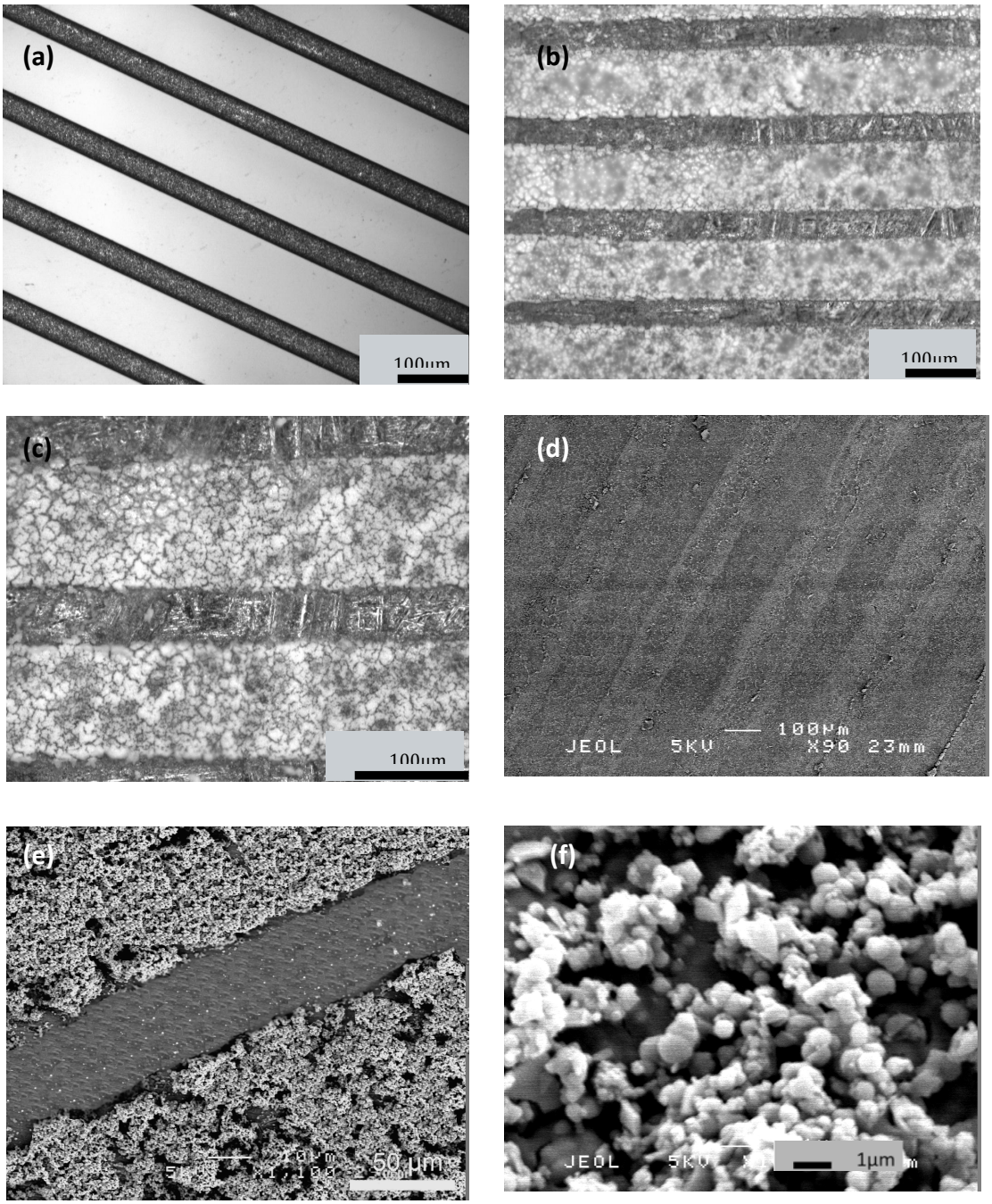

Figure 4.4: Optical micrographs of: (a) parallel copper template with strut width 50µm and inter-strut spacing of 100µm (b) TiO_2 pattern (white colour) on curved Ti substrate (grey colour) (c) Pattern at greater magnification. (d) to (f) show scanning electron micrographs of TiO_2 pattern. All images depict spraying of suspension 4wt.% TiO_2 with flow rate, applied voltage and collection time, 20µl.min^{-1}, 10kV and 300s respectively, and convex substrate is titanium of diameter 25.4mm.

During stable jetting, the spray coated both the template and the substrate, which were both grounded. This is essential in creating uniform coatings across the substrate so that after spraying, the template can be removed to leave an even pattern. **Figure 4.4** shows the development of the coatings, from the parallel copper template, the coated template and resultant coating observed by way of optical microscopy (OM) and scanning electron microscopy (SEM). The resultant patterns show that the template dimensions influence the geometry of the coatings, so they can be chosen to meet the specific clinical needs of the coating.

A clear correlation between the template shape and size and the achieved pattern was established. It was observed that the coating adhered well to the metal substrate because, on template removal, the boundary between coated and uncoated substrate was well defined (**see Figure 4.4e**). Varying the spraying time can control the height of the patterns, but this is a trade-off with the narrowness of the patterned lines.

Figure 4.4 also shows that TiO_2 patterns have been sprayed onto curved Ti substrates with uniform and ordered topography. Results for the parallel template (with strut width of 50 µm, spacing of 100 µm) show that the mean distance between patterned lines (interline spacing) is 54 µm and the mean line width is 97 µm (standard deviation 6 µm and 12 µm, respectively). This was achieved when 4 wt.% TiO_2 was applied by way of TAEA at a flow rate of 20 $\mu l.min^{-1}$, applied voltage of 10kV, collection distance 80 mm and collection time of 300s.

The same template shape was used for all experiments so the shape and size of patterns across the entire coating were kept constant. Since the collection time was

controlled at 300s during the process, the height of the patterns (normal to the substrate surface) was kept approximately constant (42 ± 5 µm measured by way of SEM image analysis). **Figure 4.4f** shows that the coatings exhibit a microporous surface, with pores less than 1 µm in diameter. This is beneficial for cell attachment and enhances bioactivity (Lewandrowski et al., 2003).

4.3.1 The effect of substrate curvature

The coating that closely resembled the negative of the templates on convex and concave substrates with diameters and 25.4mm and 23.6mm respectively. For the smaller diameters on the concave surface, it was more difficult to obtain homogenous patterns. During spraying on concave surfaces, it was observed that the edges of the smaller diameter substrates were interfering with the electrohydrodynamic jetting process, resulting in less even coatings. A schematic of this phenomenon is shown in **Figure 4.5**. In order to overcome this issue, the collection distance could be reduced to minimise this effect.

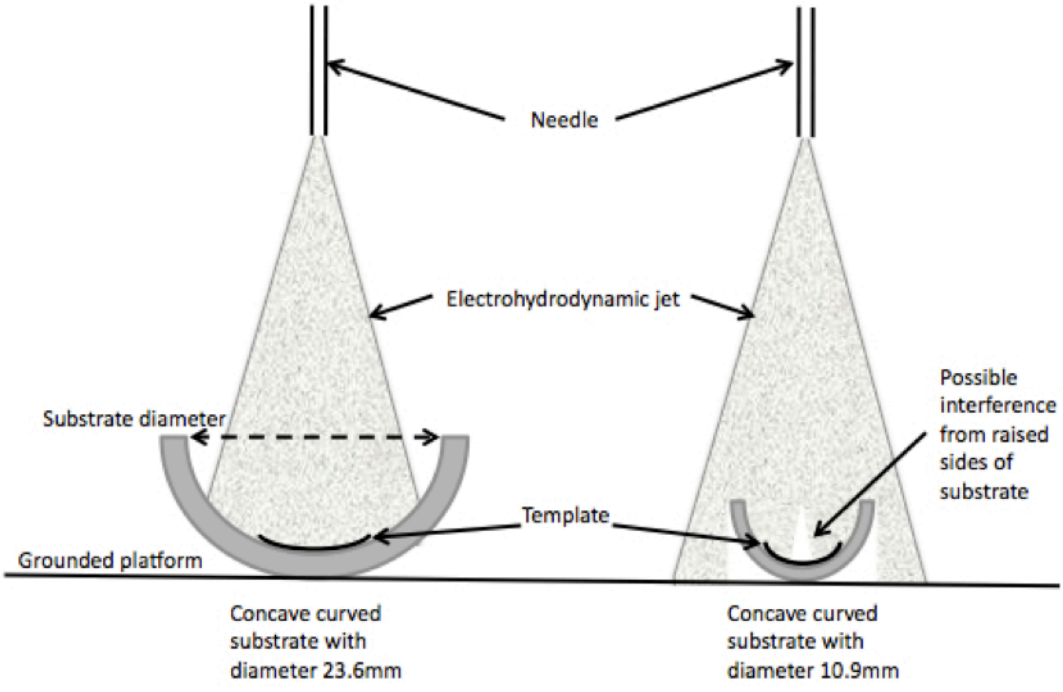

Figure 4.5: Concave curved substrate walls interfering with EHD jet

In order to compare the uniformity of the TAEA spraying across the curved substrate, mean line widths were measured at different points across the curve (see **Figure 4.2**). **Figure 4.6** shows how optimal results were obtained at Position 1, as the mean deposit width was measured as 98 µm, closest to the actual template size (100 µm). Figure 5 also shows that Position 1 yielded minimum spread as the standard deviations of both measures were lowest here. Position 1 was at the top of the curved substrate, thus the pattern surface was most parallel to the grounded platform compared with Positions 2 and 3, and means that results were most comparable to TAEA of flat substrates.

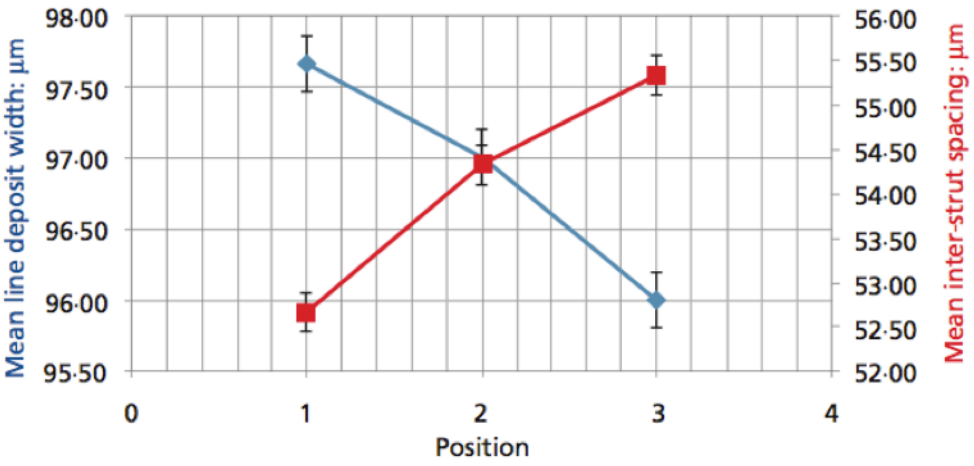

Figure 4.6: Mean deposit width and spacing variation with position on substrate curve. Error bars depict standard deviation.

As the template position increased from 1 to 3, the angle at which the patterning area lays also increased. Results showed that as this angle increased, mean deposit width decreased to 96 µm (by 2%) and mean spacing width increased from 53 to 55 µm (by 4%). Spread (standard deviation) increased for both parameters. This indicates that curvature does not greatly affect the uniformity of TAEA patterning at these diameters.

4.4 Mechanical properties

Hardness and elastic modulus of the patterns were evaluated using nanoindentation techniques adopted in previous studies (Nithyanandan et al., 2013). A three-sided pyramidal Berkovich diamond indenter with a nominal tip radius of 10nm was used throughout the experiments. The indentation load and the displacement were recorded continuously through one complete cycle of loading and unloading, and the thermal drift of the transducer was corrected during each measurement. By invoking the Oliver–Pharr method, the hardness and the effective elastic modulus were calculated from the unloading curve of the nanoindentation tests (Bhushan and Li, 2003). The effect of load, holding time and loading rate on the mechanical properties of the TiO_2 patterns were studied.

A typical load–displacement curve obtained during the nanoindentation on bioceramic TiO_2 pattern is shown in **Figure 4.7a**. The continuous curve for the complete cycle of loading and unloading indicates good adhesion of the patterns to the substrate (Bhushan and Li, 2003). This also suggests no cracking or delamination of the TiO_2 pattern on the substrate.

The hardness of the ceramic patterns was calculated from the maximum load (P_{max}) and the contact area of the indentation (A) (Oliver and Pharr, 1992).

$H=P_{max}/A$ (equation 4)

A was calculated using the following equation (Malzbender et al., 2002):

$A = 24 \cdot 5h_c^2$

$A = 24 \cdot 5h_c^2$

where h_c represents the contact depth as measured at the maximum load.

The effective elastic modulus was derived from the initial slope of the unloading cycle (S, stiffness) and contact area of the indentation (A) (Zhou and Komvopoulos, 2006).

$$E_r = \frac{\sqrt{\pi}}{2}\frac{S}{\sqrt{A}} \qquad \text{(equation 5)}$$

Figure 4.7b shows the effect of load on the TiO_2 patterns at a loading rate of 1 $\mu N.s^{-1}$ and a hold time of 1 s. Hardness decreases as load increases up to 7 µN, and then remains at that value (0·1 GPa) up to higher loads. Elastic modulus also decreases up to ~10 µN, and then remains at that value (0·3 GPa) up to higher loads. This decrease in hardness and effective elastic modulus can be attributed to the microporosity observed in the TiO_2 deposits, as higher loads are able to penetrate more easily into microporous structures. This supports the results of other coatings. Although adhesion as a function of time (storage) has not been considered in this work, there is no reason to believe that adhesion will deteriorate with time. Experimental verification of this fact is important in future exploitation of this process.

The hardness and effective elastic modulus of TiO_2 patterns with regard to loading rate were analysed and shown in **Figure 4.7c**. The hardness was 7·5 GPa at a loading rate of 0·1 $\mu N.s^{-1}$, and reduced to 7·3 GPa when the loading rate was increased to 1 $\mu N.s^{-1}$. This is only a 2% decrease, so it can be concluded that hardness is not significantly affected by loading rate within these testing limits. This means that the TiO_2 exhibits brittle properties (as expected for ceramic materials), which is why the

hardness value did not change. With respect to effective elastic modulus, this was found to be 7·5 GPa at a loading rate of 0·1 $\mu N.s^{-1}$, and reduced to 7·3 GPa when the loading rate was increased to 1 $\mu N.s^{-1}$. This again is a 2% decrease, so it can be concluded that the elastic modulus is also not significantly affected by loading rate within these parameters. This shows that both hardness and effective elastic modulus are not sensitive to loading rate.

The variation of hardness and the effective elastic modulus with hold time is shown in **Figure 4.7d**. Both parameters increased as hold time increased from 1 to 60 s by 12% and 24%, respectively. This indicates that longer hold times allowed for more energy to be dissipated across the specimen sample as high values were found for both parameters.

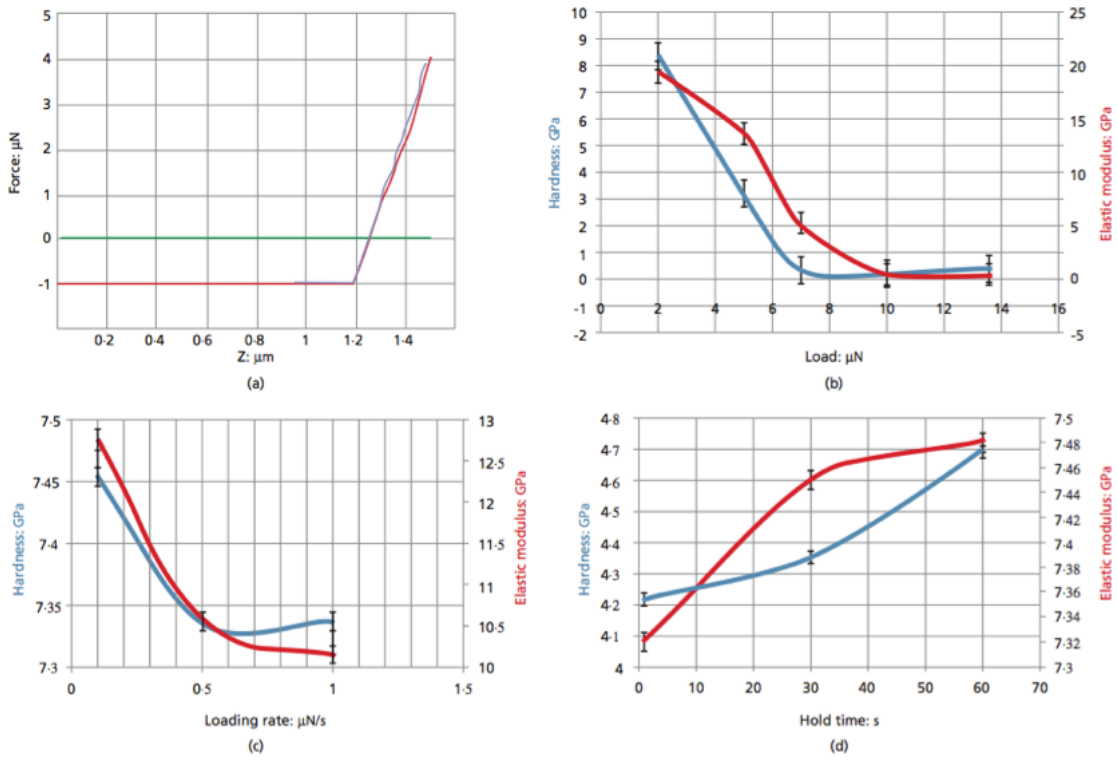

Figure 4.7: (a) A typical load–displacement curve obtained from the nanoindentation tests on TAEA TiO_2 pattern with a loading rate of 1 $\mu N.s^{-1}$. Variation of hardness and effective elastic modulus with (b) load, (c) loading rate and (d) hold time.

4.5 Summary

A method of producing TiO_2 patterns on curved Ti substrates by way of the TAEA process has been developed with a high degree of control over the pattern geometry (by way of template choice) and thickness (by way of collection time). TiO_2 patterns with parallel lines have been successfully produced on both convex and concave Ti substrate diameters of ~25mm. Optimal results were obtained with 4 wt.% TiO_2 in ethanol suspension sprayed within the stable cone jet mode window at a flow rate of 20 µl.min^{-1} for 300 s at 10 kV with a collection distance of 80 mm.

A clear correlation between the template shape and size and the achieved pattern was established, therefore the template can be chosen to reflect the specific clinical needs of the coating. Results for the parallel template (with strut width of 50 µm, spacing of 100 µm) show that the mean interline spacing is 54 ± 6 µm and the mean line width is 97±12 µm.

Since the collection time was controlled at 300 s during the process, the height of the patterns (normal to the substrate surface) was kept approximately constant at 42 ± 5 µm.

For TiO_2 patterns at a loading rate of 1µN.s^{-1} and a hold time of 1 s, hardness decreases as load increases up to 7 µN and remains at 0·1 GPa up to higher loads. Elastic modulus behaves in a similar way. This decrease can be attributed to the microporosity observed in the TiO_2 deposits as higher loads are able to penetrate

more easily into microporous structures. Hardness is 7·5 GPa at a loading rate of 0·1 $\mu N.s^{-1}$, and reduces to 7·3 GPa when the loading rate is increased to 1 $\mu N.s^{-1}$. This is only a 2% decrease, thus the hardness is not significantly affected by the loading rate due to the brittle nature of the TiO_2 ceramic. With respect to effective elastic modulus, this is found to be 7·5 GPa at loading rate 0·1 $\mu N.s^{-1}$, and reduces to 7·3 GPa when the loading rate is increased to 1 $\mu N.s^{-1}$. This again is a 2% decrease, so we can conclude that the elastic modulus is also not significantly affected by loading rate within these parameters.

5. Biopolymer template-assisted electrohydrodynamic atomisation (TAEA)

5.1 Introduction

Typical coatings for metallic orthopaedic implants are hydroxyapatite (HA) bioceramic. These have been used successfully in orthopaedic applications for several decades to improve biological response *in vivo* (de Groot et al., 1998, Thian et al., 2010). HA exhibits excellent biocompatibility as it closely resembles the mineral phase of bone and offers appropriate mechanical properties under low-load conditions, although it degrades slowly *in vivo* (Paital and Dahotre, 2009). Ceramic coatings can be successfully applied via VPS due to their high melting points. However, if the coating process temperature could be reduced to ambient temperature conditions, a greater range of materials could be used, including biodegradable polymers.

Polymers are widely used biomaterials (Balasundaram and Webster, 2006), thus a natural progression of work on TAEA. Polymer TAEA has potential applications in joint prosthesis coatings, scaffolds for hard and soft tissue engineering, low wear interfaces and orthopaedic fixation tools (Ciccone et al., 2001). Bioactive polymer coatings have exhibited bone- bonding properties and cell-mediated osteogenesis comparable with that of HA and other calcium–phosphate coatings (Heimke and Griss, 1980). The results from stress-analysis studies also suggest that polymer coatings and their associated flexibility may have mechanical advantages compared with traditional ceramic coatings, which are more brittle (Kim et al., 2006).

In addition to their mechanical properties, polymers have the scope to provide drug-delivery capabilities, where medications can be delivered intact to the implant–tissue interface through a polymer medium that can control its administration (Duncan, 2003). Polyesters such as polycaprolactone (PCL) and poly(lactic acid) (PLA) are considered the most suitable types of biodegradable polymer as they demonstrate low toxicity and immunogenicity, enhance drug-targeting specificity, improve treatment absorption rates and protect pharmaceuticals against biochemical degradation (Reed and Gilding, 1981, Anderson and Shive, 1997).

This study presents the development and assessment of the novel deposition of biodegradable polycaprolactone (PCL) polymer patterns on a metallic substrate using a jet spraying TAEA technique at ambient temperature. The parameters required for depositing uniform layers are developed and the physical characteristics of the resultant coating are measured. A range of polymer concentrations (1–15 wt.% PCL in dimethylacetamide, DMAC) and flow rates (1–25 $\mu l.min^{-1}$) are investigated. The resultant patterns are analysed via optical and scanning electron microscopy, profilometry and nanoindentation.

5.2 Comparison of PCL solutions with different concentrations

Appropriate quantities of PCL were dissolved in DMAC. The weight ratios of the polymer to the solvent were as follows: (PCL:DMAC) 1:99, 2:98, 5:95, 10:90, and 15:85, i.e. 1, 2, 5, 10 and 15 wt.% PCL in DMAC, respectively. The polymer solutions were stirred mechanically for 60 min at the ambient temperature (20 °C) to ensure that the polymer had completely dissolved and the solutions were homogenous.

The TAEA process of producing the patterns is electric field assisted; it is controlled by both the processing parameters of the technique (such as flow rate and applied voltage) as well as the physical properties of the solutions (such as density, viscosity, surface tension, and electrical conductivity). A combination of these variables determines the different jetting modes (Jaworek and Krupa, 1999). **Table 5.1** shows how the measured physical properties of the solution vary with respect to solution concentration, from pure 100 wt.% DMAC to 10 wt.% PCL in DMAC. Five values were recorded for each measurement, and the mean value was calculated. The corresponding standard errors are also given.

Table 5.1: PCL solution properties

Sample	**Density ($kg.m^{-3}$)**	**Viscosity (mPa.s)**	**Surface tension ($m.Nm^{-1}$)**	**Electrical conductivity ($\mu S.m^{-1}$)**
DMAC	938±30	2.0±0.1	30±1	6.0±0.4
PCL:DMAC 2:98	945±31	2.6±0.2	30±1	3.4±0.3
PCL:DMAC 5:95	949±35	4.6±0.4	30±1	1.8±0.1
PCL:DMAC 10:90	956±36	11.1±0.7	32±1	0.8±0.03

The electrical conductivity of the solution was decreased by 87% with an addition of 10 wt.% of PCL. This is due to the insulating nature of polymer. The density and

surface tension did not increase significantly (2% and 7% respectively), but the viscosity increased significantly by a factor of 6.

5.3 Jetting modes of PCL solutions

When spraying via TAEA, the presence of the stable cone jet mode is critical in producing even patterns. This jetting mode can be obtained within a range of applied voltage at a chosen flow rate. Therefore, it was important to first map the range at which this mode could be achieved for each flow rate and solution concentration. Subsequently, the appropriate voltage for any concentration and flow rate within the mapped range could be found.

Alongside the presence of a stable cone jet, other processing parameters such as collection time and working distance, had to be optimised. The collection time was varied from 30 s (which produced particles) to 500 s (which produced very thick patterns of $\sim$100 µm which peel away from the template). The spray time of 300 s was found to be the optimal time that produced repeatable and uniform patterns. The working distance was varied from 10 to 100 mm. It was found that 60 mm was optimal and the coating area was a uniform circle, which was less vulnerable to being affected by ambient conditions in the laboratory. By holding these parameters at these constant values, the geometry of the resultant pattern was primarily investigated by varying the solution concentration.

The shape of the jet and the nature of its break-up are documented in the literature (Jaworek and Krupa, 1999). The modes include dripping, micro-dripping, un- stable cone jet, and stable cone jet, which are shown in **Figure 5.1**. The cone jet is the most

stable mode and it generates a near-uniform particle size distribution (Cloupeau and Prunetfoch, 1990). In this work, the voltage envelope for the different modes was comparable to the literature (Enayati et al., 2010). As the voltage increased, the stable cone jet mode was achieved when the gravitational and electric forces overcame the surface tension forces. The drops become smaller regular spheres when these forces are balanced (Hartman et al., 2000).

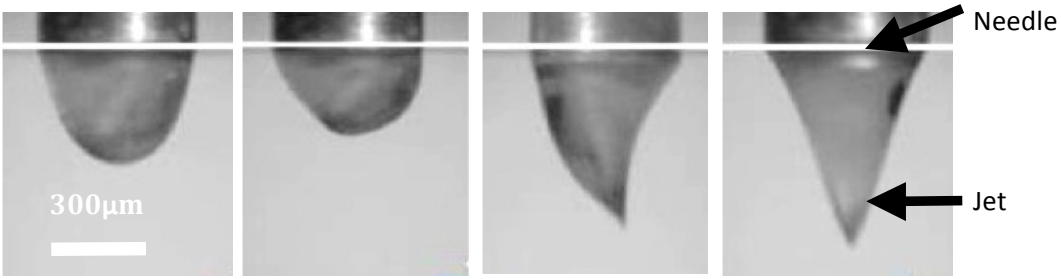

Figure 5.1: Jetting modes for 5wt.% PCL in DMAC, 0-11kV at 15µl.min^{-1} flow rate (a) dripping 0-5kV (b) micro-dripping 5.1-6.6kV (c) unstable cone jet 6.7-8.3kV (d) stable cone jet 8.4-11.5kV

Typical examples of the geometric shape of the PCL suspension as it exits the needle, relative to the changing voltage are given in **Figure 5.1**. The flow rate was set at 15µl.min^{-1} and the applied voltage increased from 0kV to 11kV. **Figure 5.1a** shows the shape of the liquid exiting the needle as the voltage applied increases from 0kV to 5kV. **Figure 5.1b** shows that size of the droplets reduces significantly as the voltage applied increases from 5.1 to 6.6 kV, thus microdripping occurs more frequently. As the voltage increases from 6.7-8.3 kV, the unstable cone jet is formed **Figure 5.1c**. These modes are uncontrolled jetting modes, which would result in uneven and inhomogeneous patterning. However, increasing the voltage up to 11.5kV results in a stable cone jet mode **Figure 5.1d**. Above 11.6kV, the jet split into multi-jet mode.

The modes were investigated in detail for three different polymer concentrations (2, 5 and 10 wt.% PCL in DMAC) and the findings are presented as parametric maps of the operating range of applied voltage versus flow rate. Applied voltage and flow rate are crucial parameters when creating a stable cone jet for spraying. These maps show that it can be achieved only when the flow rate and the applied voltage are in a distinctive range. The regions above and under the envelope give unstable jetting. **Figure 5.2a** shows the shape of the jet as it exits the needle, relative to change in voltage for 2 wt.% of PCL solution.

These operating range maps show that in more viscous solutions, a greater voltage (both upper and lower limits) is required to form the stable cone jet mode of jetting. For example, when the flow rate of the solutions was 20 $\mu l.min^{-1}$, a stable cone jet could be achieved when the applied voltage was 7.1 kV at 5 wt.% PCL in DMAC (the least concentrated solution i.e. the least viscous), but increased to 10 kV at 10 wt.% PCL in DMAC (the most concentrated solution i.e. the most viscous). This is mainly due to the lower electrical conductivity of the more viscous solutions, as polymers are less conductive than the solvent. Therefore, a greater electric field is needed to overcome the surface tension and viscosity to form a cone jet.

In more viscous solutions, the overall region between dripping and the upper limit for a stable cone jet increased in kV range and transition between modes occurred less rapidly, apart from the transition from unstable to stable cone jet modes. This could be due to the polymer concentration and its associated surface tension, which means the balance of electrical force is achieved more slowly. The electrical stresses could be more efficiently transmitted through liquid by viscous diffusion at higher flow rates (Enayati et al., 2010).

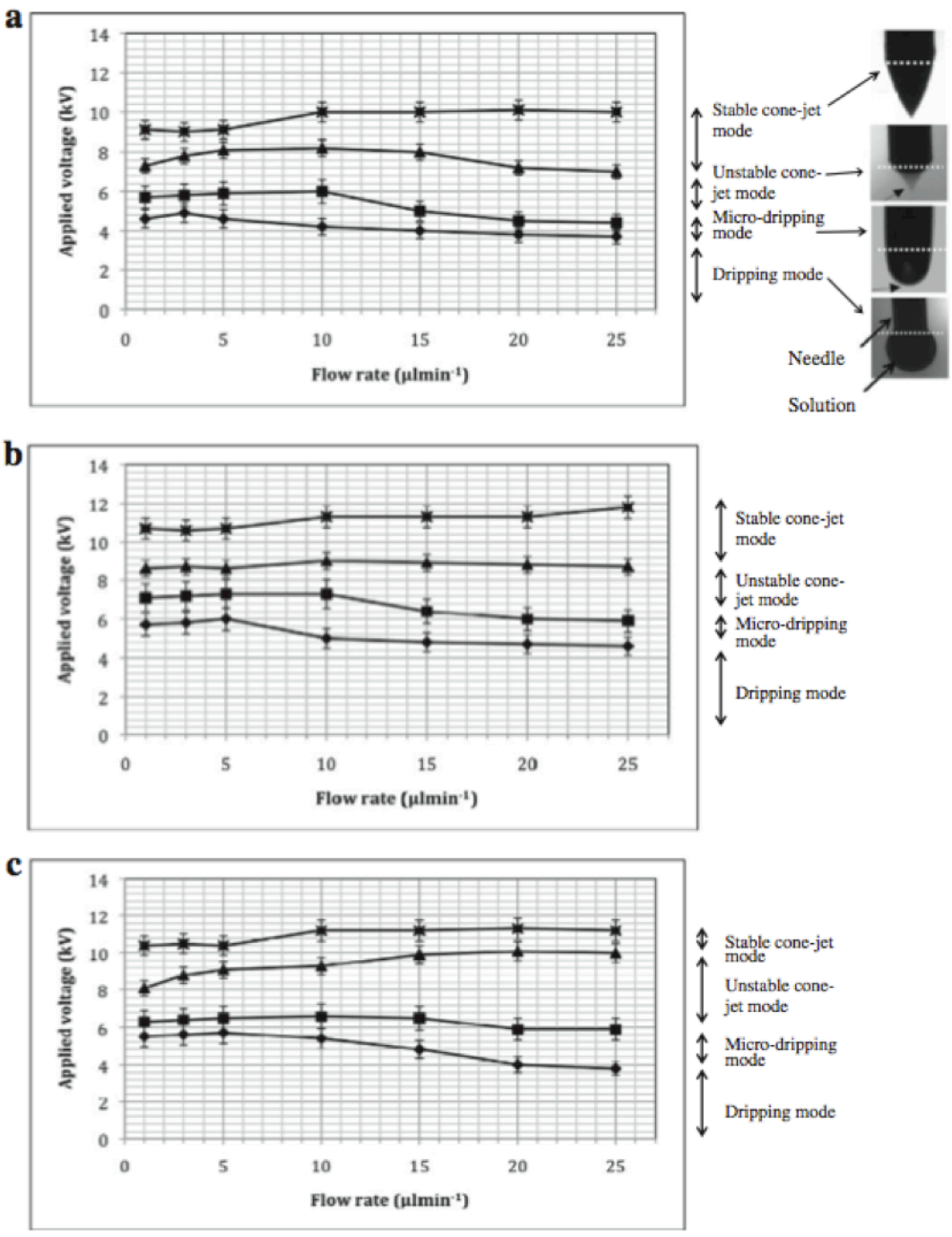

Figure 5.2: (a). Operating flow rate and applied voltage range for TAEA spraying modes for 2 wt.% PCL solution in DMAC. Images to the right show the geometry of the needle and the solution. The white dotted line indicates the needle exit. (b). Operating flow rate and applied voltage range for TAEA spraying modes for 5 wt.% PCL solution in DMAC. (c). Operating flow rate and applied voltage range for TAEA spraying modes for 10 wt.% PCL solution in DMAC.

5.4 PCL pattern geometry

During cone jet mode jetting, the spray uniformly coats the template and the substrate as they are both grounded. This is essential in creating uniform patterns across the substrate so that after spraying, the template can simply be removed leaving behind an even pattern. A strong correlation between the template size and shape, and the achieved pattern was established. It was observed that the pattern adhered well to the metal substrate as the boundary between coated and uncoated substrates was defined and straight. **Figure 5.3** shows the development of the patterns, from the hexagonal copper template, the coated template and resultant pattern observed via OM and SEM.

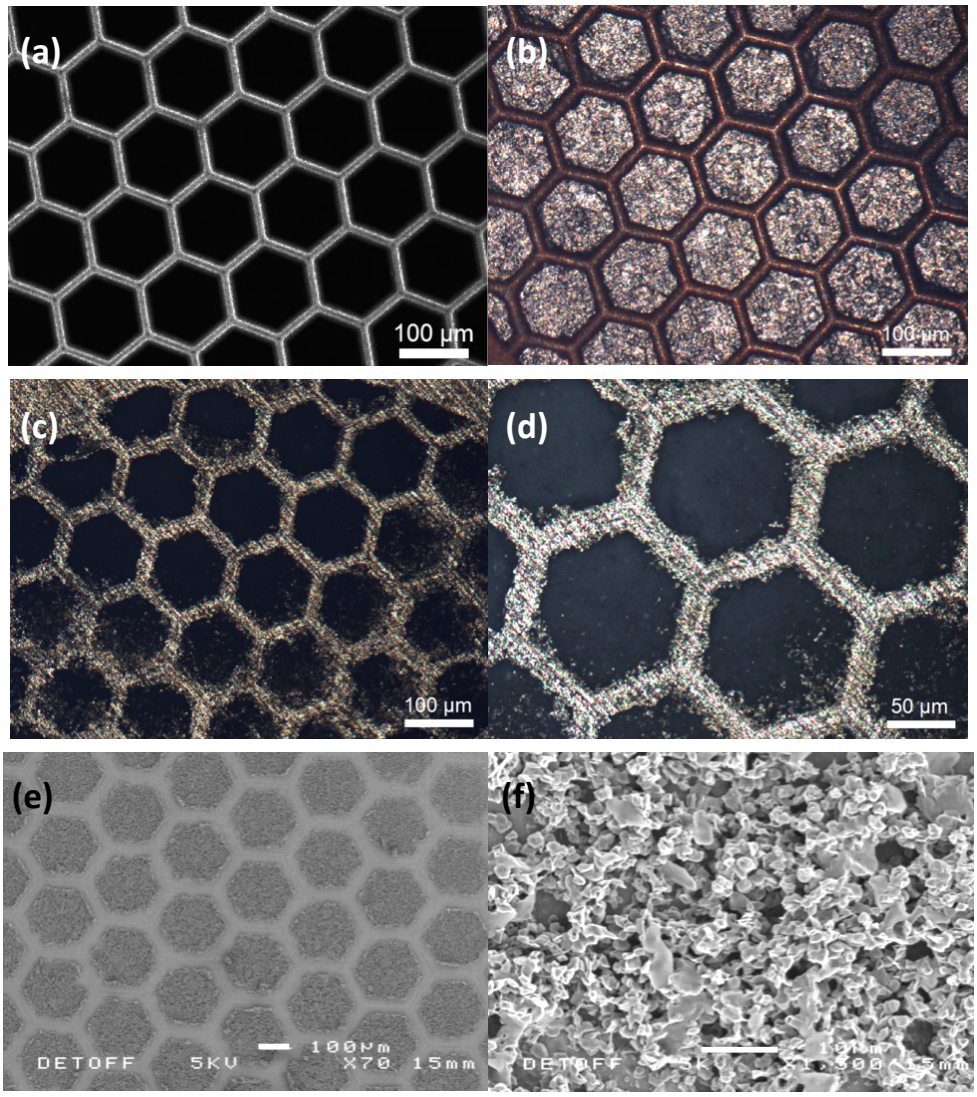

Figure 5.3: (a)–(d) show optical micrographs of: (a) hexagonal template, (b) pattern with template on substrate, (c) pattern on substrate at 5x magnification, (d) pattern on substrate at 10x magnification, and (e)–(f) show scanning electron micrographs of (e) pattern on substrate at 70x magnification and (f) pattern on substrate at 1500x magnification. (b)–(f) pattern is 5 wt.% PCL; flow rate, applied voltage and collection time, 10 µl.min-1, 11 kV and 300 s respectively.

The equivalent diameters of the hexagonal islands were controlled at 95 μm (standard deviation 6 μm) and the spaces between the islands have a mean of 35 μm. The spaces between the islands were kept constant and varied by only a few micrometres. The same template was used for all experiments so the shape and size of islands across the entire pattern were kept constant. Since the spray time was controlled at 300 s during the process, the height of the 'islands' in the patterns was kept constant and had a mean of 33.4 μm.

Figure 5.3f shows that the pattern exhibits a microporous surface. This is beneficial for cell attachment as the surface more closely mimics the natural microstructure of cancellous bone, thereby enhancing bioactivity (Lewandrowski et al., 2003).

5.5 The effect of flow rate and solution concentration on pattern thickness

The effect of flow rate and solution concentration on the thickness of the surface patterns was compared. **Figure 5.2b** shows that the stable cone jet mode was maintained over the largest range of applied voltage when the solution was 5 wt.% PCL in DMAC. The flow rate was varied from 1–25 $\mu l.min^{-1}$. The lower flow rate reduced the speed at which the solution reaches the tip of the nozzle, and decreased the droplet size of the spray.

Scattering was increased as the flow rate increased and the patterns appeared denser. This can be observed where the pattern produced when flow rate was 20 $\mu l.min^{-1}$ (**Figure 5.4c)** is denser than the 10 $\mu l.min^{-1}$ pattern **Figure 5.4a.**

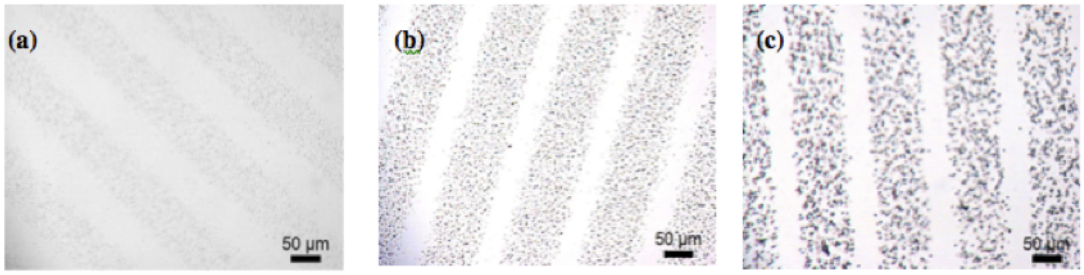

Figure 5.4: The effect of flow rate on coating geometry for 5 wt.% PCL in DMAC, 30 s collection time with flow rate: (a) 10 µl.min^{-1}, (b) 15 µl.min^{-1} and (c) 20µl.min^{-1}.

However, when the flow rate reached 25 µl.min^{-1}, the jet became ineffective in producing clear patterns as the templates lifted up from the surface of the substrate as a greater proportion of the solvent had not evaporated. The templates became difficult to remove as much of the pattern would peel away. The more viscous solutions (15 wt.% PCL in DMAC) also tended to block the needle at low flow rates. At very low flow rates, the patterns were very thin after the fixed collection time. The optimal flow rate for 2, 5 and 10 wt.% PCL was found to be 10 µl.min^{-1}.

It was observed that as flow rate increased from 10–20 µl.min^{-1}, the thickness of the deposit increased by 4.3%, therefore the deposit thickness is directly proportional to the flow rate. It was also observed that as solution concentration increased from 2 to 15 wt.% PCL, the thickness of the deposit increased by 9.14%, therefore the deposit thickness is directly proportional to the solution concentration. These relationships are shown in **Figure 5.5**.

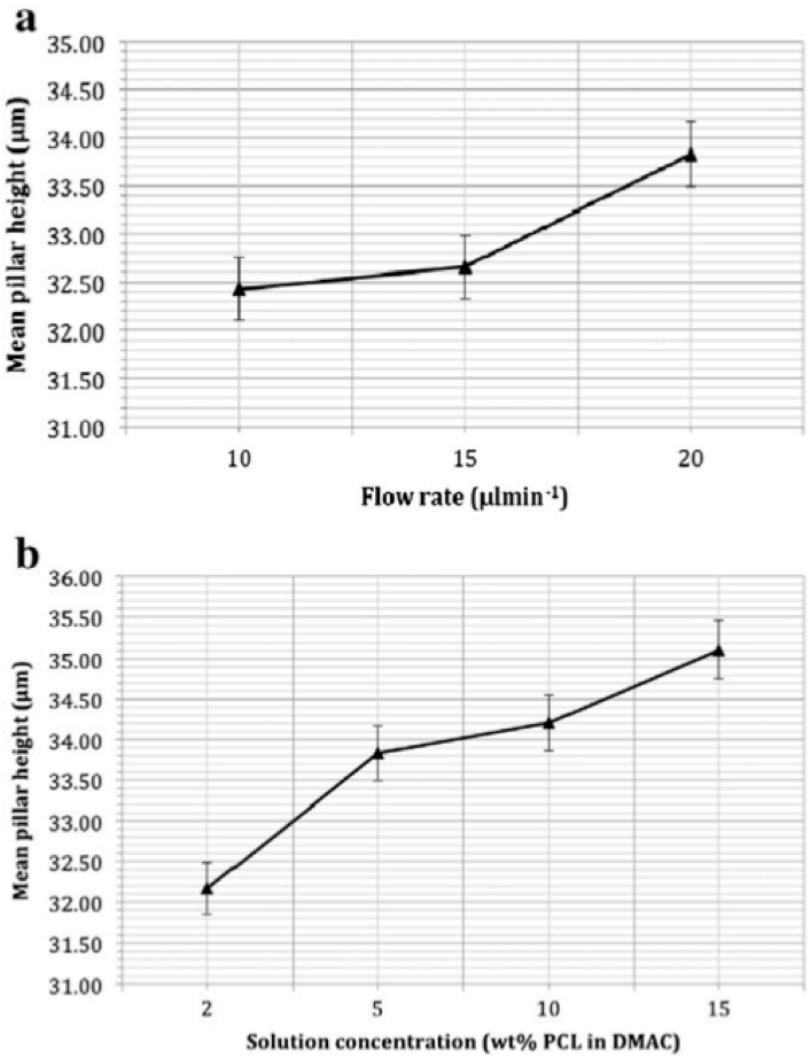

Figure 5.5: (a). Flow rate vs. mean pattern height for 5 wt.% PCL at flow rate 10–20 µl.min^{-1}. (b). Solution concentration vs. mean pattern height for 2–15 wt.% PCL at 20 µl.min^{-1}.

5.6 Mechanical properties of PCL patterns

A typical load–displacement curve obtained during the nanoindentation on a polymer pattern is shown in **Figure 5.6a**. The continuous curve for the complete cycle of loading and unloading indicates good adhesion of the patterns to the substrate. It is also suggesting that there is no cracking or delamination of the polymer pattern on the substrate. The hardness of the polymer patterns was calculated from the

maximum load and the contact area of the indentation. The effective elastic modulus was derived from the initial slope of the unloading cycle and the contact area of the indentation (Zhou and Komvopoulos, 2006).

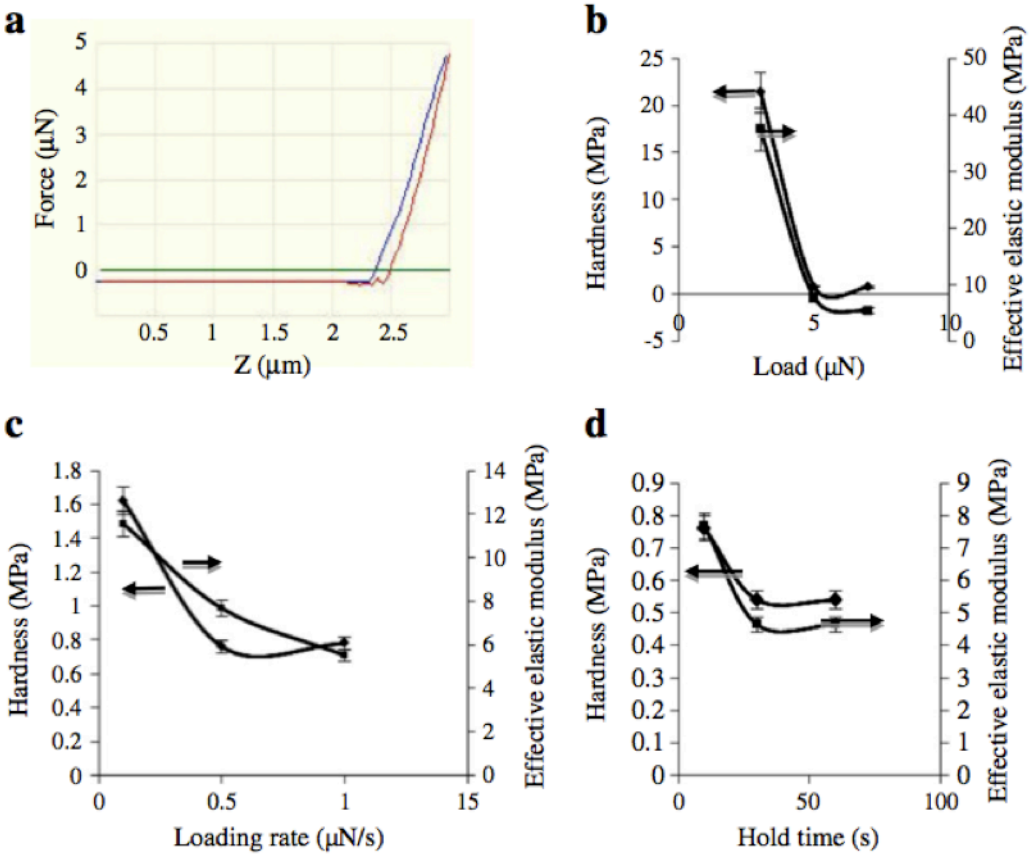

Figure 5.6: (a) A typical load–displacement curve obtained from the nanoindentation test on the polymeric pattern with a loading rate of 1 μN.s^{-1}. Variation of hardness and effective elastic modulus with (b) load, (c) loading rate, and (d) holding time.

Figure 5.6b shows the effect of load on the polymer patterns at a loading rate of 0.5 μN.s^{-1} and a hold time of 10 s. The hardness is decreased with the increase of load and was unchanged thereafter. A similar trend is seen for effective elastic modulus where it is reduced from ~37 MPa to ~8 MPa.

The decrease in hardness and effective elastic modulus is due to micropores observed in the polymer patterns where higher loads penetrate easily in the microporous

polymer structures. This is in good agreement with the results of Fang and Chang (Fang and Chang, 2004) for polycarbonate polymer films. However, in contrast Geng et al. (Geng et al., 2005) observed an increase in effective elastic modulus with the applied load. They attributed this effect to the substrate of the polymer films. Moreover, the film thickness was ≤1 μm and this may have played a part. In this work the thickness of the polymer pattern is >1 μm.

Recently, Mammeri et al. (Mammeri et al., 2012) investigated the increase in hardness and the effective elastic modulus of the polymethylmethacrylate-based hybrid coating as a function of indentation depth. At a lower indentation depth the mechanical response is dominated by film properties whereas at a higher indentation depth the properties were controlled by the substrate. Indeed, the effect of substrate could be considered as two springs in series and calculated using the reciprocal exponential function (Mencik et al., 1997). It has been demonstrated that the indentation depth of <30% of the thickness of the film assists to eliminate the substrate effect. During the indentation measurements in the present work, the indentation depth was kept at <30% of the thickness of the film and the possible reason for decrease in mechanical properties is solely due to micropores observed in the polymer patterns.

The hardness and effective elastic modulus of polymer patterns with regard to loading rate was analysed and shown in **Figure 5.6c**. The hardness is 1.6 MPa at a loading rate of 0.1μN.s^{-1} and nearly halved when the load rate was increased to 1 N.s^{-1}. The effective elastic modulus of ~12 MPa is obtained for a load rate of 0.1 μN.s^{-1}. This is double the value calculated for a loading rate of 1 μN.s^{-1}. This shows that both of these properties are sensitive to loading rate. Beake et al. (Beake et al., 2002) reported that there is little influence of loading rate on the hardness and the effective

elastic modulus of plasma polymerised films. This is opposed to the observation of Fang and Chang (Fang and Chang, 2004) where there is a decrease in both of these proper- ties with the loading rate. It is well known that the grain size, segregation and the morphology of the metals, alloys and ceramics play a vital role in mechanical properties (Pellicer et al., 2011, Yaghoubi et al., 2010). It is less known how mechanical properties change in polymer films with different conditions. Zhou and Komvopoulos (Zhou and Komvopoulos, 2006) attributed a remarkable increase of stiffening at the vicinity of the film/substrate interface to loading rate to restricted molecular movement. In fact, they have shown that for larger indentation depth, increase in loading rate dramatically increased the stiffness compared to lower indentation depth. This observation suggests that there is different viscoelastic behaviour through thickness. In addition, the surface of the polymer has a rapid response to any change in condition compared to the bulk of the polymer due to less entanglement interaction (Zhou and Komvopoulos, 2006). Zhao et al. (Zhao et al., 2006) have shown that elastic-plastic indentation of porous materials is different to dense materials. Indeed, the porosity is shown to decrease the hardness of the materials.

The variation of hardness and the effective elastic modulus with the hold time is shown in **Fig 5.6d**. At a shorter hold time both the hardness and the effective elastic modulus are higher compared to a longer hold time. It is also seen that in increasing the hold time, both of these properties were kept constant. This agrees well with observations of Geng et al. (Geng et al., 2005) on ultra-thin polymeric films. It is generally accepted that the deformation of polymers is viscoelastic. The viscoelastic relaxation behaviour of polymer thin films is influenced by both the bulk viscoelastic material properties, and interface effects. Johnson and Stafford (Johnson and Stafford, 2010) have shown that the thickness of the film, cross-link density and the

chemical bond near the interface affect the relaxation behaviour of polymer films. On the one hand, at a shorter holding time, the dominant mechanical response results from the surface of the polymer film and its relaxation. On the other hand, at a longer holding time, the effect of bulk polymer and the interface between the film and the substrate will dominate. The relaxation behaviour of the polymer chains at these length scales will be different and results in the change in mechanical properties of the films.

5.7 TAEA of other polymers onto flat titanium substrates

This section demonstrates that the range of polymer materials applied via TAEA can be extended to include other biopolymers including polymethylsilsesquioxane (PMSQ) in ethanol solution, and polyurethane (PU) in dimethylformamide (DMF) solution. This is the first time a range of polymers has been used as a coating material for TAEA. As before, solutions were characterised in terms of density, viscosity, surface tension and electrical conductivity to investigate how they affect the TAEA process and resultant patterns. The substrates used here are flat pure titanium. The physical properties of the polymer solutions are detailed in **Table 5.2**.

Table 5.2: Solution properties of PU in DMF and PMSQ in ethanol

Solution	Density ($kg.m^{-3}$)	Viscosity (mPa.s)	Surface tension ($mN.m^{-1}$)	Electrical conductivity ($S.m^{-1}$)
DMF	945±37	0.92±0.1	36±3	4.5±0.4
5wt.% PU in DMF	962±37	0.95±0.1	42±4	2.6±0.3
10wt.% PU in DMF	976±37	0.97±0.1	46±3	2.1±0.3
15wt.% PU in DMF	989±37	0.99±0.1	48±4	1.1±0.2
Ethanol	790±23	1.3±0.01	23±0.3	$0.1x10^{-4}$
5wt.% PMSQ in ethanol	806±24	1.01±0.01	21.4±0.3	$4.9x10^{-4}$
10wt.% PMSQ in ethanol	812±17	1.03±0.01	22±0.2	$6.6x10^{-4}$
15wt.% PMSQ in ethanol	820±18	1.04±0.02	22.3±0.2	$7.3x10^{-4}$

In this study, TAEA is further developed for the application of predetermined polymer patterns on flat titanium substrates for the first time. **Figure 5.7** shows typical results for PMSQ and PU. They show that TAEA of these polymers is possible. The results obtained are verified by way of analysis of the pattern morphology.

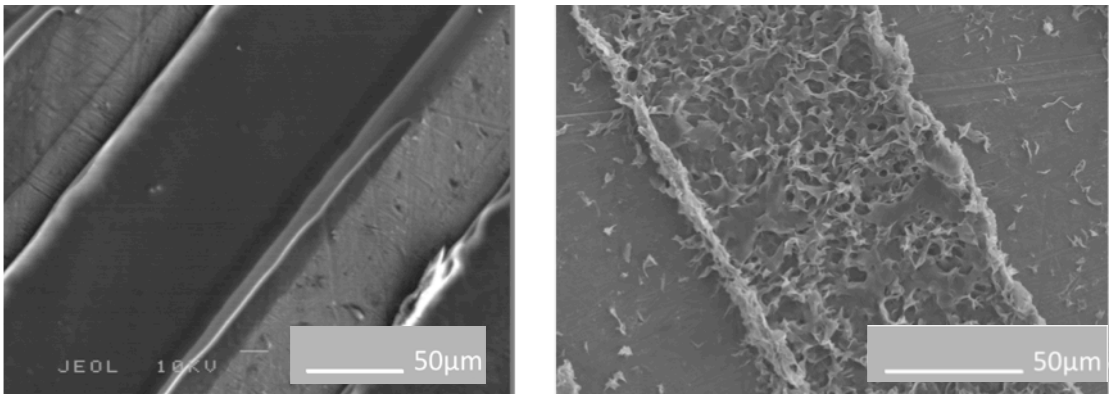

Figure 5.7: Scanning electron micrographs of (a) 50µm parallel line pattern (from template) of 10wt.% PMSQ in ethanol (b) Same template pattern yielded from 10wt.% PU in DMF solution. Flat Ti substrates. Parallel line copper templates with strut width of 50 µm and inter-strut spacing of 100 µm were employed. Flow rate, applied voltage and collection time, 20 µl.min^{-1}, 11 kV and 300 s respectively for both.

A clear correlation between the template shape and size and the achieved pattern was established. It was observed that the coating adhered well to the metal substrate because, on template removal, the boundary between coated and uncoated substrate was well defined.

Results for 10wt.% PMSQ in ethanol, using a parallel template with strut width of 50 µm, spacing of 100 µm, show that the mean distance between patterned lines (interline spacing) is 52 µm and the mean line width is 96 µm (standard deviation 3 µm and 9 µm, respectively). Flow rate was 20 µl.min^{-1}, applied voltage of 10kV, collection distance 80 mm and collection time of 300s.

Results for 10wt.% PU in DMF, using a parallel template with strut width of 50 µm, spacing of 100 µm, show that the mean distance between patterned lines (interline spacing) is 54 µm and the mean line width is 92 µm (standard deviation 7 µm and 12

µm and 9 µm, respectively). Flow rate was 20 µl.min^{-1}, applied voltage of 10kV, collection distance 80 mm and collection time of 300s.

Results for 10wt.% PU in DMF, using a parallel template with strut width of 50 µm, spacing of 100 µm, show that the mean distance between patterned lines (interline spacing) is 54 µm and the mean line width is 92 µm (standard deviation 7 µm and 12 µm, respectively). Flow rate was 20 µl.min^{-1}, applied voltage of 10kV, collection distance 80 mm and collection time of 300s.

This images show that this pattern exhibited porosity on the pattern surface. Mean pore size for 10wt.%PU is 3.29µm ± 0.8µm i.e. macroporosity. When the solution concentration was increased to 15wt.% PU, pore size increased by 7% to 3.52µm ± 0.9µm. When the solution concentration was decreased 5wt.% PU, pore size decreased by 6% to 3.09µm ± 0.5µm. This is likely due to the increasing viscosity and surface tension as solution concentration increases. Future work could further investigate this phenomenon.

Macroporosity greatly induces bioactivity and cell-spreading process as it supports cell intrusion in the materials or cells ingrowth and cell attachments. Therefore it may be desirable for the pattern to have a macroporous surface as it mimics the natural surface of bone in the human body. The ability to control porosity morphology of a surface is beneficial to the control of the rate of cell growth. On initial contact, cells stretch across macropores and then deeper into the coating, aiding cell migration. The optimal size for macroporosity is dependent on the type of cell and the bioactivity of the materials. However, porosity compromises the mechanical properties of the pattern. There is potential to best utilise this porous microstructure by applying it as a

surface layer to improve bioactivity, without compromising mechanical properties of the bulk coating material.

The same template shape was used for all experiments so the shape and size of patterns across the entire coating were kept constant. Since the collection time was controlled at 300 s during the process, the mean height of the patterns (normal to the substrate surface) was approximately constant (42 ± 7 µm measured by way of SEM image analysis) on all substrates.

5.8 Summary

A method of producing polymeric patterns has been developed with a high degree of control over the pattern geometry (via template choice) and thickness (via collection time). Optimal results were obtained with 5 wt.% PCL in DMAC solution sprayed within the stable cone jet mode window at a flow rate of 15 µl.min^{-1} for 300 s at 11.1 kV with a working distance of 60 mm. Hexagonal patterns were repeatable and well-defined, with a thickness of ~34 µm.

The TAEA method can be carried out at ambient temperature, and key processing control parameters such as applied voltage and flow rate are easily adjustable. The ideal processing window of stable jetting was defined in terms of operating parameter ranges for flow rate, and applied voltage, as well as physical solution properties such as viscosity and electrical conductivity. More viscous solutions (10 wt.% PCL in DMAC as opposed to 5 wt.%) were found to require increased upper and the lower limits of applied voltage to form stable cone jetting. The polymer concentration was systematically varied from 2 to 15 wt.% PCL in DMAC, with flow

rate from 1 to 25 µl.min^{-1}. The diameters of the hexagonal islands were controlled at 95 µm (standard deviation 6 µm) and the spaces between the islands have a mean of 35 µm. The spaces between the islands were kept constant and varied only by a few micrometers.

The height of the 'islands' in the patterns had a mean of ~34 µm after 300 s of spraying. It was observed that as collection time increased, the thickness of the deposit increased. The patterns exhibit a microporous surface.

The mechanical properties of the polymer patterns were evaluated using nanoindentation. The hardness is 1.6 MPa at a loading rate of 0.1 µN.s^{-1} and nearly halved when the load rate was increased to 1 µN.s^{-1}. The effective elastic modulus of ~12 MPa is obtained for a loading rate of 0.1 µN.s^{-1}. This is double the value calculated for a load rate of 1 µN.s^{-1}. There is a clear variation of hardness and the effective elastic modulus with change in load, loading rate and the hold time.

Results using PU and PMSQ as coating materials for TAEA have shown that the TAEA process is versatile and can apply patterns of other polymers onto titanium substrates suitable for orthopaedic implant applications. 10wt.% PMSQ in ethanol yielded patterns with interline spacing 52 µm and mean line width 96 µm (standard deviation 3 µm and 9 µm, respectively). 10wt.% PU in DMF yielded patterns with interline spacing 54 µm and mean line width 92 µm (standard deviation 7 µm and 12 µm, respectively). For both, flow rate was 20 µl.min^{-1}, applied voltage of 10kV, collection distance 80 mm and collection time of 300s.

The PU patterns exhibited porosity on the pattern surface, with mean pore size 3.29µm ± 0.8µm for 10wt.% PU patterns. As solution concentration increases, it was

observed that pore size also increases, likely due to the increasing viscosity and surface tension of the solution. There is potential to best utilise this porous microstructure by applying it as a surface layer to improve bioactivity, without compromising mechanical properties of the bulk coating material.

6. Template-assisted electrohydrodynamic atomisation (TAEA) of ceramic patterns on metallic substrates

6.1 Introduction

Adapting template-assisted electrohydrodynamic atomisation (TAEA) spraying for application on a range of metallic substrate materials will further evidence the versatility of the process, demonstrating its potential for coating orthopaedic implants. The process parameters and the coating suspensions can be adjusted in order to achieve the appropriate chemistry and microstructures for orthopaedic implants like total hip replacements (THRs).

A suspension of titanium dioxide in ethanol was patterned onto various flat metallic substrates, followed by an interlocked coating of hydroxyapatite (HA) to improve coating adhesion (Chi et al., 2013). Physical properties of the coating suspensions, including density and surface tension were characterised so that their effect on resultant coating microstructures could be ascertained. Pure titanium, titanium alloys Ti90-Al6-V4 and Ti78.8-Mo15-Nb3-Al3-SiO(0.2) and 316L stainless steel were the metallic substrates used. These were chosen due to their wide use in joint replacements and medical implants for orthopaedics. After coating, the microstructure and surface morphology of the patterns/coatings deposited on each substrate was analysed via optical and scanning electron microscopy.

One of the key benefits of TAEA over more common, high-temperature (15,000°C) industrial deposition techniques such as vacuum plasma spraying is that it can be carried out at ambient temperature. Therefore, the effect of heating the titanium dioxide deposits was investigated to ascertain whether further consolidation of the 'green' unsintered samples had an effect on hardness and elastic modulus of the patterns. Separate sets of TiO_2 TAEA-patterned flat Ti substrate samples (three used for each temperature) were heated to 100°C, 200°C, 300°C, 400°C, 500°C, 600°C, 700°C and 800°C, from ambient temperature at a ramp rate of 1°C.min^{-1}, and cooled slowly back to ambient temperature by way of annealing. They were then analysed by way of nanoindentation in the same way as the initial, unheated patterns, and the hardness and elastic modulus were recorded.

6.2 The effect on TAEA patterns and coatings on different metallic substrates

Titanium and its alloys suitable for use in load-bearing orthopaedic implants because they are relatively lightweight with high fatigue strength, and have good corrosion resistance and biocompatibility. Their biocompatibility is derived from the thin oxide layer that forms on its surface *in vivo*. This layer on its own is insufficient for biological fixation as it can be inconsistent and biologically inactive. A layer of titanium dioxide can be applied via TAEA to create an interface onto which hydroxyapatite (HA) can adhere, improving the biological fixation of bone onto the coated implant (Sebbowa et al., 2011). TAEA process parameters were varied, including the suspension concentration of TiO_2 in ethanol (1-10 wt.%) and HA in ethanol (1-10 wt.%), and flow rate (10-20µl.min^{-1}).

6.2.1 Suspension characterisation of TiO_2 and HA in ethanol

Suspension properties for titanium dioxide in ethanol suspension were given in Chapter 4, **Table 4.1**, and the HA suspensions are given in **Table 6.1**. This table shows how the measured physical properties of the suspension vary with respect to concentration, from 100 wt.% ethanol to 10 wt.% HA in ethanol. The electrical conductivities of the suspensions were in the range $0{\cdot}1\text{-}1.6 \times 10^{-4}$ $S.m^{-1}$. The addition of 10wt.% HA caused the density to increase by 19%, viscosity by 4.5 times and surface tension by 28% respectively. This affects the ability and readiness of the suspension material to achieve stable jetting under the influence of an electric field. Therefore, it was found that 6wt.% HA was ideal for coating in the stable cone jet mode (not too viscous but electrically conductive enough), which is necessary to generate homogeneous droplets.

Table 6.1: HA suspension properties

Suspension	**Density ($kg.m^{-3}$)**	**Viscosity (mPa.s)**	**Surface tension ($mN.m^{-1}$)**	**Electrical conductivity ($S.m^{-1}$)**
Ethanol	790	1.3	23	$0.1x10^{-4}$
1wt.% HA in ethanol	902	4.6	25	$0.8x10^{-4}$
2wt.% HA in ethanol	910	5.2	26	$0.8x10^{-4}$
4wt.% HA in ethanol	926	5.7	27	$1.0x10^{-4}$
6wt.% HA in ethanol	**930**	**6.8**	**28**	**$1.2x10^{-4}$**
8wt.% HA in ethanol	937	7.1	29	$1.4x10^{-4}$
10 wt.% HA in ethanol	943	7.2	32	$1.6x10^{-4}$

6.2.2 Interlocked pattern characterisation on metallic substrates

In this study, TAEA is further developed for the application of predetermined TiO_2 patterns and HA interlocked coatings on flat titanium alloy and stainless steel substrates for the first time. **Figure 6.1** shows typical results for titanium, 316L stainless steel and titanium alloys. They show that this is indeed possible, with results

comparable to that of existing research on pure titanium flat substrates. The results obtained are verified by way of analysis of the pattern morphology.

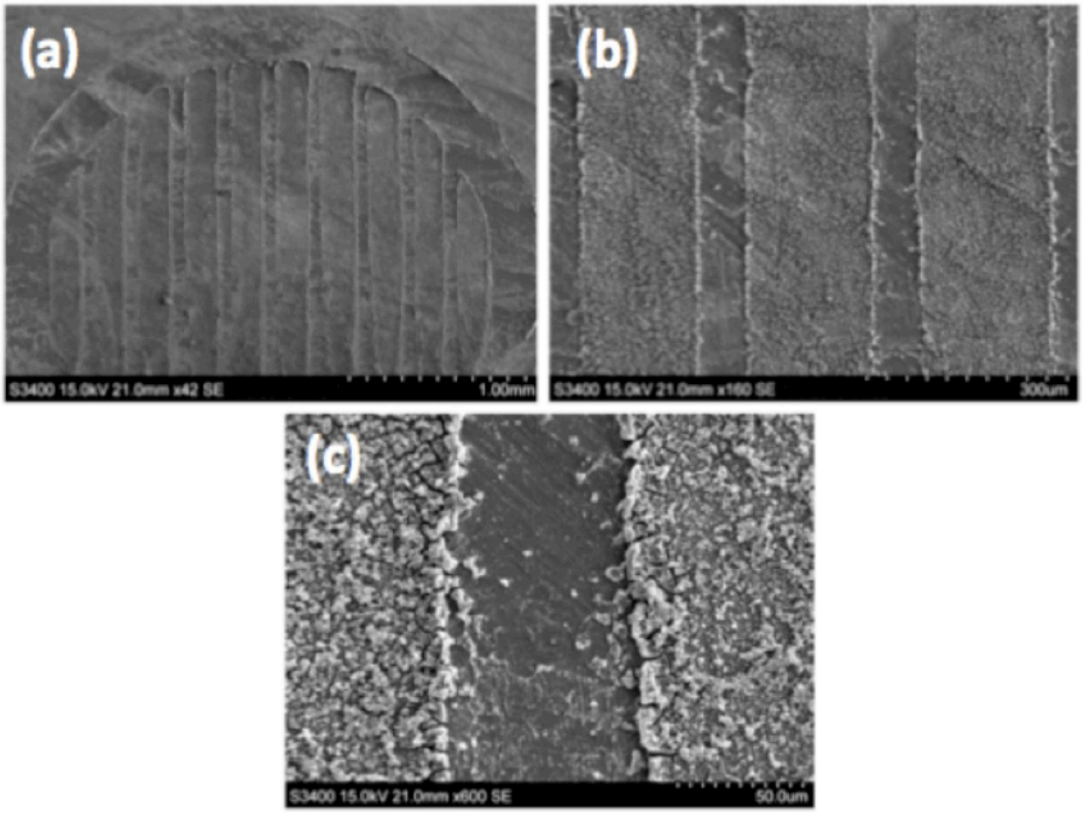

Figure 6.1: Optical micrographs of: (a)-(c) Interlocked HA on TiO_2 pattern on flat 316L stainless steel substrate using parallel copper template with strut width of 50 µm and inter-strut spacing of 100 µm. All images depict spraying of suspension 4 wt.% TiO_2 and 6wt.% HA with flow rate, applied voltage and collection time 20 $\mu l.min^{-1}$, 10 kV and 300s, respectively.

A clear correlation between the template shape and size and the achieved pattern was established. It was observed that the coating adhered well to the metal substrate because, on template removal, the boundary between coated and uncoated substrate was well defined. The template geometry was still visible after the application of the interlocked overlay of HA. **Figure 6.2** shows how the two layers fit onto the substrate.

Figure 6.2: Schematic cross-section of TiO_2 buffer layer and HA overlay on a substrate (Edirisinghe, 2010)

Figure 6.1 also shows that interlocked HA coatings have been sprayed onto flat 316L stainless steel substrates with uniform and ordered topography. Results for the parallel template (with strut width of 50 µm, spacing of 100 µm) show that the mean distance between patterned lines (interline spacing) is 56 µm and the mean line width is 95 µm (standard deviation 6 µm and 11 µm, respectively). This was achieved when 4 wt.% TiO_2 was applied as a pattern, with 6wt.% HA was sprayed continuously over the top. For both suspensions, flow rate was 20 $\mu l.min^{-1}$, applied voltage of 10kV, collection distance 80 mm and collection time of 300s.

For interlocked HA coatings sprayed on flat Ti alloy substrates, the mean distance between patterned lines (interline spacing) is 58 µm and the mean line width is 95 µm (standard deviation 5 µm and 11 µm, respectively). For coatings on flat Ti substrates, the mean distance between patterned lines (interline spacing) is 52 µm and the mean line width is 96 µm (standard deviation 6 µm and 11 µm, respectively).

The same template shape was used for all experiments so the shape and size of patterns across the entire coating were kept constant. Since the collection time was controlled at 300s during the process, the height of the patterns (normal to the substrate surface) was kept approximately constant (75 ± 13 µm measured by way of SEM image analysis) on all substrates.

6.2 Effect of heat treatment in air to TiO_2 patterns on Ti

One of the key benefits of TAEA over more common, high temperature (15,000°C) industrial deposition techniques such as vacuum plasma spraying is that it can be carried out at ambient temperature. Therefore, the effect of heating the titanium dioxide deposits was investigated to ascertain whether further consolidation of the 'green' unsintered samples had an effect on hardness and elastic modulus of the patterns. Separate sets of TiO_2 TAEA-patterned flat Ti substrate samples (three used for each temperature) were heated to 100°C, 200°C, 300°C, 400°C, 500°C, 600°C, 700°C and 800°C, from ambient temperature at a ramp rate of 1°C.min^{-1}, and cooled slowly back to ambient temperature by way of annealing. They were then analysed by way of nanoindentation in the same way as the initial, unheated patterns, and the hardness and elastic modulus were recorded.

Figure 6.3 shows that hardness is not significantly affected by post- pattern heating to consolidate the TiO_2 on the metallic substrate, as this increases by only 5 to 2% from 100°C to 800°C. In fact, the elastic modulus reduces by 2 to 8% on heating to 500°C and then remains comparatively unaffected. However, if other organic bioactive species are included in the TAEA process at ambient temperature, post-deposition heating is to be avoided as it can lead to the degradation of these species. Therefore

it is encouraging that the results in **Figure 6.3** do not show marked mechanical property enhancement by post-deposition heat treatment, although this aspect will be further investigated in future work.

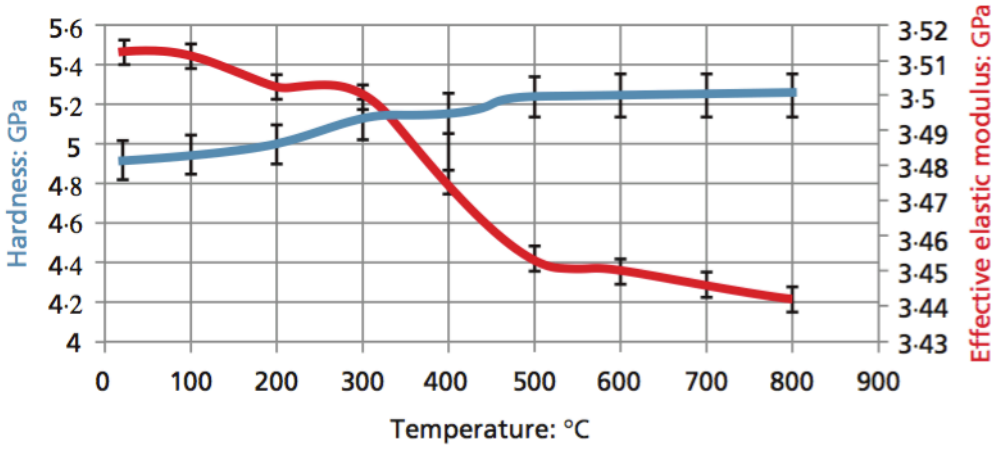

Figure 6.3: Variation of hardness and effective elastic modulus with heat treatment temperature from 20°C (ambient temperature, i.e. no heat treatment) to 800°C. Load is 5 µN, loading rate is 1 µN.s^{-1}. Values are means of three separate samples.

6.3 Summary

Interlocked TiO_2 coatings and HA coatings on pure titanium, titanium alloys and 316L stainless steel have been successfully produced via TAEA. This is the first time this process has been applied to these metallic substrates, all of which are relevant to orthopaedic applications. 4wt.% TiO_2 in ethanol and 6wt.% HA in ethanol were found to yield the most repeatable and accurate results on all metallic substrates investigated. Post-patterning heat treatment does not show marked enhancement of deposit mechanical properties and, although this requires more intensive investigation on curved surface TAEA samples, is a positive finding in terms of incorporating other temperature-sensitive bioactive materials during manufacture.

7. Conclusions

The conclusions of this research are summarised as follows:

1. The TAEA spraying of bioceramic suspension and polymer solutions in the stable cone jet mode was studies. It was found that the media concentration, the flow rate, the applied voltage and the spraying time had a significant influence on the morphology of the resultant coatings.

2. TAEA has been shown to produce TiO_2 patterns on curved Ti substrates with a high degree of control over the pattern geometry (by way of template choice) and thickness (by way of collection time). TiO_2 patterns with parallel lines have been successfully produced on both convex and concave Ti substrate diameters of $\sim$25mm. Optimal results were obtained with 4 wt.% TiO_2 in ethanol suspension sprayed within the stable cone jet mode window at a flow rate of 20 $\mu l.min^{-1}$ for 300 s at 10 kV with a collection distance of 80 mm.

3. A clear correlation between the template shape and size and the achieved pattern was established, therefore the template can be chosen to reflect the specific clinical needs of the coating.

4. Since the collection time was controlled at 300 s during the process, the height of the patterns (normal to the substrate surface) was kept approximately constant.

5. For TiO_2 patterns at a loading rate of 1μN.s^{-1} and a hold time of 1 s, hardness decreases as load increases up to 7 μN and remains at 0·1 GPa up to higher loads. Elastic modulus behaves in a similar way. This decrease can be attributed to the microporosity observed in the TiO_2 deposits, as higher loads are able to penetrate more easily into microporous structures.

6. For TiO_2 patterns, hardness is 7·5 GPa at a loading rate of 0·1 μN.s^{-1}, and reduces to 7·3 GPa when the loading rate is increased to 1 μN.s^{-1}. This is only a 2% decrease, thus the hardness is not significantly affected by the loading rate due to the brittle nature of the TiO_2 ceramic. With respect to effective elastic modulus, this is found to be 7·5 GPa at a loading rate of 0·1 μN.s^{-1}, and reduces to 7·3 GPa when the loading rate is increased to 1 μN.s^{-1}. This again is a 2% decrease, so we can conclude that elastic modulus is also not significantly affected by loading rate within these parameters.

7. It was also found that for TiO_2 patterns, hardness was not significantly affected by post-pattern heating to consolidate the bioceramic on the metallic substrate, as this increased by only 5·2% from 100°C to 800°C. In fact, the elastic modulus reduced by 2·8% on heating to 500°C and then remained comparatively unaffected. No marked mechanical property enhancement was observed by post-deposition heat treatment, although this aspect will be further investigated in future work. Post-patterning heat treatment does not show marked enhancement of deposit mechanical properties.

8. For PCL polymer patterns, hardness was found to be 1.6 MPa at a loading rate of 0.1 μN.s^{-1} and nearly halved when the load rate was increased to 1 μN.s^{-1}. The effective elastic modulus of ~12 MPa was obtained for a loading rate of 0.1 μN.s^{-1}. This is double

the value calculated for a load rate of 1 $\mu N.s^{-1}$. There is a clear variation of hardness and the effective elastic modulus with change in load, loading rate and the hold time.

9. A method of producing polymeric patterns has been developed with a high degree of control over the pattern geometry (via template choice) and thickness (via collection time). Optimal results were obtained with 5 wt.% PCL in DMAC solution sprayed within the stable cone jet mode window at a flow rate of 15 $\mu l.min^{-1}$ for 300 s at 11.1 kV with a working distance of 60 mm. Hexagonal patterns were well-defined and repeatable with thickness of ~34 µm.

8. Future work

Based on the research conducted and its outcomes, the following aspects of further investigations are recommended:

1. Pure ethanol was used as the solvent to suspend titanium dioxide (TiO_2) and hydroxyapatite (HA) in a liquid so that they could be applied via template-assisted electrohydrodynamic atomisation (TAEA). Future work could involve further expanding the range of solvent liquid carriers for bioceramics, comparing how physical and spray properties affect the nature of jet break-up process and the microstructure of resultant patterns and coatings. This can be extended for solvents required for polymer TAEA. Solvents dictate the minimum concentration of the coating material in solution for a Taylor cone to form and stable cone jetting to occur, thus TAEA spraying to be carried out. This will then affect the morphology of the resultant particles and patterns deposited on the substrate.

2. A greater range of ceramic coatings could also be investigated, including silicon-substituted hydroxyapatite, other calcium phosphates, and mixtures of ceramics (for example a mixture of TiO_2 sol and HA in suspension). Hydroxyapatite with different powder particle sizes and shapes could also be investigated, and how this affects the microstructure and mechanical strength to the HA patterns and coatings. For these materials, similar optimal process parameters should be evaluated, including flow rate, applied voltage, collection distance and collection time.

3. Future work could investigate the co-feeding of other bioactive species during TAEA as this is easily accommodated if co-axial nozzles are used curved surface TAEA heat treatment mechanical property enhancement by post-deposition heat treatment, although this aspect will be further investigated in future work.

4. The literature shows that TAEA has previously been employed to produce interlocked ceramic HA coatings (Li et al., 2011, Li et al., 2008) on flat titanium substrates. This consisted of a patterned TiO_2 buffer layer and an HA coating on top. Thus, initial experimentation yielded parallel line deposits with a mean diameter of 45µm (standard deviation 5µm), spaced 20µm apart. The literature shows HA patterns from hexagonal templates can be produced and controlled within 30µm (standard deviation 2µm) spaced ~7µm apart (Li et al., 2011). Therefore, future work could be carried out to further improve the resolution of HA coatings by using finer template (with smaller island diameter and spacing than 30µm and 7µm respectively) during the patterning process for use with ceramics. The characterisation results from these coatings could then be used as a control to compare the influence of polymer and ceramic-polymer composite coatings compared to the industry standard of HA coatings.

5. Results from Chapter 6 on biopolymer TAEA showed that polyurethane, thus potentially other polymers too, can deposit macroporous patterns on metallic substrates. Further work could investigate how to control the mean pore size of these pores, and the porosity in terms of % volume vacant space. It would be valuable to better understand this so that the reasons for this porosity could be better understood, and thus further controlled. Another area of investigation is the development of TAEA for use with ceramic-polymer composites and sandwich

coatings of HA and PCL. A similar range of processing parameters will be followed so the results can be compared with pure PCL coatings and pure HA coatings.

6. It would be beneficial to develop this processing technique onto curved surfaces, as these substrates are more representative of the three-dimensional metallic implants utilised in orthopaedic treatments such as total joint replacement. The range of diameters would be increased for both convex and concave substrates. An automated linear conveyor mechanism could be developed to move substrates during coating, to simulate an automated process. The platform could rotate to facilitate the homogenous coating of substrates. This may not be necessary as TAEA spraying is not a line-of-sight process, but it could speed up the coating process when coating may substrates in quick succession.

7. A greater range of polymers as coating materials could also be investigated, including non-biodegradable polymers onto which active ingredients could be covalently bonded. This would mean that any implant using this type of coating would not have to be classified as a drug-eluting medical implant, and therefore would have a range of potential applications with fewer regulatory requirements than polymer coatings that serve as vehicles for drug delivery. This would increase the applicability and versatility of material produced via TAEA. A greater range of substrate materials could be investigated, including polymer substrates suck as polyether ether ketone (PEEK).

8. Interlocked coatings derived from TAEA have already been proven to control and guide cellular responses of HOB *in vitro* on flat surfaces (Munir et al., 2011). TAEA is capable of applying highly controllable lines and patterns of selected materials onto substrates at ambient temperature. Coating topography has been historically found

to provide powerful signalling for cells, whilst forming contact guidance to influence orientation. The biocompatibility of the coatings could also be determined using cell studies on human osteoblast-like (HOB) cell models.

From the literature, bone-like apatite formed on HA coatings on titanium, after immersion in simulated body fluid. This demonstrates the high *in vitro* bioactivity of HA. Primary human osteoblast (HOB) cells responded to HA patterns by stretching of the filopodia (projections of cytoplasm that extend from migrating cells, beyond the leading edge). The filopodia is bound by the cell membrane, which contains receptors and cell adhesion molecules important for growth and guidance. The filopodia extended between track and pillar deposits, attaching to the apex of the pillar pattern and stretching between two. HOB cells responded to the track pattern by elongating along and between the track, and the length of HOB cells was proportional to the gaps between track patterns, but this relationship was not observed on the pillar patterns. The study therefore provides an insight for the design of future implant surfaces that can control and guide cellular responses. TAEA patterning provides a controllable technique to provide topography to medical implants.

This existing cell work can be extended to TAEA-derived interlocked coatings on curved metallic substrates. Cellular adhesion and proliferation could be investigated, as well as the control of cell alignment on curved 3D titanium substrates on a range of diameters (e.g. 10 to 25mm). Identical parallel line deposits of TiO_2 (100micron wide, 50micron spacing, 10micron thick) with an interlocked overlay of HA could been applied onto curved titanium substrates, as well as flat substrates as a control group. After being sterilised via gamma irradiation, cytotoxicity could be tested via MTT assays (24hr and 72hr elution studies of HOB

media tested at 24 and 48hrs), cell proliferation via Alamar Blue assays, and cell viability via live/dead staining. The biological properties of any coating and substrate materials could be assessed in this way.

9. The mechanical properties of TAEA patterns and coatings could be further investigated and extended beyond nanoindentation. It would be valuable to measure shear strength of the TAEA coatings as this is also particularly relevant to implants such as total hip replacements. Results should be compared to coatings produced via vacuum plasma spraying as well to further demonstrate the benefits of TAEA over the industry standard process. Future work could also further investigate whether marked mechanical property enhancement was observed by post-deposition heat treatment on a wider range of coating materials, including hydroxyapatite and other calcium phosphates, thus extending the current work on TiO_2. No surface treatments were carried out on the substrates, other than cleaning and polishing them. It would be useful to verify that roughening the surface of the substrate does not significantly improve the mechanical adhesion of the coating in the short and long term in biological environments.

10. The shape of the needle could also influence the nature of the electrohydrodynamic jet, and how it breaks up. Parameters to investigate would include needle diameter, needle material, and the geometry of the needle exit. A stainless steel needle with an inner diameter of 300µm and a blunt flat end was used in this study. It was mounted in the resin and was electrically conductive. A range of needle diameters could be investigated, and their tips could be polished to specific angles (e.g. 10-80° diagonal slants), and the resultant impact relics and their size distribution could be analysed. Ideally, relic size (and its size distribution) could be reduced further so that more intricate patterns could be applied repeatedly.

11. A greater range of templates could also be investigated. Copper templates with a diameter of 5mm were used in this study. Future work could use larger templates with a greater range of pattern geometries, particularly smaller strut spacing and different shapes. The effect of template material on pattern microstructure could be analysed so as to optimise control over pattern geometry.

12. Following on from the interlocked TiO_2 and HA coatings produced via TAEA in this study, a systematic comparison of these coatings compared to those produced via vacuum plasma spraying could be carried out. Their mechanical and chemical properties could be compared, as well as the results of biological cell studies. This could give further evidence that TAEA is an improved coating method compared to the industry standard process of vacuum plasma spraying and bring TAEA closer to commercialisation.

References

ABERTURAS, M. R., MOLPECERES, J., GUZMAN, M. & GARCIA, F. 2002. Development of a new cyclosporine formulation based on poly(caprolactone) microspheres. *Journal of Microencapsulation,* 19**,** 61-72.

ABU-AMER, Y., DARWECH, I. & CLOHISY, J. C. 2007. Aseptic loosening of total joint replacements: mechanisms underlying osteolysis and potential therapies. *Arthritis Research & Therapy,* 9, 1-7.

AHMAD, Z., HUANG, J., EDIRISINGHE, M. J., JAYASINGHE, S. N., BEST, S. M., BONFIELD, W., BROOKS, R. A. & RUSHTON, N. 2006. Electrohydrodynamic print-patterning of nano-hydroxyapatite. *Journal of Biomedical Nanotechnology,* 2**,** 201-207.

ANDERSON, J. M. & SHIVE, M. S. 1997. Biodegradation and biocompatibility of PLA and PLGA microspheres. *Advanced Drug Delivery Reviews,* 28**,** 5-24.

BALASUNDARAM, G. & WEBSTER, T. J. 2006. Nanotechnology and biomaterials for orthopedic medical applications. *Nanomedicine,* 1**,** 169-176.

BARBUCCI, R. 2002. *Integrated biomaterial science,* New York, Kluwer/Plenum.

BEAKE, B. D., ZHENG, S. & ALEXANDER, M. R. 2002. Nanoindentation testing of plasma-polymerised hexane films. *Journal of Materials Science,* 37**,** 3821-3826.

BEHIRI, J. C. & BONFIELD, W. 1984. Fracture-mechanics of bone - The effects of density, specimen thickness and crack velocity on longitudinal fracture. *Journal of Biomechanics,* 17**,** 25-34.

BHUSHAN, B. & LI, X. D. 2003. Nanomechanical characterisation of solid surfaces and thin films. *International Materials Reviews,* 48**,** 125-164.

BLACK, J. & HASTINGS, G. 1998. *Handbook of biomaterial properties*, Chapman and Hall.

BONFIELD, W. 1988. Composites for bone replacement. *Journal of Biomedical Engineering,* 10**,** 522-526.

BOURNE, R. B., MALONEY, W. J. & WRIGHT, J. G. 2004. An AOA critical issue the outcome of the outcomes movement. *Journal of Bone and Joint Surgery-American Volume,* 86A**,** 633-640.

BRADBURY, T. A. R., JAMES 2013. *Medical Management of the Surgical Patient*, Cambridge University Press.

CABRINI, M., CIGADA, A., RONDELLI, G. & VICENTINI, B. 1997a. Effect of different surface finishing and of hydroxyapatite coatings on passive and corrosion current of Ti6Al4V alloy in simulated physiological solution. *Biomaterials,* 18**,** 783-787.

CAPELLO, W. N., DANTONIO, J. A., FEINBERG, J. R. & MANLEY, M. T. 1997. Hydroxyapatite-coated total hip femoral components in patients less than fifty years old - Clinical

and radiographic results after five to eight years of follow-up. *Journal of Bone and Joint Surgery-American Volume,* 79A**,** 1023-1029.

CHEANG, P. & KHOR, K. A. 1996. Addressing Processing Problems Associated With Plasma Spraying of Hydroxyapatite Coatings. *Biomaterials,* 17**,** 537-544.

CHEN, H., YUAN, L., SONG, W., WU, Z. K. & LI, D. 2008. Biocompatible polymer materials: Role of protein-surface interactions. *Progress in Polymer Science,* 33**,** 1059-1087.

CHI, M.-H., TSOU, H.-K., CHUNG, C.-J. & HE, J.-L. 2013. Biomimetic hydroxyapatite grown on biomedical polymer coated with titanium dioxide interlayer to assist osteocompatible performance. *Thin Solid Films,* 549**,** 98-102.

CICCONE, W. J., 2ND, MOTZ, C., BENTLEY, C. & TASTO, J. P. 2001. Bioabsorbable implants in orthopaedics: New developments and clinical applications. *The Journal of the American Academy of Orthopaedic Surgeons,* 9**,** 280-8.

CLOUPEAU, M. & PRUNETFOCH, B. 1990. Electrostatic spraying of liquids: Main functioning modes. *Journal of Electrostatics,* 25**,** 165-184.

COATHUP, M. J., COBB, J. P., WALKER, P. S. & BLUNN, G. W. 2000. Plate fixation of prostheses after segmental resection for bone tumours. *Journal of Orthopaedic Research,* 18**,** 865-872.

CURREY, J. D. 1983. Biological Composites. *Handbook of Composites,* 4**,** 503-563.

CURTIS, A. & WILKINSON, C. 1997. Topographical control of cells. *Biomaterials,* 18**,** 1573-1583.

D'ANTONIO, J. A., CAPELLO, W. N., MANLEY, M. T. & GEESINK, R. 2001. Hydroxyapatite femoral stems for total hip arthroplasty - 10-to 13-year followup. *Clinical Orthopaedics and Related Research***,** 101-111.

DAVIS, J. R. 2004. *Handbook of thermal spray technology*, ASM International.

DE GROOT, K., JANSEN, J. A., WOLKE, J. G. C., KLEIN, C. P. A. T. & VAN BLITTERSWIJK, C. A. 1993. Developments in bioactive coatings. *Hydroxylapatite coatings in orthopaedic surgery***,** 49-62.

DE GROOT, K., WOLKE, J. G. C. & JANSEN, J. A. 1998. Calcium phosphate coatings for medical implants. *Proceedings of the Institution of Mechanical Engineers Part H - Journal of Engineering in Medicine,* 212**,** 137-147.

DEARNLEY, P. A. 1999. A review of metallic, ceramic and surface-treated metals used for bearing surfaces in human joint replacements. *Proceedings of the Institution of Mechanical Engineers Part H-Journal of Engineering in Medicine,* 213**,** 107-135.

DERAM, V., MINICHIELLO, C., VANNIER, R. N., LE MAGUER, A., PAWLOWSKI, L. & MURANO, D. 2003. Microstructural characterizations of plasma sprayed hydroxyapatite coatings. *Surface & Coatings Technology,* 166**,** 153-159.

DRAKE, C., ACE, M. & MAALE, G. E. 2002. Revision total hip arthroplasty. *AORN journal,* 76**,** 414-7, 419-27; quiz 428, 431-2.

DUNCAN, R. 2003. The dawning era of polymer therapeutics. *Nature Reviews Drug Discovery,* 2**,** 347-360.

EDIRISINGHE, M. A. N., M. R. 2010. *Investigation of interlocked bioactive coating for orthopaedic applications* [Online]. Available: http://www.oruk.org/funding-research/research-projects/474/.

ELLIOTT, J. C. & YOUNG, R. A. 1967. Conversion of single crystals of chlorapatite into single crystals of hydroxyapatite. *Nature,* 214**,** 904-6.

ENAYATI, M., AHMAD, Z., STRIDE, E. & EDIRISINGHE, M. 2010. Size mapping of electric field-assisted production of polycaprolactone particles. *Journal of the Royal Society Interface,* 7**,** S393-S402.

FANG, T. H. & CHANG, W. J. 2004. Nanoindentation characteristics on polycarbonate polymer film. *Microelectronics Journal,* 35**,** 595-599.

GARCIA-ALONSO, D., PARCO, M., STOKES, J. & LOONEY, L. 2012. Low-Energy Plasma Spray (LEPS) Deposition of Hydroxyapatite/Poly-epsilon-Caprolactone Biocomposite Coatings. *Journal of Thermal Spray Technology,* 21**,** 132-143.

GENG, K. B., YANG, F. Q., DRUFFEL, T. & GRULKE, E. A. 2005. Nanoindentation behavior of ultrathin polymeric films. *Polymer,* 46**,** 11768-11772.

GLEDHILL, H. C., TURNER, I. G. & DOYLE, C. 1999. Direct morphological comparison of vacuum plasma sprayed and detonation gun sprayed hydroxyapatite coatings for orthopaedic applications. *Biomaterials,* 20**,** 315-322.

GRACE, J. M. & MARIJNISSEN, J. C. M. 1994. A review of liquid atomization by electrical means. *Journal of Aerosol Science,* 25**,** 1005-1019.

GROSS, K. A., CHAI, C. S., KANNANGARA, G. S. K., BEN-NISSAN, B. & HANLEY, L. 1998. Thin hydroxyapatite coatings via sol-gel synthesis. *Journal of Materials Science-Materials in Medicine,* 9**,** 839-843.

HARRIS, W. H., SCHILLER, A. L., SCHOLLER, J. M., FREIBERG, R. A. & SCOTT, R. 1976. Extensive localized bone-resorption in femur following total hip replacement. *Journal of Bone and Joint Surgery-American Volume,* 58**,** 612-618.

HARTMAN, R. P. A., BORRA, J. P., BRUNNER, D. J., MARIJNISSEN, J. C. M. & SCARLETT, B. 1999. The evolution of electrohydrodynamic sprays produced in the cone-jet mode, a physical model. *Journal of Electrostatics,* 47, 143-170.

HARTMAN, R. P. A., BRUNNER, D. J., CAMELOT, D. M. A., MARIJNISSEN, J. C. M. & SCARLETT, B. 2000. Jet break-up in electrohydrodynamic atomization in the cone-jet mode. *Journal of Aerosol Science,* 31**,** 65-95.

HAYWOOD, K. 2008. *The Skeletal System*, Marshall Cavendish.

HEIMKE, G. & GRISS, P. 1980. Ceramic implant materials. *Medical & Biological Engineering & Computing,* 18**,** 503-510.

HENCH, L. L. 1991. Bioceramics - From concept to clinic. *Journal of the American Ceramic Society,* 74**,** 1487-1510.

HENCH, L. L. 1998. Bioceramics. *Journal of the American Ceramic Society,* 81**,** 1705-1728.

HING, K. A. 2004. Bone repair in the twenty-first century: biology, chemistry or engineering? *Philosophical Transactions of the Royal Society of London Series a-Mathematical Physical and Engineering Sciences,* 362**,** 2821-2850.

HUANG, J., BEST, S. M., BONFIELD, W., BROOKS, R. A., RUSHTON, N., JAYASINGHE, S. N. & EDIRISINGHE, M. J. 2004. In vitro assessment of the biological response to nano-sized hydroxyapatite. *Journal of Materials Science-Materials in Medicine,* 15**,** 441-445.

IGNATIUS, A. A., BETZ, O., AUGAT, P. & CLAES, L. E. 2001. In vivo investigations on composites made of resorbable ceramics and poly(lactide) used as bone graft substitutes. *Journal of Biomedical Materials Research,* 58**,** 701-709.

JAFFE, W. L. & SCOTT, D. F. 1996. Total hip arthroplasty with hydroxyapatite-coated prostheses. *Journal of Bone and Joint Surgery-American Volume,* 78A**,** 1918-1934.

JAWOREK, A. & KRUPA, A. 1999. Classification of the modes of EHD spraying. *Journal of Aerosol Science,* 30**,** 873-893.

JAYADEVAN, K. P. & TSENG, T. Y. 2002. Composite and multilayer ferroelectric thin films: processing, properties and applications. *Journal of Materials Science-Materials in Electronics,* 13**,** 439-459.

JAYASINGHE, S. N. & EDIRISINGHE, M. J. 2002. Effect of viscosity on the size of relics produced by electrostatic atomization. *Journal of Aerosol Science,* 33**,** 1379-1388.

JAYASINGHE, S. N., EDIRISINGHE, M. J. & WANG, D. Z. 2004. Controlled deposition of nanoparticle clusters by electrohydrodynamic atomization. *Nanotechnology,* 15**,** 1519-1523.

JOHNSON, P. M. & STAFFORD, C. M. 2010. Effect of Interfacial Adhesion on Viscoelastic Relaxation Processes in Thin Polymer Film Indentation. *Acs Applied Materials & Interfaces,* 2**,** 2108-2115.

JONES, A. R. & THONG, K. C. 1971. Production of charged monodisperse fuel droplets by electrical dispersion. *Journal of Physics D-Applied Physics,* 4**,** 1159-66.

KAWANISHI, M., USHIDA, T., KANEKO, T., NIWA, H., FUKUBAYASHI, T., NAKAMURA, K., ODA, H., TANAKA, S. & TATEISHI, T. 2004. New type of biodegradable porous scaffolds for tissue-engineered articular cartilage. *Materials Science & Engineering C-Biomimetic and Supramolecular Systems,* 24**,** 431-435.

KIM, H. W., KNOWLES, J. C. & KIM, H. E. 2004. Hydroxyapatite/Poly(epsilon-caprolactone) Composite Coatings on Hydroxyapatite Porous Bone Scaffold for Drug Delivery. *Biomaterials,* 25**,** 1279-1287.

KIM, H. W., LEE, E. J., KIM, H. E., SALIH, V. & KNOWLES, J. C. 2005. Effect of fluoridation of hydroxyapatite in hydroxyapatite-polycaprolactone composites on osteoblast activity. *Biomaterials,* 26**,** 4395-4404.

KIM, S. S., PARK, M. S., JEON, O., CHOI, C. Y. & KIM, B. S. 2006. Poly(lactide-co-glycolide)/hydroxyapatite composite scaffolds for bone tissue engineering. *Biomaterials,* 27**,** 1399-1409.

KRZAKALA, A., SLUZALSKA, K., WIDZIOLEK, M., SZADE, J., WINIARSKI, A., DERCZ, G., KAZEK, A., TYLKO, G., MICHALSKA, J., IWANIAK, A., OSYCZKA, A. M. & SIMKA, W. 2013. Formation of bioactive coatings on a Ti-6Al-7Nb alloy by plasma electrolytic oxidation. *Electrochimica Acta,* 104**,** 407-424.

KUKLA, R. 1997. Magnetron sputtering on large scale substrates: an overview on the state of the art. *Surface & Coatings Technology,* 93**,** 1-6.

KUMAR, P. A. C., M. 2005. *Clinical Medicine.*, Elsevier Saunders.

KUO, J. 2007. Electron Microscopy: Methods and Protocols. 2nd ed.: Humana Press.

KURZWEG, H., HEIMANN, R. B., TROCZYNSKI, T. & WAYMAN, M. L. 1998. Development of plasma-sprayed bioceramic coatings with bond coats based on titania and zirconia. *Biomaterials,* 19**,** 1507-1511.

KUTZ, M. 2003. Standard Handbook of Biomedical Engineering & Design. McGraw-Hill.

LAVERNIA, C., D'APUZZO, M., HERNANDEZ, V. & LEE, D. 2004. Thigh pain in primary total hip arthroplasty - The effects of elastic moduli. *Journal of Arthroplasty,* 19**,** 10-16.

LEARMONTH, I. D., YOUNG, C. & RORABECK, C. 2007. The operation of the century: total hip replacement. *Lancet,* 370**,** 1508-1519.

LEE, K. & GOODMAN, S. B. 2008. Current state and future of joint replacements in the hip and knee. *Expert Review of Medical Devices,* 5**,** 383-393.

LEEUWENBURGH, S. C. G., HEINE, M. C., WOLKE, J. G. C., PRATSINIS, S. E., SCHOONMAN, J. & JANSEN, J. A. 2006. Morphology of calcium phosphate coatings for biomedical applications deposited using Electrostatic Spray Deposition. *Thin Solid Films,* 503**,** 69-78.

LEGEROS, R. Z. 1993. Biodegradation and bioresorption of calcium phosphate ceramics. *Clinical Materials,* 14**,** 65-88.

LEWANDROWSKI, K. U., BONDRE, S. P., WISE, D. L. & TRANTOLO, D. J. 2003. Enhanced bioactivity of a poly(propylene fumarate) bone graft substitute by augmentation with nano-hydroxyapatite. *Bio-Medical Materials and Engineering,* 13**,** 115-124.

LI, X., HUANG, J., AHMAD, Z. & EDIRISINGHE, M. 2007. Electrohydrodynamic coating of metal with nano-sized hydroxyapatite. *Bio-Medical Materials and Engineering,* 17**,** 335-346.

LI, X., HUANG, J. & EDIRISINGHE, M. J. 2008. Novel Patterning of Nano-Bioceramics: Template-Assisted Electrohydrodynamic Atomization Spraying. *Journal of the Royal Society Interface,* 5**,** 253-257.

LI, X., KOLLER, G., HUANG, J., DI SILVIO, L., RENTON, T., ESAT, M., BONFIELD, W. & EDIRISINGHE, M. 2010. A Novel Jet-Based Nano-Hydroxyapatite Patterning Technique For Osteoblast Guidance. *Journal of the Royal Society Interface,* 7**,** 189-197.

LI, X. A., HUANG, J., EDIRISINGHE, M. & BONFIELD, W. 2011. An electrically driven jetting technique for diverse high-resolution surface structures of nanometre hydroxyapatite crystals. *Colloids and Surfaces B-Biointerfaces,* 82**,** 562-570.

LIEBERMAN, J., R. & FRIEDLAENDER, G. E. 2005. *Bone Regeneration and Repair: Biology and Clinical Applications.*, Humana Press.

LIN, C. M. & YEN, S. K. 2005. Characterization and bond strength of electrolytic HA/TiO2 double layers for orthopaedic applications. *Journal of Materials Science-Materials in Medicine,* 16**,** 889-897.

LIU, X. Y., CHU, P. K. & DING, C. X. 2004. Surface modification of titanium, titanium alloys, and related materials for biomedical applications. *Materials Science & Engineering R-Reports,* 47**,** 49-121.

LIU, Y., LI, J. P., HUNZIKER, E. B. & DE GROOT, K. 2006. Incorporation of growth factors into medical devices via biomimetic coatings. *Philosophical Transactions of the Royal Society a-Mathematical Physical and Engineering Sciences,* 364**,** 233-248.

LOWMAN, E. W. 1955. OSTEOARTHRITIS. *Jama-Journal of the American Medical Association,* 157**,** 487-488.

LUO, C. J., NANGREJO, M. & EDIRISINGHE, M. 2010. A novel method of selecting solvents for polymer electrospinning. *Polymer,* 51**,** 1654-1662.

MA, J., SHI, L. H., SHI, Y. Y., LUO, S. U. & XU, J. 2002. Pyrolysis of polymethylsilsesquioxane. *Journal of Applied Polymer Science,* 85**,** 1077-1086.

MALCHAU, H., HERBERTS, P., EISLER, T., GARELLICK, G. & SODERMAN, P. 2002. The Swedish total hip replacement register. *Journal of Bone and Joint Surgery-American Volume,* 84A**,** 2-20.

MALZBENDER, J., DEN TOONDER, J. M. J., BALKENENDE, A. R. & DE WITH, G. 2002. Measuring mechanical properties of coatings: a methodology applied to nano-particle-filled sol-gel coatings on glass. *Materials Science & Engineering R-Reports,* 36**,** 47-103.

MAMMERI, F., TEYSSANDIER, J., CONNAN, C., LE BOURHIS, E. & CHEHIMI, M. M. 2012. Mechanical properties of carbon nanotube-PMMA based hybrid coatings: the importance of surface chemistry. *Royal Society of Chemistry, Advances Journal,* 2**,** 2462-2468.

MANSUR, M. R., WANG, J. & BERNDT, C. C. 2013. Microstructure, composition and hardness of laser-assisted hydroxyapatite and Ti-6Al-4V composite coatings. *Surface & Coatings Technology,* 232**,** 482-488.

MENCIK, J., MUNZ, D., QUANDT, E., WEPPELMANN, E. R. & SWAIN, M. V. 1997. Determination of elastic modulus of thin layers using nanoindentation. *Journal of Materials Research,* 12**,** 2475-2484.

MONSEES, T. K., BARTH, K., TIPPELT, S., HEIDEL, K., GORBUNOV, A., POMPE, W. & FUNK, R. H. W. 2005. Effects of different titanium alloys and nanosize surface patterning on adhesion, differentiation, and orientation of osteoblast-like cells. *Cells Tissues Organs,* 180**,** 81-95.

MUNIR, G., HUANG, J., EDIRISINGHE, M., NANGREJO, R. & BONFIELD, W. 2012. Electrohydrodynamic processing of calcium phosphates: coating and patterning for medical implants. *Nano LIFE,* 2**,** 1-17.

MUNIR, G., KOLLER, G., DI SILVIO, L., EDIRISINGHE, M. J., BONFIELD, W. & HUANG, J. 2011. The pathway to intelligent implants: Osteoblast response to nano silicon-doped hydroxyapatite patterning. *Journal of the Royal Society Interface,* 8**,** 678-688.

MUTOH, M., KAIEDA, S. & KAMIMURA, K. 1979. Convergence and disintegration of liquid jets induced by an electrostatic-field. *Journal of Applied Physics,* 50**,** 3174-3179.

NAG, S. & BANERJEE, R. 2012. Fundamentals of Medical Implant Materials. *ASM Handbook Materials for Medical Devices,* 23**,** 6-17.

NARAYAN, R. 2009. *Biomedical Materials*, Springer.

NITHYANANDAN, A., MAHALINGAM, S., HUANG, J., REHMAN, S., DRAPER, E. & EDIRISINGHE, M. 2013. Template-assisted electrohydrodynamic atomization of polycaprolactone for orthopedic patterning applications. *Materials Science and Engineering: C*, 33, 8, 4608-15.

NITHYANANDAN, A., MAHALINGAM, S., HUANG, J., REHMAN, S., DRAPER, E. & EDIRISINGHE, M. 2015. Bioinspired electrohydrodynamic ceramic patterning of curved metallic substrates. *Bioinspired Biomimetic and Nanobiomaterials,* 4**,** 59-67.

OKAYAMA, S., AKAO, M., NAKAMURA, S., SHIN, Y., HIGASHIKATA, M. & AOKI, H. 1991. The mechanical properties and solubility of strontium-substituted hydroxyapatite. *Bio-medical materials and engineering,* 1**,** 11-7.

OLIVER, W. C. & PHARR, G. M. 1992. An Improved Technique for Determining Hardness and Elastic-Modulus Using Load and Displacement Sensing Indentation Experiments. *Journal of Materials Research,* 7**,** 1564-1583.

ONG, J. L., BESSHO, K., CAVIN, R. & CARNES, D. L. 2002. Bone response to radio frequency sputtered calcium phosphate implants and titanium implants in vivo. *Journal of Biomedical Materials Research,* 59**,** 184-190.

PAITAL, S. R. & DAHOTRE, N. B. 2009. Calcium phosphate coatings for bio-implant applications: Materials, performance factors, and methodologies. *Materials Science & Engineering R-Reports,* 66**,** 1-70.

PANYAM, J. & LABHASETWAR, V. 2003. Biodegradable nanoparticles for drug and gene delivery to cells and tissue. *Advanced Drug Delivery Reviews,* 55**,** 329-347.

PARK, J. B. 1987. Biomaterials Science and Engineering. London: Pleum Press.

PELLICER, E., VAREA, A., SIVARAMAN, K. M., PANE, S., SURINACH, S., DOLORS BARO, M., NOGUES, J., NELSON, B. J. & SORT, J. 2011. Grain Boundary Segregation and Interdiffusion Effects in Nickel-Copper Alloys: An Effective Means to Improve the Thermal Stability of Nanocrystalline Nickel. *ACS Applied Materials & Interfaces,* 3**,** 2265-2274.

PLACE, E., EVANS, N. & STEVENS, M. 2009. Complexity in biomaterials for tissue engineering. *Nature Materials,* 8**,** 457-470.

POPA, M. V., MORENO, J. M. C., POPA, M., VASILESCU, E., DROB, P., VASILESCU, C. & DROB, S. I. 2011. Electrochemical deposition of bioactive coatings on Ti and Ti-6Al-4V surfaces. *Surface & Coatings Technology,* 205**,** 4776-4783.

POSNER, A. S., PERLOFF, A. & DIORIO, A. F. 1958. Refinement of the hydroxyapatite structure. *Acta Crystallographica,* 11**,** 308-309.

QIU, H. J., YANG, J., KODALI, P., KOH, J. & AMEER, G. A. 2007. A citric acid-based hydroxyapatite composite for orthopedic implants (vol 27, pg 5845, 2006). *Biomaterials,* 28**,** 2068-2068.

RADIN, S. R. & DUCHEYNE, P. 1992. Plasma spraying induced changes of calcium-phostphate ceramic characteristics and the effect on in-vitro stability. *Journal of Materials Science-Materials in Medicine,* 3**,** 33-42.

RAYLEIGH, F. R. S. 1978. On the instability of jets. *Proc. London. Math. Soc.,* 10**,** 4-13.

REED, A. M. & GILDING, D. K. 1981. Biodegradable polymers for use in surgery - Poly(glycolic)-poly(lactic acid) homo and co-polymers. 2. In vitro degradation. *Polymer,* 22**,** 494-498.

REILLY, D. T. & BURSTEIN, A. H. 1975. Elastic and ultimate properties of compact bone tissue. *Journal of Biomechanics,* 8**,** 393-405.

REUTER, H. 1991. Sol-gel processes. *Advanced Materials,* 3**,** 258-259.

RULISON, A. J. & FLAGAN, R. C. 1994. Electrospray atomization of electrolytic solutions. *Journal of Colloid and Interface Science,* 167**,** 135-145.

SEBBOWA, T., EDIRISINGHE, M., SALIH, V. & HUANG, J. 2011. Effect of deposition parameters and post-deposition annealing on the morphology and cellular response of electrosprayed TiO2 films. *Biofabrication,* 3**,** 045001.

SERGO, V., SBAIZERO, O. & CLARKE, D. R. 1997. Mechanical and chemical consequences of the residual stresses in plasma sprayed hydroxyapatite coatings. *Biomaterials,* 18**,** 477-482.

SHACKELFORD, J. F. 2005. *Introduction to Materials Science for Engineers*, Pearson Prentice Hall.

SMITH, D. P. H. 1986. The electrohydrodynamic atomization of liquids. *Ieee Transactions on Industry Applications,* 22**,** 527-535.

SUCHANEK, W. & YOSHIMURA, M. 1998. Processing and properties of hydroxyapatite-based biomaterials for use as hard tissue replacement implants. *Journal of Materials Research,* 13**,** 94-117.

SUN, L. M., BERNDT, C. C., GROSS, K. A. & KUCUK, A. 2001. Material fundamentals and clinical performance of plasma-sprayed hydroxyapatite coatings: A review. *Journal of Biomedical Materials Research,* 58**,** 570-592.

TANAHASHI, M., YAO, T., KOKUBO, T., MINODA, M., MIYAMOTO, T., NAKAMURA, T. & YAMAMURO, T. 1994. Apatite coating on organic polymers by a biomimetic process. *Journal of the American Ceramic Society,* 77**,** 2805-2808.

TAYLOR, G. 1964. Disintegration of water drops in electric field. *Proceedings of the Royal Society of London Series a-Mathematical and Physical Sciences,* 280**,** 383-90.

THIAN, E. S., AHMAD, Z., HUANG, J., EDIRISINGHE, M. J., JAYASINGHE, S. N., IRELAND, D. C., BROOKS, R. A., RUSHTON, N., BONFIELD, W. & BEST, S. M. 2010. The role of surface wettability and surface charge of electrosprayed nanoapatites on the behaviour of osteoblasts. *Acta Biomaterialia,* 6**,** 750-755.

TSUI, Y. C., DOYLE, C. & CLYNE, T. W. 1998. Plasma sprayed hydroxyapatite coatings on titanium substrates Part 2: optimisation of coating properties. *Biomaterials,* 19**,** 2031-2043.

URAL, E., KESENCI, K., FAMBRI, L., MIGLIARESI, C. & PISKIN, E. 2000. Poly(D,L-cactide/epsilon-caprolactone)/hydroxyapatite composites. *Biomaterials,* 21**,** 2147-2154.

VELASCO-ORTEGA, E., JOS, A., CAMEAN, A. M., PATO-MOURELO, J. & SEGURA-EGEA, J. J. 2010. In vitro evaluation of cytotoxicity and genotoxicity of a commercial titanium alloy for dental implantology. *Mutation Research-Genetic Toxicology and Environmental Mutagenesis,* 702**,** 17-23.

VELEMA, J. & KAPLAN, D. 2006. Biopolymer-based biomaterials as scaffolds for tissue engineering. *Tissue Engineering I: Scaffold Systems for Tissue Engineering,* 102**,** 187-238.

WANG, M. 2009. Surface Modification of Metallic Biomaterials for Orthopaedic Applications. *Light Metals Technology 2009,* 618-619**,** 285-290.

WANG, W., OUYANG, Y. H. & POH, C. K. 2011. Orthopaedic Implant Technology: Biomaterials from Past to Future. *Annals Academy of Medicine Singapore,* 40**,** 237-244.

WEI, M., RUYS, A. J., MILTHORPE, B. K. & SORRELL, C. C. 1999. Solution ripening of hydroxyapatite nanoparticles: Effects on electrophoretic deposition. *Journal of Biomedical Materials Research,* 45**,** 11-19.

WILHELM, O., MADLER, L. & PRATSINIS, S. E. 2003. Electrospray evaporation and deposition. *Journal of Aerosol Science,* 34**,** 815-836.

WOOLF, A. D. & PFLEGER, B. 2003. Burden of major musculoskeletal conditions. *Bulletin of the World Health Organization,* 81**,** 646-656.

XIAO, F.-J., PENG, L., ZHANG, Y. & YUN, L.-J. 2009. Silicon-substituted hydroxyapatite composite coating by using vacuum-plasma spraying and its interaction with human serum albumin. *Journal of Materials Science-Materials in Medicine,* 20**,** 1653-1658.

YAGHOUBI, H., TAGHAVINIA, N., ALAMDARI, E. K. & VOLINSKY, A. A. 2010. Nanomechanical Properties of TiO2 Granular Thin Films. *ACS Applied Materials & Interfaces,* 2**,** 2629-2636.

YAMADA, H., YOSHIHARA, Y., HENMI, O., MORITA, M., SHIROMOTO, Y., KAWANO, T., KANAJI, A., ANDO, K., NAKAGAWA, M., KOSAKI, N. & FUKAYA, E. 2009. Cementless total hip replacement: past, present, and future. *Journal of Orthopaedic Science,* 14**,** 228-241.

ZELENY, J. 1914. The electrical discharge from liquid points, and a hydrostatic method of measuring the electric intensity at their surfaces. *Physical Review,* 3**,** 69-91.

ZHAO, M. H., CHEN, X., YAN, J. & KARLSSON, A. M. 2006. Determination of uniaxial residual stress and mechanical properties by instrumented indentation. *Acta Materialia,* 54**,** 2823-2832.

ZHOU, J. & KOMVOPOULOS, K. 2006. Surface and interface viscoelastic behaviors of thin polymer films investigated by nanoindentation. *Journal of Applied Physics,* 100, 3291-8.